Tampereen yliopisto

Juha-Matti Hakojärvi

DEVELOPMENT OF A FAST AND ACCURATE ROTATIONAL MOTOR

Master's Thesis
Faculty of Information Technology and Communication Sciences (ITC)
Karri Palovuori
Katja Laine
3/2023

ABSTRACT

Juha-Matti Hakojärvi : Development of a fast and accurate rotational motor
Master's Thesis
Tampere University
MSc, Electrical Engineering
2/2023

Cameras are devices which appear in most handset devices nowadays. From the early days of mobile phones, a transition from the occurrence of a single camera to multiple different cameras has occurred. As cameras have become a standard feature of a handset, the development of optics and computational image processing has set new standards for mobile imaging quality. Competition in the mobile phone market makes the manufacturers push the limits of mechanical and optical performance and seek better solutions for enhancing image quality. As the limitations in size and power consumption are strict, new technologies have to be introduced. A way to bypass the space limitation of the devices is to make folding structure, that can be included in smaller space when not in use. This kind of structure needs a suitable actuator but also sets new requirements for camera actuators with the increased mechanical load, while still requiring precision.

This thesis is a description of the development process of a camera actuator from technology scouting to a manufactured actuator. First, different types of linear and rotary actuators and their characteristics was studied. As the design requirements were introduced, further comparison of suitable actuator types was enabled. Taking all the requirements into account, the actuator types were limited to electromagnetic actuators with the least mechanical contact possible, while still maintaining the high torque production capability as well as the capability of precise positioning. The options were narrowed down to stepper motors, the first design of an actuator was based on hybrid type of stepper motors, as commercial motors of that kind occurred to be capable of producing high enough torque for the intended purpose. However, simulations and attempts to make a prototype rendered the opportunities to none, the plans were headed towards a design of a stepper motor, whose torque production based on permanent magnets only.

The permanent magnet stepper motor was simulated and the results were compared to a stepper motor modified out of 2 BLDC (Brushless Direct Current) motor's components. As the rough prototype was somewhat successfully made, the design was further developed into a prototype motor with sufficient positioning precision, bearings and suitable dimensions for the available manufacturing capabilities. The machined parts were ordered from a third party and the prototype was assembled. The first assembled version with the original parts was unsuccessful, as the motor's rotating parts collided with each other. A solution for the problem was sought from reassembling the motor with modified (3D-printed) stator parts, which resulted in a motor that did rotate but didn't have high enough torque to move the load.

There are several possibilities to enhance the torque of the prototype. First and foremost, the iron stator parts should be modified to provide enough clearance between the rotor's magnets and the stator. In case this wouldn't enhance the torque sufficiently, another solution would be to alter the properties of the coils (turns and wire diameter as well as the density of the windings). In case this was insufficient to produce the desired torque, an undesired option would be to sacrifice positioning precision by decreasing the pole count and making a single pole bigger. The least desired means to increase the torque would be to increase it by means of gears.

Keywords: Actuator design, actuator types, hybrid stepper motor, permanent magnet stepper motor, FEM simulation, handset development, camera mechanics and electronics development

TIIVISTELMÄ

Juha-Matti Hakojärvi : Development of a fast and accurate rotational motor
Diplomityö
Tampereen yliopisto
Sähkötekniikan Di-ohjelma
2/2023

Kamera on laite, joka löytyy useimmista nykypäivän matkapuhelimista. Matkapuhelinten alkuajoista on tapahtunut siirtymä kameran mukaantulosta useamman kameran järjestelmiin. Koska kameroista on tullut puhelinten vakio-ominaisuus, optiikan kehitys ja laskennallinen kuvanprosessointi on asettanut kuvanlaatuvaatimukset uudelle tasolle. Matkapuhelinmarkkinoiden kilpailu saa valmistajat venyttämään mekaanisen ja optisen suorituskyvyn rajoja ja etsimään parempia ratkaisuja kuvanlaadun parantamiseksi. Koska koon ja tehonkulutuksen vaatimukset ovat tiukkoja, uutta teknologiaa on tehtävä. Eräs tapa kokorajoituksen kiertämiseksi on toteuttaa kokoontaittuva ratkaisu, joka mahtuu pienempään tilaan, ollessaan käyttämätön. Tällainen rakenne tarvitsee sopivan aktuaattorin, mutta asettaa myös uusia vaatimuksia kamera-aktuaattoreille lisääntyneen mekaanisen kuorman myötä vaatien kuitenkin edelleen tarkkuutta.

Tämä diplomityö on kuvaus kamera-aktuaattorin kehitysprosessista teknologiakartoituksesta valmistettuun aktuaattoriin asti. Ensiksi perehdyttiin lineaarista ja pyörivää liikettä tekeviin aktuaattorityyppeihin. Kun suunnitteluvaatimukset esiteltiin, eri aktuaattorityyppien vertailu mahdollistui. Kaikki suunnitteluvaatimukset huomioon ottaen aktuaattorityypit rajattiin sähkömagneettisiin aktuaattoreihin, joissa mekaanisen kontaktin määrä on vähäisin mahdollinen, mutta jotka kuitenkin pystyvät niin suureen vääntöön kuin tarkkuuteen. Vaihtoehdot rajattiin hybridistepperimoottoreihin, koska tämäntyyppiset kaupallisesti saatavilla olevat moottorit tuottivat riittävästi vääntöä käyttötapaukseen nähden. Simulaatiot ja prototyypinrakennusyritykset kuitenkin osoittivat mahdollisuudet olemattomiksi, joten suunnitelmat suunnattiin stepperimoottoriin, joka perustuu vain kestomagneettien tuottamaan vääntöön.

Kestomagneettistepperimoottoria simuloitiin ja tuloksia verrattiin stepperimoottoriin, joka muokattiin 2:sta BLDC-moottorista (Brushless Direct Current, hiiliharjaton tasavirtamoottori). Koska karkea prototyyppi oli jokseenkin onnistuneesti kokoonpantu, mallia kehitettiin edelleen moottoriksi, jossa on riittävä tarkkuus, laakerointi ja sopivat mittasuhteet saatavilla olevaan valmistuskyvykkyyteen nähden. Koneistetut osat tilattiin kolmannelta osapuolelta ja prototyyppi rakennettiin. Ensimmäinen kokoonpano oli epäonnistunut, sillä moottorin pyörivät osat törmäsivät toisiinsa. Ratkaisua ongelmaan etsittiin uudelleenkokoonpanosta muokatuilla (3D-tulostetuilla) osilla, mikä sai aikaan moottorin, joka pyöri, mutta joka ei tuottanut riittävästi vääntöä kuorman liikuttamiseen.

On useita mahdollisuuksia, joilla voisi parantaa prototyypin väännöntuottoa. Ensinnäkin, rautaosat pitäisi muokata siten, että roottorin magneettien ja staattorin välillä olisi riittävästi välystä. Siinä tapauksessa, että tämä ei olisi riittävä parannus väännöntuotossa, toinen ratkaisu olisi muuttaa kelojen ominaisuuksia (kierroksia, langan halkaisijaa sekä käämityksien tiheyttä). Siinä tapauksessa, että sekään ei riittäisi tuottamaan haluttua vääntöä, eräs ei-haluttu vaihtoehto olisi uhrata asentotarkkuutta vähentämällä napojen lukumäärää, suurentaen yksittäistä puolaa. Vähiten haluttu tapa väännön lisäämiseksi olisi lisätä sitä rattaiden avulla.

Avainsanat: Aktuaattorisuunnittelu, aktuaattorityypit, hybridiaskelmoottori, kestomagneettiaskelmoottori, FEM-simulaatio, matkapuhelinkehitys, kameroiden mekaniikka- ja elektroniikkakehitys

PREFACE

This thesis was done at the faculty of Information Technology and Communication Sciences, for Huawei Technologies Finland Oy. There were 3 supervisors of my work, of which one was my supervisor Eero Tuulos. The development process was led mostly by the project and its demands, and this thesis was written as its byproduct.

Little did I know at the time of starting this thesis work, what it was about to teach me. The goal of the thesis was clear from the very beginning but as for many projects, there were delays and redirections of plans. Along the way I got to take an introduction to the world of FEM simulations and quite vast amount of information on actuators and actuator technologies. An important instructor for the simulation part of the work was Patrick Grahn from Comsol, whom I'd like to thank for assistance on that part. I am grateful for the guidance on mechanical side of things, which my colleague Markus Virta gave to me during the design of the motor as well as Marko Eromäki's help in brainstorming the concept. I would like to thank all of my instructors for guiding the work and giving the feedback I needed. And not to forget one of the most vital ones, thank you to my friends for support and necessary distractions outside the writing task itself.

Tampere, 24th of February 2023

Juha-Matti Hakojärvi

CONTENTS

ABBREVIATIONS AND MARKINGS

AC	alternating current
BJT	bipolar junction transistor
BLAC	brushless AC
BLDC	brushless DC
CAD	computer assisted design
CNC	computer numerical control
DC	direct current
DSLR	digital single lens reflex
emf	electromotoric force
FEM	finite element method
mmf	magnetomotive force
MOSFET	metal oxide semiconductor field-effect transistor
MTBF	mean time between failures
NEMA	National Electrical Manufacturers Association
Nitinol	marketing name for nickel-titanium shape memory alloy
PMLM	permanent magnet linear motor
PMSM	permanent magnet synchronous motor
RC	radio control
SMA	shape memory alloy
SME	shape memory effect
TOF	time-of-flight
USM	ultrasonic motor
VXD	Voice-Coil Extreme-Torque Drive, marketing name for Tamron's lens linear autofocus motor
XD	Extreme Dynamic, marketing name for Sony's lens linear autofocus motor

F	force
$\Re$	reluctance
ϕ	magnetic flux
t	magnetic path length
μ_m	permeability of a medium
A	cross-sectional area of a magnetic path
μ_0	permeability of free space
μ_r	relative permeability of a medium
N	the number of turns of a coil
i	current
λ	flux linkage
W_f	work done by magnetic flux
L	inductance
x	displacement
f_{mech}	mechanical force
T	torque
L_d	radial inductance
L_q	tangential inductance
γ	torque angle (angle between a motor's direct axis and radial force)
B	magnetic flux density
l	length of a conductor (in a magnetic field)
r	radius of a motor's rotor
K_T	torque constant
V	voltage
n	rotational speed
v	velocity of a conductor relative to field
s	reluctance stack count

1. INTRODUCTION

During the previous years, there has been an increasing demand of miniaturizing devices, especially in mobile devices like cell phones. The development of manufacturing processes and heavily increased processing capability of phone chipsets has led to wide possibilities in camera development. Such are the prevalent multi-camera systems and other technical and computational solutions to enhance picture quality. Combining different types of cameras, such as monochromatic and TOF (time-of-flight) sensors, has been a widely used opportunity in image quality enhancing. Some phones take the advantage of several sensors by combining them with different optics that complement each other, for example providing the user a variety of focal distances.

There are some limitations, though, when it comes to small sensors: despite the recent advances in the quality of the optics, the small sensor size makes low light situations difficult. Some cell phones have already been published with larger sensor sizes than so far has been usual. This, however might demand using technical solutions that have never been utilized yet.

One of a kind is pop-up optical system, which is a structure that folds into smaller space, when not in use and extends itself to take up larger space when in use. Pop-up structures have been utilized in pocket cameras but now they are also seen as a solution to equip handsets with better cameras. The room from expanding structure can be utilized for better optics as well as the aforementioned larger sensors, while still keeping the size (mainly thickness) of the handset reasonable.

This as a solution needs an actuator, for example a rotating one. In the use case at hand, the target was to replace a geared stepper motor system with a directly driven stepper motor. A thing that’s not quite that widely used yet is using hollow shaft motors. Using the peripheral space of the optics by building an autofocus and pop up actuation capable motor would be feasible, considering that the possibilities of a highly space-economical design. Utilizing a hollow shaft motor with a larger sensor would mean larger diameter, enabling greater torque.

This thesis work is a description of designing a fast but also precisely rotating electrical motor. For the time of doing the thesis work, there is no commercialized motor that would be of hollow stucture that would be an exact fit to a certain camera module. There are

several stepper motors that are small in their size but one of their greatest problems is that they need gear drive in order to produce motion demanded in the camera system. The downside of mechanical transmission inside the camera module, tough, is that it produces more noise than the motor that is connected directly to the moving part of the camera. Some solutions alike have already been seen on the digital camera market, such as the linear focus motor of Sony mirrorless system camera lenses. This thesis work was done to find out, whether a hollow-core motor of handset form factor is manufacturable with sufficient torque production. Other points of examination are, whether it can provide enough precision, while still maintaining gearless structure.

The idea stems from the fact that there was a need for both kinds of movement in separate time windows. This, in turn, awoke the idea of taking an advantage of two different motor types integrated: a brushless direct current motor for fast, torque-demanding motion and a stepper for precise motion, where precision was needed with less torque.

In the second Chapter, different types of linear and rotary motors are reviewed. This Chapter also includes an overview of motor technology used in cameras. Third Chapter introduces the starting point of the development process with the requirements for the design. The first version of the solution follows in fourth Chapter. The findings of the hybrid stepper motor simulations steered the design forward to the second revision of the motor, which is a permanent magnet stepper motor introduced in fifth Chapter. In the sixth Chapter, the structure of the permanent magnet stepper motor is changed. Along with the new design and its simulations a reference prototype is introduced to provide proof of concept. The seventh Chapter develops this proof-of-concept motor into a design that matches the dimensional requirements and is compatible with the designed load. This Chapter is followed by wrap-up in Chapter 8.

2. AVAILABLE TECHNOLOGIES

In research and development, implementation and investigating the feasibility of new ideas starts from qualitative analysis. That is, finding out, what is the value proposed by the product. In this particular case, we delve into the industry analogies, i.e. what has already been developed, and talking about mass production units, what is currently available on the market. That helps us to get to know, what actually is the current competition, and where the new invention can actually thrive. [1, pp. 29, 191, 196, 200]

The starting point of this project is finding a direct-drive-capable type of an actuator in order to get rid of the possible noise-causing mechanics and compare different possibilities to achieve that. [2] The aim of the analysis is to pick the most feasible alternative to a mobile phone camera module and create a real scale prototype of that.

2.1 Rotary electromagnetic motors

Rotary electric motors produce rotational motion with electrical energy. There are multiple types of rotary electric motors, and some of them have been used for decades. Historically, AC motors have been prevalent in electricity production and machinery, more widely used technology being induction (asynchronous AC) motors, that are estimated to cover about 80% of the energy used in all electrical motors. [3]

Nowadays BLDC (brushless direct current, also brushless DC) motors have begun frequenting in smaller machines, e.g. battery powered hand tools and RC (radio-controlled) airplanes. They have also found their place even in electric vehicle industry, ranging from electrical scooters to cars. In addition to that, stepper motors have become even more prevalent in the consumer market due to consumer-available 3D-printers and other CNC (computer numerical control) equipment aimed for hobbyists. Nowadays, it's by no means unusual that a lens of a DSLR or a mirrorless system camera utilizes a wave propagation piezoelectric drive focus system and stepper motors are utilized in objectives, too. DSLR is an abbreviation of digital single lens reflex, which describes the widely used system camera structure with an optical viewfinder and a single lens. [4] [5] [6] [7]

There are also a few solutions that utilize linear motors in camera lenses, too. The solutions are kept well behind undescriptive marketing materials but they are claimed to be voice coil motors as well as linear stepper motors. They are manufactured by multiple well-known manufacturers, such as Sony (XD motor), Samyang and Tamron (VXD

motor). However, when it comes to the illustration of the focus mechanism, the marketing names may sometimes be misleading. For example, Samyang's solution – Linear Stepping Motor as they call it – does look like more like a rotational stepper motor with lead screw and not, for example, a permanent magnet linear motor. Linear motors will be addressed in detail later on on Chapter 2.3. [8] [9] [10]

Electrical motors can be divided into two main categories (in addition to the common AC and DC motor categories): those, that have a single magnetic field, i.e. variable reluctance motors, and two magnetic field motors. Both of the styles are shown in Figure 1. The way of torque production in these two is different: The two-magnetic-field motor produces torque by the attraction and repulsion two magnetic field sources – one on the rotor and one on the stator. Both of these can be of electromagnetic type, requiring commutators while permanent magnets provide an alternative with no need for excitation alongside with improved efficiency and higher power density. [11] [3]

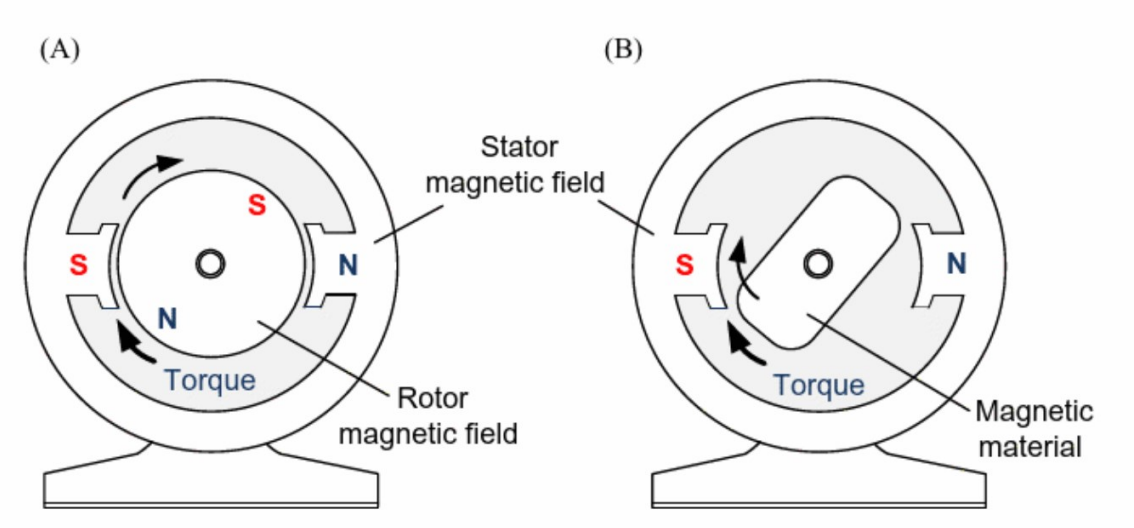

Figure 1. *The operation of an electric motor in a simplified form. On the left, there is the structure with the magnetized rotor, and on the right, there is the variable reluctance type of a motor. [3]*

The operation of the single-magnetic-field type motor (the structure on the right in Figure 1) relies on the reluctance torque, which is based on magnetomotive force (mmf):

$$F = \Re\phi \tag{1}$$

Where F is the magnetomotive force, $\Re$ is the reluctance of the magnetic circuit and ϕ is the magnetic flux of the magnetic circuit. Reluctance is a quantity that describes the tendency of a substance to resist magnetic flux and its behavior can be seen as analoguous to resistance and Equation 1 analoguous to Ohm's law. The reluctance itself is defined by the length (t) of the magnetic path as well as the permeability of the material (μ_m) and the cross-sectional area of the path (A) [12] [13]:

$$\Re = \frac{t}{\mu_m A} \quad (2)$$

Reluctance (Equation 2) is a case-sensitive property of the machine, as it's inversely proportional to the permeability of the magnetic circuit. Permeability of the material is often split into two separate parts, permeability of free space $\mu_0$and material's relative permeability μ_r, and $\mu_m = \mu_0\mu_r$. [3] [14]

On the other hand, the source of the magnetomotoric force is an activated coil. The magnetomotoric force induced by the coil is affected by two factors, turns and the current the coil is driven with:

$$F = Ni \quad (3)$$

Where N is the amount of turns per coil and i is the current flowing through the coil. [12]

Reluctance torque (in Figure 1) which follows from the magnetomotive force (Equation 1) of the activated coil (Equation 3), is induced in unaligned positions. When the rotor is not aligned with the poles, and the air gap between the magnetic elements and the rotor is not minimal. Since the reluctance path of the magnetic circuit isn't minimized, the rotor tends to rotate into a position, where the reluctance is minimum, i.e. the rotor is aligned with the salient poles of the stator. In aligned position, the inductance of the coil is also maximized as can be seen from Figure 8 in Chapter 2.1.2. The reluctance torque will be discussed in detail in Chapter 2.1.3. [3] [11] [15] [16]

2 magnetic field motors produce torque by interaction between two magnets but the separation between them comes from magnet types. Both of them can be of electromagnets (powered coils), such as in asynchronous AC (alternating current) motors in Chapter 2.1.2. Another alternative, brushless DC (direct current) motor, introduced in Chapter 2.1.5 includes a permanent magnet (rotor) and a coil. The foundation of operation is the same for permanent magnet synchronous motors introduced in Chapter 2.1.1. [3]

2.1.1 Synchronous AC motors

The AC motors can be divided into two main categories: synchronous and asynchronous (induction) motors. The operating principle differs with these by the magnetic field of the rotor. Alternatives for magnetic field production in the rotor are limited to two different ones, which are a DC powered coil and a permanent magnet. Since the magnetic field of the rotor remains still in relation to the rotor itself, it should rotate as fast as the external magnetic field changes. Hence the name, synchronous motor. [3]

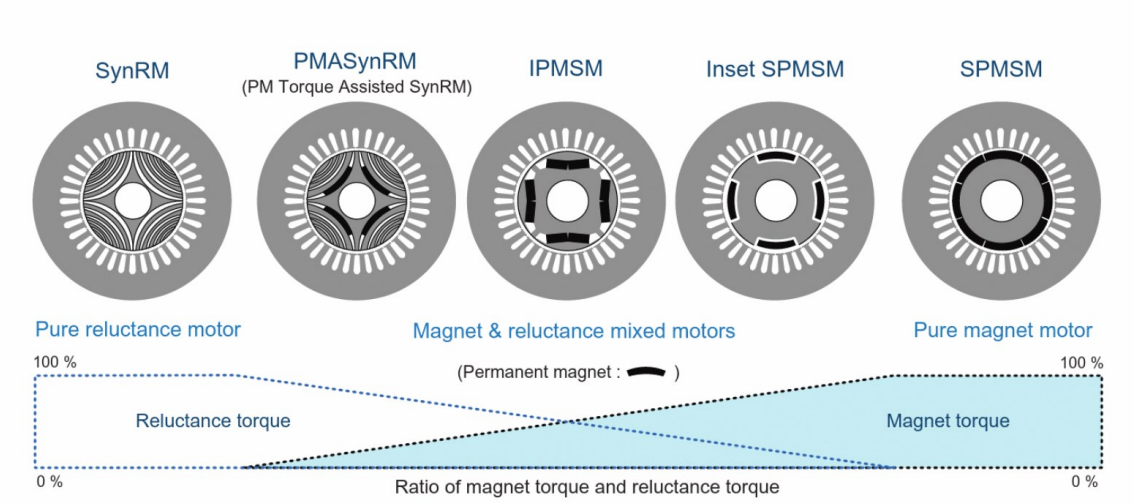

Figure 2. *The different rotor structures of synchronous permanent magnet motors and their torque production distribution. [3]*

Figure 2 above shows the different types of rotors of synchronous motors. SynRM is an abbreviation from synchronous reluctance motor, which is a pure reluctance motor. PMASynRM, i.e. permanent magnet synchronous reluctance motor uses permanent magnets to assist reluctance torque. IPMSM's, internal permanent magnet synchronous motors, produce torque with both reluctance and permanent magnets, with approximately even balance. A step further towards magnetic torque production is inset SPMSM (surface-mounted permanent magnet synchronous motor) motor type. They still produce torque partially by reluctance, versus the SPMSM's, which have only magnets facing the stator structure, meaning solely magnetic torque production. As from the image can be observed, the rotor does not nesessarily have to be magnetic but also reluctance torque can be utilized. According to the use case, the balance between reluctance and magnet torque can be set by affecting the motor structure. The principle of reluctance torque production will be introduced later in Chapter 2.1.3 Reluctance motors. [3]

2.1.2 Asynchronous AC motors

Asynchronous AC motors are more commonly called AC induction motors. Typical AC induction motor structure involves winding in the stator and a conductor cage in the rotor. In the case of an AC induction motor, torque is provided by two electromagnets. [14] The distinction from the synchronous AC motor is that as the AC current is lead to the rotor, the magnetic field doesn't remain static but it revolves. The name asynchronous stems from the fact that the magnetic field of the rotor is also in different phase compared with that of the stator. The magnetic field also rotates faster than the rotor itself. [11] To produce the necessary magnetic field in the rotor, the commutators connect the slip rings

of the rotor to a non-rotating commutation surface via carbon brushes, such as in the motor of Figure 3. [3]

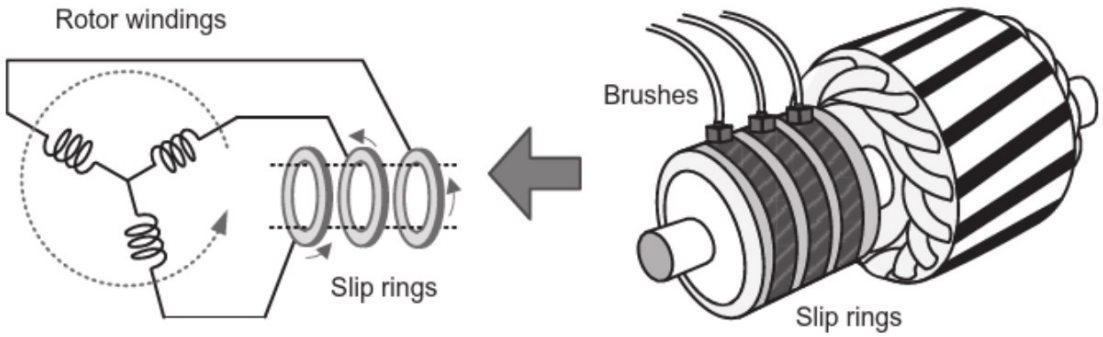

Figure 3. *Structure of the commutated rotor. [3]*

AC induction motors are widely used in both industrial and consumer applications. Power-wise different sizes of AC induction motors range from 10 W to 10 MW, including single-phase mains connected motors as well as three-phase connected motors. [14]

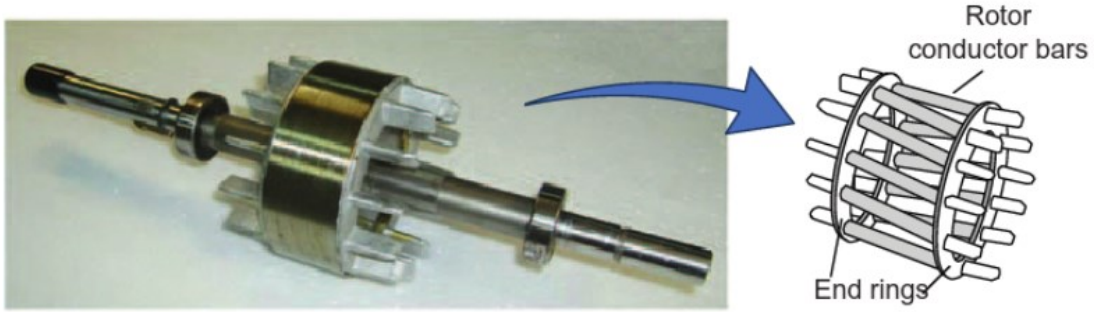

Figure 4. *Structure of a squirrel-cage rotor. [3]*

Squirrel cage rotor is by far the most commonly used rotor type due to the construction's simplicity and ruggedness. The structure consists of parallel-to-rotational-axis conductor bars, which are interconnected electrically by the end rings shown in Figure 4. As also shown in the Figure 4, the conductor bars can be parallel to the rotational axis of the motor but most often they're a little skewed, because it reduces cogging torque as well as acoustic noise. Cogging torque is the torque caused by magnet passing the stator slots. As the magnet passes the ferromagnetic pole, the anisotropic reluctance during the motion between the poles causes a torque towards the point with smallest possible reluctance path. This torque can be felt by rotating the motor by hand but it also affects the torque while operating the motor. An alternative to skewing of the conductor bars, is modifying the pole saliency, however both solutions, result in slightly less average torque and in some cases efficiency. [3] [11] [14] [17] [18] [19] [20] [21]

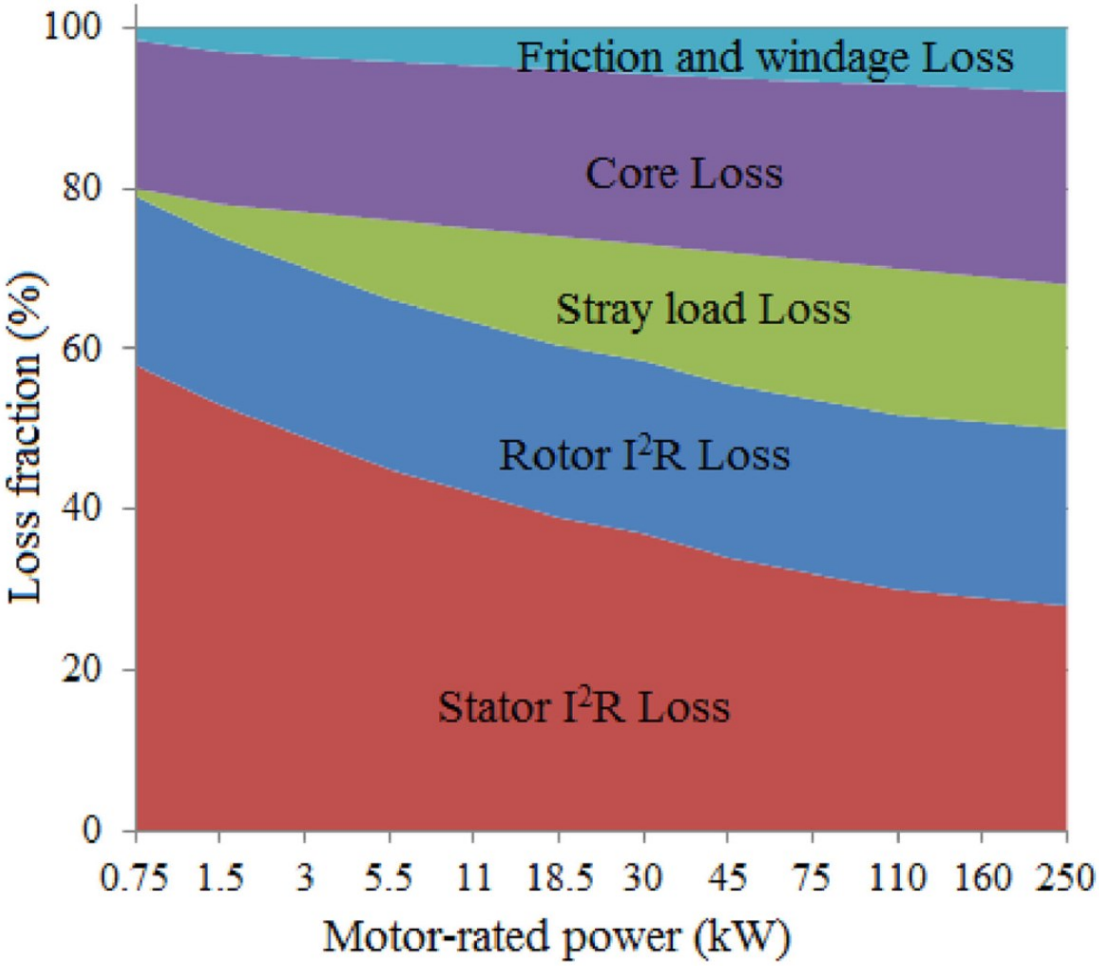

Figure 5. *Distribution of losses over rated power of a four-pole induction machine. [22]*

For AC induction motors, the losses in the motor by the rotation speed, the distribution of which is shown in Figure 5, are mostly defined by resistive losses in both stator and rotor. Almost equal to resistive (I^2R) losses in the rotor is core loss, which is caused by eddy currents inside the ferromagnetic materials of the motor. For ferromagnetic materials, temperature is not usually causing functional changes. For most coil insulators and permanent magnets electrical steels' Curie temperature – in which the magnetic properties of the material changes – is too high. To prevent eddy currents inside the ferromagnetic parts of the motor, the steel is layered and a layer of insulator is annealed between the layers. [14] [22]

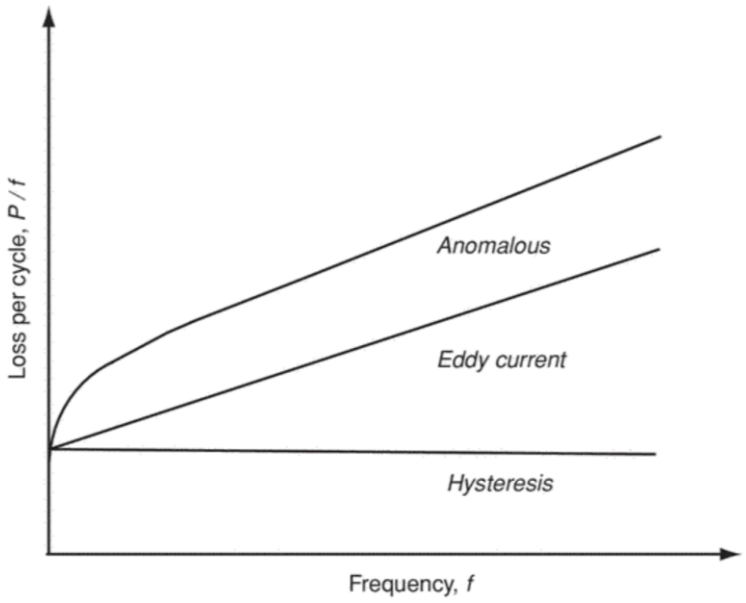

Figure 6. *Magnetic loss types in magnetic materials by frequency. [14]*

Figure 6 shows the distribution of major loses per cycle by used control frequency. Eddy currents induce extraneous heat in the motor but also limit the skin depth, i.e. depth, where the flux can penetrate into. Hysteresis losses are independent of the frequency. [14]

2.1.3 Reluctance motors

Unlike some AC motors and motors that have coils in their rotors, reluctance motors don't rely on the basic principle of force towards a current-fed wire. Thus, the rotor of a reluctance motor doesn't have coils in it, except for the optional starting cage, that may be necessary, when operating below synchronous speed of the motor. Since the rotor is formed to a certain form, it tends to rotate to an orientation feasible for magnetic field propagation [15] [23]. [13]

With a solid, completely uniform cylinder, the magnetic circuit wouldn't change despite rotor rotation, because as the motor is rotationally symmetric, it will not change the magnetic circuit either. However, if we change the cylinder by cutting pieces out of it, like in Figure 8, Figure 9 and Figure 10, the magnetomotive force will attempt to align the rotor into a position with the lowest reluctance path. [13]

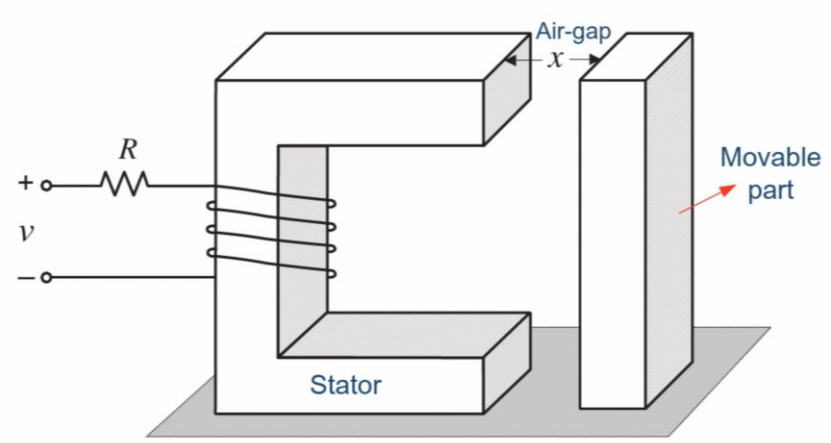

Figure 7. *A simple reluctance machine for linear motion production. [3]*

Understanding the torque production of a motor involves understanding the operation of a basic reluctance machine as shown in Figure 7. This structure is also known as a clapper actuator [24]. The self-inductance of a coil is determined by the flux linkage of the coil to itself divided by the current flowing through its conductors. Alternatively, it can be declared by using the conductor revolutions and flux:

$$L = \frac{\lambda}{i} = \frac{N\phi}{i} \tag{4}$$

Where L is the self-inductance of a coil, λ is the flux-linkage, i the electrical current through the coil, ϕ the magnetic flux passing through the coil and N the number of conductor rounds of the coil. [3] [24]

Although, it's not possible to understand the torque production of the motor completely, it can be made by delving into the magnetic circuit, and further, the work done by the coil: [3]

$$W_f = \int i\, d\lambda = \int \frac{\lambda}{L(x)} d\lambda = \frac{\lambda^2}{2L(x)} = \frac{1}{2} L(x) i^2 \tag{5}$$

As can be seen from Equations 4 and 5, the force caused by the magnetic energy can be exerted by differentiating the Equation by the motion of the armature: [3]

$$f_{mech} = -\frac{dW_f(i,x)}{dx} = -\frac{d}{dx}\left(\frac{\lambda^2}{2L(x)}\right) = \frac{\lambda^2}{2L^2(x)} \frac{dL(x)}{dx} = \frac{1}{2} i^2 \frac{dL(x)}{dx} \tag{6}$$

It must be noted, though, that Equation 5 holds true only assuming the flux linkage (λ) is constant. The energy of the magnetic circuit in Equation 4 can also be described by reluctance ($\Re$): [3]

$$W_f = \int_0^{\lambda} i\, d\lambda = \int_0^{\phi} F\, d\phi = \int_0^{\phi} \Re\phi\, d\phi = \frac{1}{2} \Re(x) \phi^2 \tag{7}$$

Similarly, to the force derived in Equation 5, the force by reluctance can be derived from Equation 7: [3]

$$f_{mech} = -\frac{d}{dx}\left(\frac{1}{2}\Re(x)\phi^2\right) = -\frac{1}{2}\phi^2\frac{d\Re(x)}{dx} \quad (8)$$

What can be deducted from Equation 8 is that the torque produced by a reluctance motor can most effectively be enhanced by increasing the flux as the dependency is quadratic. As can be seen from Equation 4, the relationship between the flux and winding turns or current is linear, so the means of torque enhancement is case-sensitive.

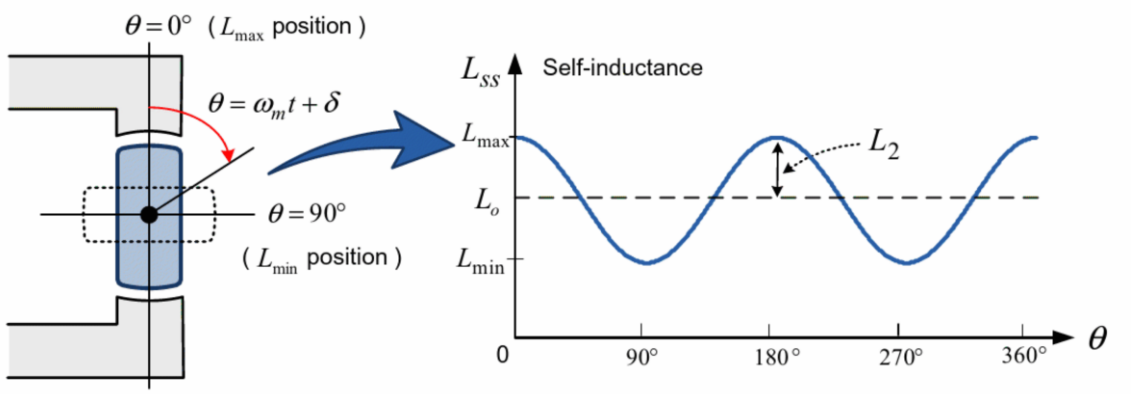

Figure 8. *Self-inductance variation over time on a single-magnetic-field (reluctance) motor. [3]*

Figure 8 shows the basic structure of a rotary reluctance motor and the variation of the inductance. As with the linear inductance machine, the inductance of the rotary machine is at maximum, when the rotor is aligned with the ferromagnetic stator, i.e. the air gap on the magnetic circuit is the smallest.

Equations 5 to 8 don't directly apply to the case of a rotary reluctance motor, but the torque can be derived from them, since torque is defined as the work done per rotation (θ): [3]

$$T = \frac{dW_{mech}}{d\theta} = \frac{1}{2}i_s^2\frac{dL(\theta)}{d\theta} = -\frac{1}{2}\phi^2\frac{d\Re(\theta)}{d\theta} \quad (9)$$

Equation 9 shows that the torque is at its largest, when the rotor is approximately in the middle of 0° and 90° positions. On the other hand, the 0° and 90° positions are the ones, where torque is zero. A graphical presentation of information in Equation 9 and Figure 8 appears below in Figure 9.

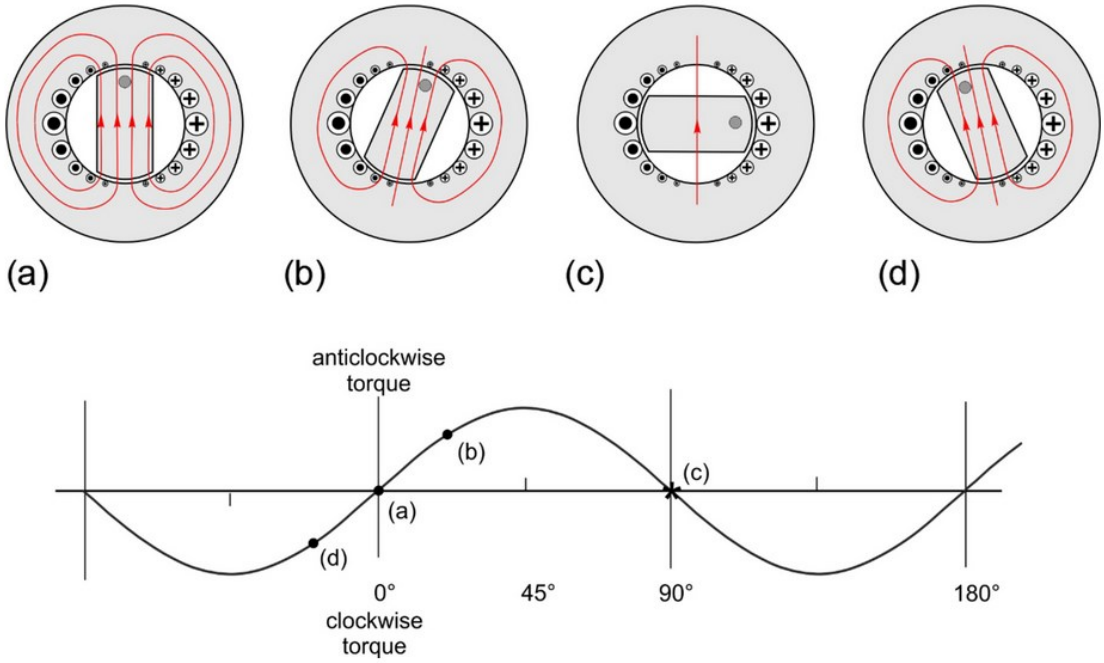

Figure 9. *Revolution of a reluctance motor with magnetic fields illustrated (red color). The graph below illustrates the form of torque output curve of this kind of a reluctance machine. [13]*

The inductance of the system in the position (a) in Figure 9 is referred as direct-axis inductance. However, the same torque can be seen in the position (c) of the same Figure. This inductance is called the quadrature-axis inductance. Since there is relatively much air on the reluctance path, the reluctance is high, while the flux through it is low. In these positions, the torque is zero, but in the situations (b) and (d), the situation's different. [13]

In squirrel-cage and AC induction motors introduced above, as well as the brushed DC motors that will be introduced next, the torque is based on the force towards a current-conducting wire in a magnetic field. In the case of a reluctance motor, for example in the rotor orientation (b) the stator wire on the top right is in a magnetic field, lead from the bottom left conductors. That causes a force towards the stator wire, but it being clamped to the stator, it produces an opposite reaction force towards the rotor, producing a counterclockwise torque. As one can infer, the point of maximum torque is found from between the two positions, (a) and (c). However, from position (c), the rotor will not return back to its position when displaced but actually enhances the displacement force, until it reaches the stable equilibrium in position (a). This is why the position (c) is called unstable equilibrium, meaning that this type of motor has only two zero-torque positions, one of which is stable. [13]

From the explanation above, can be reasoned that if the magnetic field is rotated, the rotor will also rotate along it. Even tough the basic principle is not too hard to grasp, it

isn't too easy to obtain the mathematical expression for the torque, since the inductance of the stator is dependent on the variable reluctance that follows from the rotating rotor. A correlation of different factors is presented in the following Equation (Equation 10) so as to get an approximate grasp on how the torque in a reluctance motor is produced. This won't be addressed more in depth in the scope of this thesis. [13]

$$T \propto I_S^2(L_d - L_q)sin(2\gamma) \tag{10}$$

Where T is the torque, I_s is the stator current, L_d is the inductance in the radial direction (codirectional with F_d), L_q the inductance in tangential direction (codirectional with F_q), both presented in Figure 10. The angle γ comes from the component division of F_S, which in turn, is the stator mmf, pointing in the direction of the motor's direct axis, seen in Figure 9 case (a). [13]

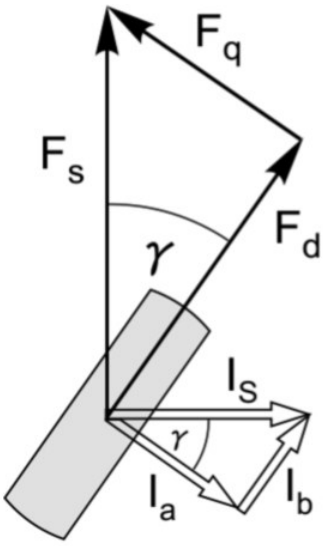

Figure 10. *Graphical representation of the component division and relevant measures to Equation 10. [13]*

However, reluctance motors haven't risen to be a generally good choice for electrical motor uses for a couple of reasons. One significant of them is the saturation of the iron rotor. The saturation of the alloy causes the torque produced to be rather linear than quadratic in relation to current in practice, as opposed to Equation 10. [13]

2.1.4 Brushed DC motors

Brushed motors have been used for a long time in car starters, blowers and fans, pumps, machine tools, drilling and milling machines, etc. They've been beneficial in the past since the rotor is a cage or a wound coil pack of copper that's connected to the power

line by carbon commutator brushes. That was especially feasible, when strong permanent magnets weren't widely available. [21]

Brushed DC motors can be split into 4 different categories: ironless rotor, iron rotor, torque and printed circuit motors. Another way of categorizing DC motors is dividing them into two categories, separately excited and self-excited ones. Separately excitated DC motors have separate power supplies for field winding and armature winding. Self-excitated motors, such as shunt motors, series motors and compound motors, are excitated by the same power supply. [3] [19]

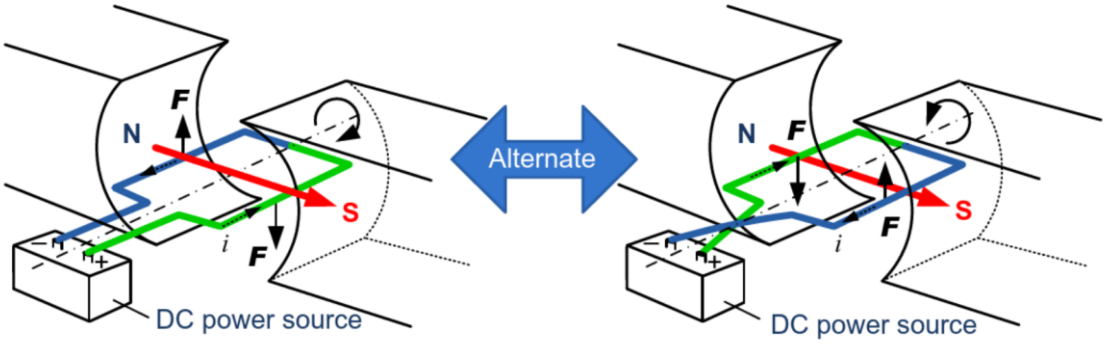

Figure 11. *Single conductor loop armature DC motor. On the left, the armature rotates clockwise due to the force (F) towards the coil wire induced by magnetic field (S). If the current (i) direction in the armature is reversed (on the right), so are the forces towards the wire loop rotation direction. In the source, magnetic field is depicted with letter S. [3]*

DC motor operation is based on the force towards the conductor loop. The rotational force towards the loop is caused by Lorenz forces towards the wires adjacent to the stators of the motor. [24] As presented in Figure 11, the rotation direction can simply be reversed by changing current direction in the armature. However, the current direction cannot remain static in the case of a rotating motor as the the field of the armature tends to align itself with the external magnetic field, pictured with symbol S in the source. [3]

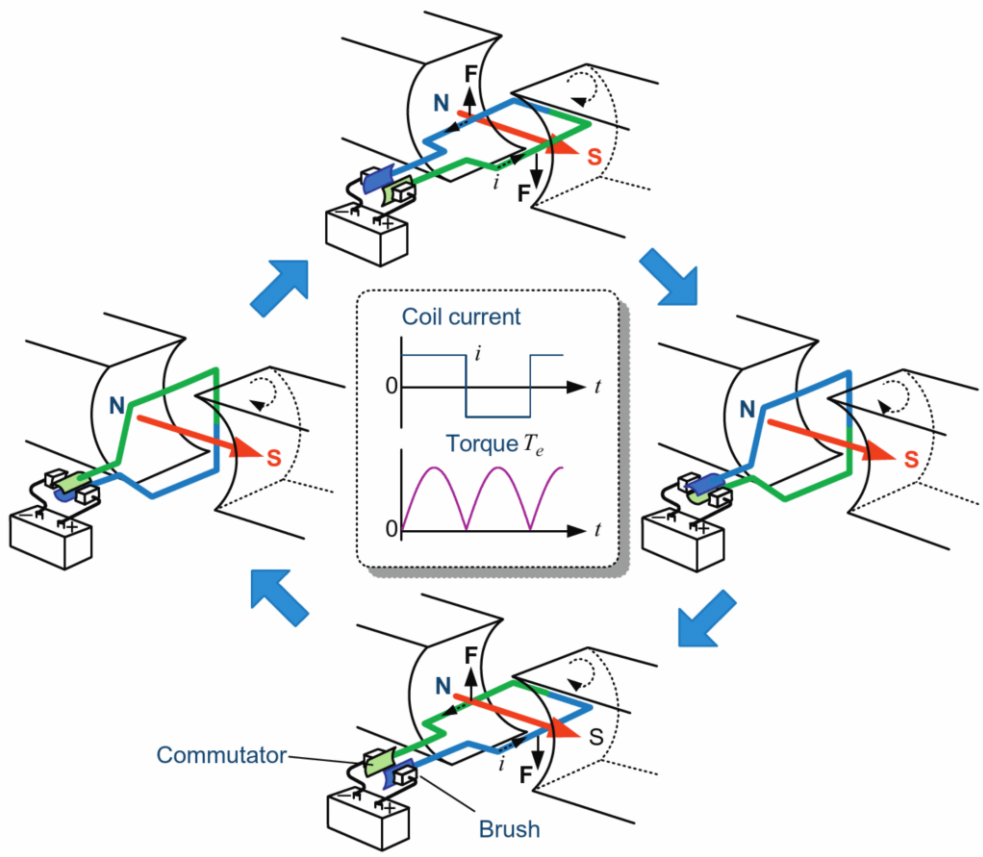

Figure 12. *Operation of a single-conductor-loop DC motor. A solution to switching the direction of the armature current (i(t)) is brushes, that change the direction of the armature current as the armature rotates. This way, the torque ($T_e(t)$) remains codirectional over rotation. As in Figure 11, the letter S represents the direction of the magnetic field. [3]*

The working principle of a brushed DC motor described in Figure 12 is rather close to the one of the AC asynchronous motor. A DC current is lead to the stator coils, which form a magnetic field in them. The rotor is connected to the same power line, inducing a magnetic field in the rotor coils, forcing the rotor's magnetic field parallel to that of the stator. However, while turning, the rotor rotates the commutators attached to it. The commutation surface on the stator consists of alternating voltage and ground contacts. This, in turn, causes the polarity of the rotor power change. As the power polarity reverses, as presented in Figure 12, so does the magnetic field in the rotor, inducing torque. [3]

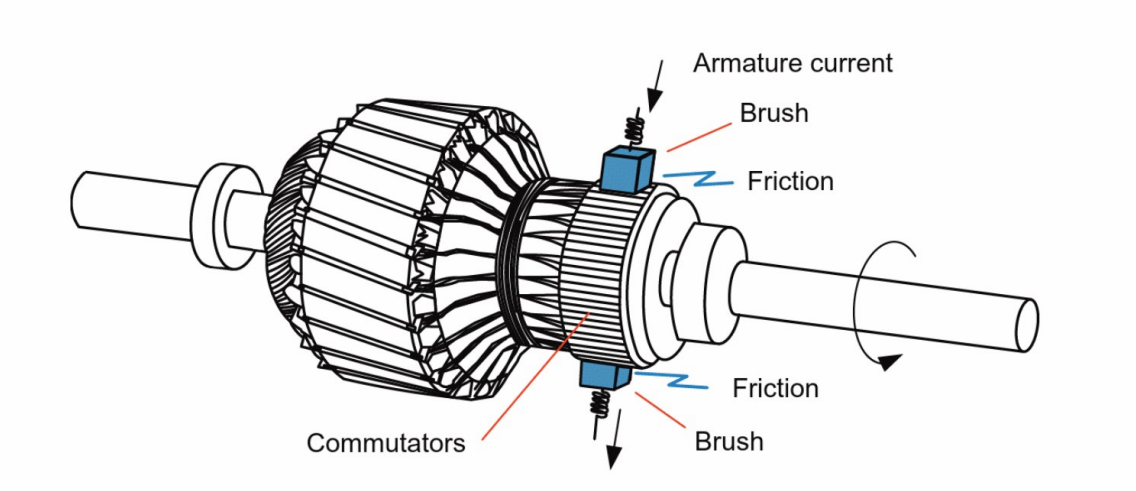

Figure 13. *Structure of a DC brushed motor's rotor and commutator brushes. Compared to the principled 12, this design uses multiple poles and skewed rotors. [3]*

The brushed DC motor's structure presented in Figure 13 assimilates the one of the AC induction motor with the difference that separate commutators are spread along the lateral surface of the instead of being constantly connected to carbon brushes. Commutation causes torque ripple in brushed DC motors, too, but can be reduced by increasing the pole count (compare Figure 12 with Figure 13). [3]

To get a grasp on the basic characteristics of a motor and to compare it with other types, one needs to understand what factors the motor's torque depends on. As concluded in previous Chapter, magnetomotoric force is the torque-producing phenomenon in reluctance motors but with dual excitation motors, the basis is different. Figure 14 shows a section view of a permanent magnet DC motor with magnetic fields during operation.

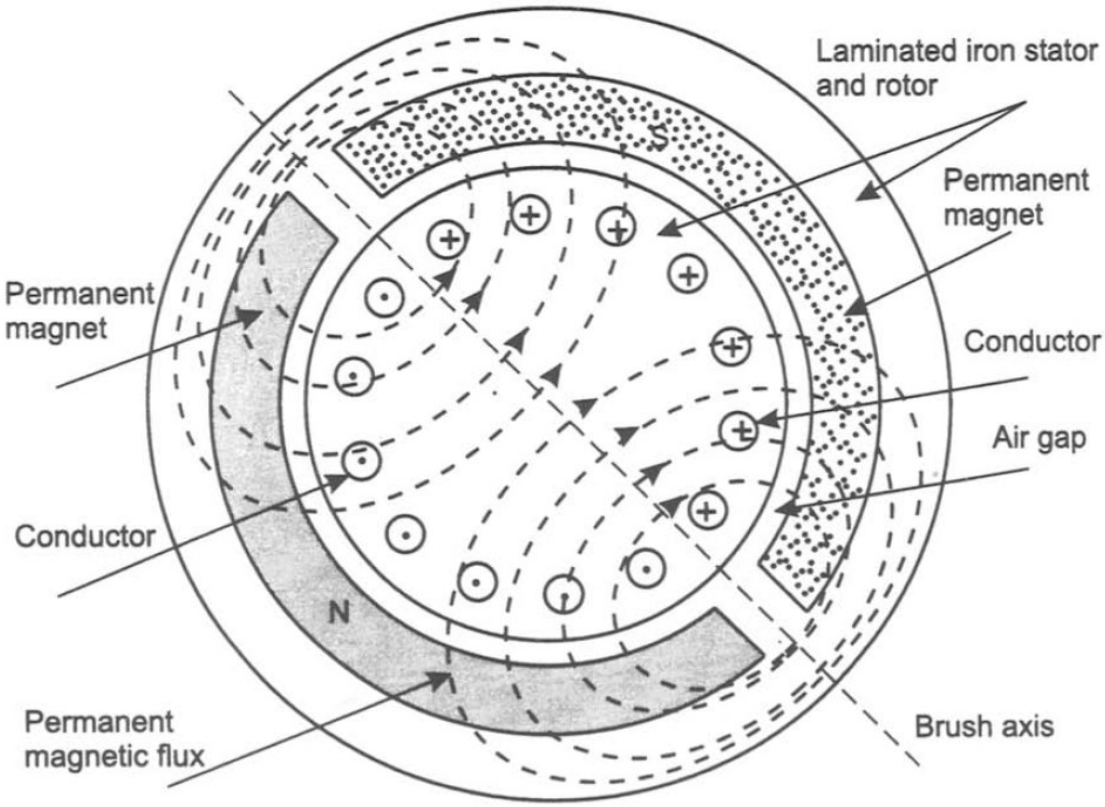

Figure 14. *Cross-section view of a permanent magnet DC motor's rotor. Magnetic fields induced by the permanent magnets represented by dashed lines and current directions are indicated by the symbols inside them. [25]*

Magnetic force to a conductor (Lorenz Force) that is in a magnetic flux with density B and current I flowing through it is expressed by Equation 11: [24]

$$F = BIl \tag{11}$$

From this follows that as the wires in a structure like in Figure 14, the magnetic parts cause force towards the wires, which in this kind of an assembly translates into torque towards the rotor. The torque strength is determined by the coil winding turns N, magnetic flux density B, axial length of the conductors l, current flow in the conductors I and the radius r of the rotor as follows: [25]

$$T = NBlIr \tag{12}$$

By defining the magnetic flux density B by magnetic flux ϕ, $B = \frac{\phi}{\pi r l}$, Equation 12 gets the following form:

$$T = \frac{N\phi I}{\pi} \tag{13}$$

As the magnetic flux density Φ and number of turns N are constants, the $\frac{N\phi}{\pi}$ is often described as torque constant K_T, the Equation 13 gets eventually into form: [13] [25]

$$T = K_T I \tag{14}$$

When it comes to torque characteristics, the torque of a series DC motor is dependent on the drive voltage and rotation speed:

$$T \propto \left\{\frac{V}{n}\right\}^2 \tag{15}$$

Where V is the voltage the motor is driven with and n is the rotational speed of the motor. [13]

However, as opposed to Equation 15 the torque at the low end of rotation speed, is limited by the resistance and saturation of the magnetic fields. For most series motors, it's necessary to limit the initial current, because the windings have too little a resistance in order to limit the initial current. For smaller motors, the resistance of the coils is high enough to limit the initial current to reasonable limits. The torque gap following from limited current is expressed in Figure 16. [13]

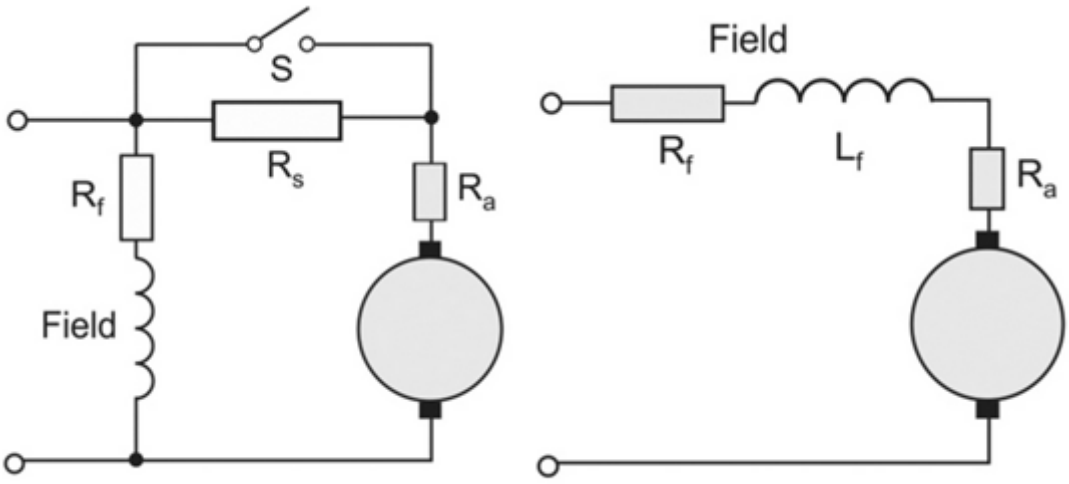

Figure 15. *Series and shunt motors' electrical models. Field winding is indicated by* $\boldsymbol{L_f}$*, and its parasitic resistance by* $\boldsymbol{R_f}$*. Armature is the grey round symbol and its resistance the* $\boldsymbol{R_a}$*. The series motor is presented on the right and shunt motor on the left. With shunt connection, there is the additional resistance* $\boldsymbol{R_s}$*, which can be switched off by using the switch represented by symbol* $\boldsymbol{S}$*. [13]*

The series and shunt DC motors' electrical models are shown in Figure 15. The evident difference is the shunt vs. series connection of the motor and the other, consequential, difference is the external starting resistance R_S and the switch connected in parallel with it. The external resistance is used in the startup of the motor and is switched off, as the back e.m.f. increases. In the start, the armature resistance may not suffice to prevent excessively large currents, and there is no back e.m.f. either, to limit the current flow. [13]

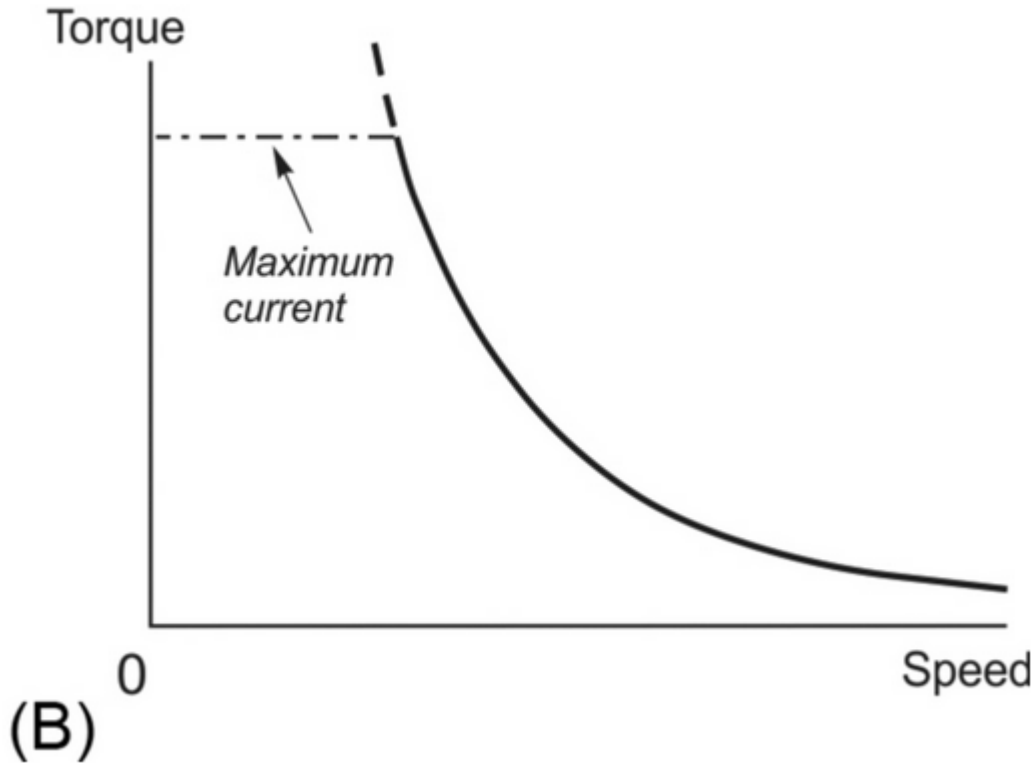

Figure 16. *Typical torque curve for a series type motor. [13]*

Series motors and shunt motors differ significantly regarding speed limitations. They don't have the inherent rotation speed gap without load, except for infinity. This is also why series motors have historically been used for traction purposes. Large series motors can neither be run unloaded, since the no-load speed is dangerously high for the motor's mechanics. [13]

The demand of mechanical connection doesn't come without downsides. The commutation, the switching between poles as well as sparking does cause significant disturbance in the power lines from which the motor takes its energy. There is a solution, namely adding the so-called interpoles or compoles to the stator, in between of the main poles. Their purpose is to enhance commutation and lessen the sparking effect. Brushes of the motor in question also possess the risk of overheating in high speeds and loads. [22]

DC motors are promising competitors to stepper motor when it comes to efficiency, as can be judged by Figure 17 but as a downside they require gears. It is also possible to obtain performance comparable to a stepper motor with a geared DC motor but it doesn't come without difficulties. The relative slip error per revolution, namely, is at higher speeds in an unacceptable level. A stepper-motor-like performance has been achieved in rotational speed of up to 2 rpm. The precision review in question, performed by Dadi

et al., were done with two different geared stepper motors: one with 30 rpm maximum speed and one with 10 rpm maximum speed, the corresponding stepper-like rotation speeds, being 1 rpm and 2 rpm. The geared DC motor is not specified to be of brushless type, but as we can confirm by the structural analysis on different motor types later on, the motor must be of the brushed DC type due to its two input conductors. [26]

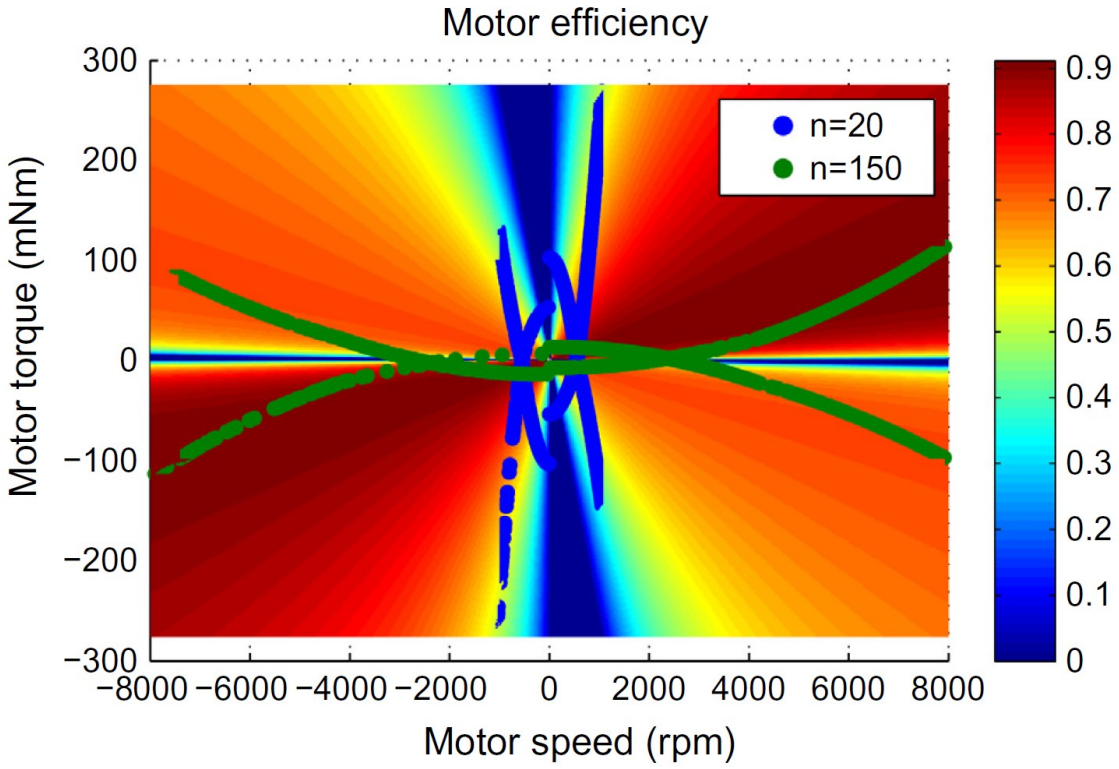

Figure 17: *Efficiency map of a DC brushed motor. The base color tones (on the right) describe efficiency on different torques and speeds. Blue zones on top of the graph describe efficiency rates the motor performs at with a gear ratio 1:20 and the green overlay describes gear ratio of 1:150. [27]*

It's useful to take a note on the fact that using gears will let the brushed DC motor work in high efficiency rates. Despite gears reduce dampening losses, the downside is that the resistive losses increase in case of a low gear ratio. With higher gear ratios, resistive losses also decrease, increasing the overall efficiency. [27]

2.1.5 Brushless DC motors

Brushless DC motors, alias BLDCs, rely on the same principle of the alignment of the codirectional magnetic fields. Five alternative BLDC structures are shown in Figure 18. Using permanent magnets eliminates the need for directing current into the rotor. The magnetic field in the rotor magnets isn't alternating, so the alternating field for producing torque must be produced in the stator coils. This requires more complicated control of the motor than just simply connecting it to DC power, but can be made with

semiconductor switches. Not only does the BLDC have the advantage of less disturbances (EMI, electromagnetic interference, i.e. electromagnetic effects on other devices in the proximity of the device) [28] [29] by the non-commuting structure, it also adds the benefit of higher achievable drive speeds. What increases the MTBF (mean time between failures) of a BLDC is the fact that there is no need for carbon brush replacement but bearings only. Mean time between failures is a metric by which the lifetime between repairable failures are expected [30] [29] [31] [32]. [3]

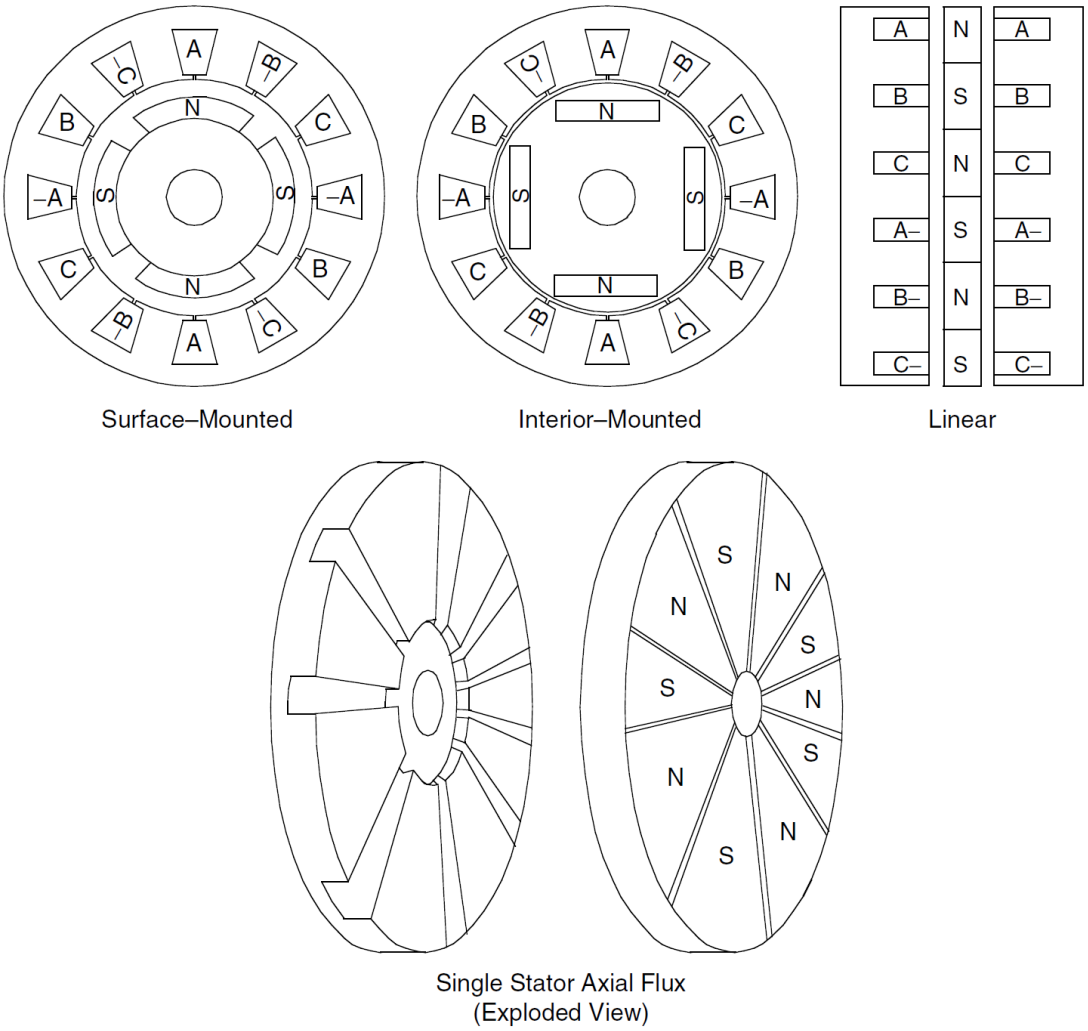

Figure 18. *Different BLDC structures. [33]*

As well as other motor types, BLDCs also have different structures (see Figure 18 above and Figure 19 below) that can be utilized in different use cases. Firstly, the form and positioning of the magnets can be varied between surface-mounted and interior-mounted types with radial flux. Axial flux motors, in turn can be used in shallow spaces, and lastly, the linear structure can be utilized in need of a linear actuator.

Development in magnetic materials from the early axial flux motors and decrease in the price of powerful hard magnetic materials has enabled the use of axial flux motors. As the volume of radial flux motors isn't completely utilized for magnetic circuits, axial motors are capable of producing higher torque densities. Axial flux motors are advantageous in modularity: the stack number can be varied to match the performance requirement for the use case. Compared to slotted stator radial permanent magnet motor machines can also have reduced cogging torque by utilizing to slotless armature winding. Yet, they have their downsides: More magnetic material is needed compared to radial flux machines, and low winding inductances may cause problems with inverter drives. [34]

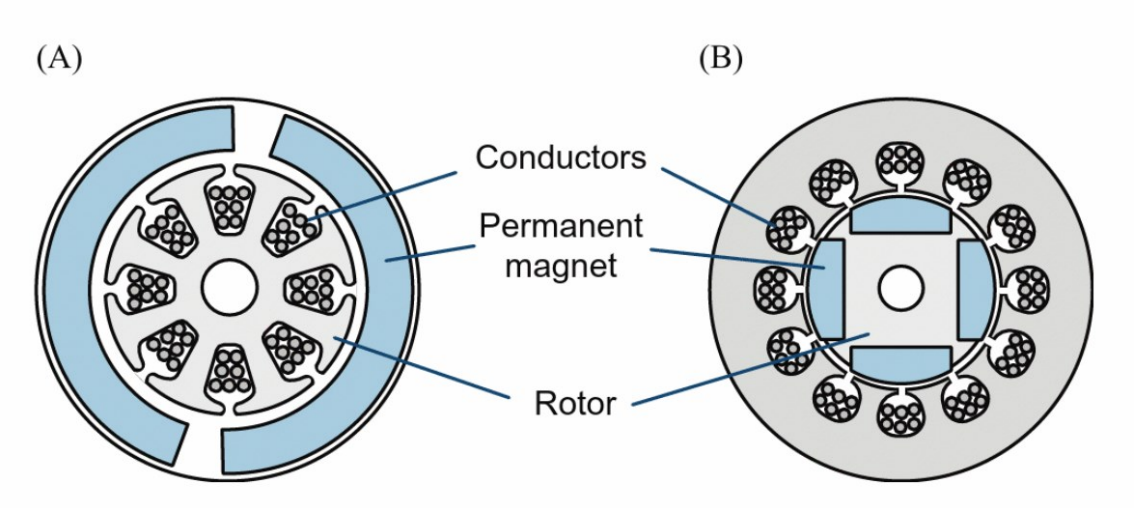

Figure 19. *Two different configurations of a BLDC motor. On the left, there is the so-called outrunner structure and on the right there is the inrunner structure. [3]*

Before, in Chapter 2.1.4, where the torque production of a brushed DC motor was evaluated, flux-cutting approach was used. In the real world, the magnetic flux doesn't pass through the conductor but passes through the iron core surrounding the coil wires. It's overcome by assuming the coil wires being at the distance of the stator bore, in the air gap instead of further away in the stator. It has been evaluated that this assumption leads to proper results in the evaluation of torque and back emf. Using the same approach, electromotoric force (emf) can be defined by Equation 16:

$$e = Blv \tag{16}$$

Where B is the flux, l the length of the conductor, and v is the speed the conductor relative to the field. The average torque output, in turn, can be determined with the same Equation as with a brushed motor, Equation 14. [25]

BLDC structures can have any number of phases but among the phase count the performance of the motor is changed as well. Single-phase BLDCs are widely utilized in small machines but despite their low cost and simplicity, they have the downside of

rotating in a single direction only. More common are the cases of 2 and 3 phase motors, which can rotate in both directions. When extra reliability and higher torque density is demanded, multi-phase motors can be utilized. [3]

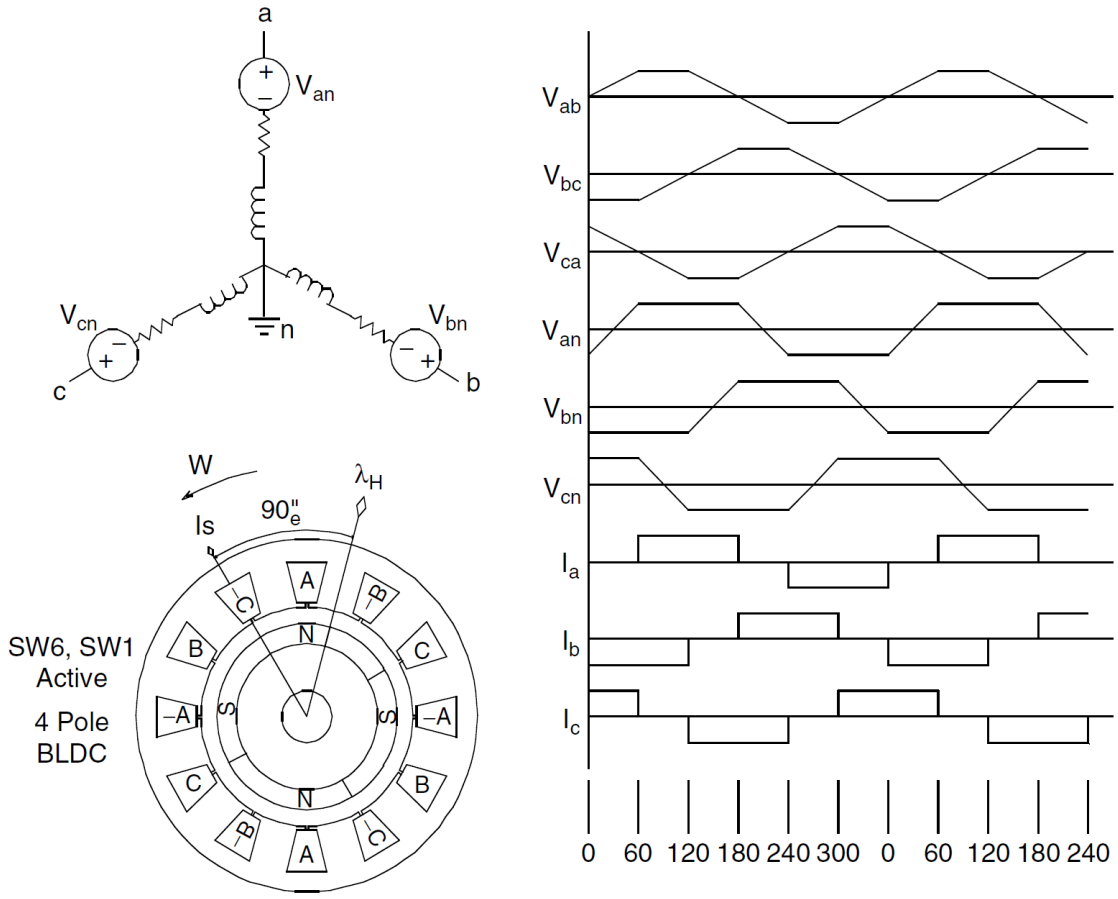

Figure 20. *Delta connection of a brushless DC motor (upper left section) its voltage and current waveforms (right half) and corresponding structure (lower left section).*

A commonly used design in the brushless DC motors is a three-phase design with varying number of poles. The phases are configured to either a delta (Figure 20, above) or a star pattern (Figure 22, below). The benefit of the star pattern is the real middle connection, which can be utilized for determining the position of the rotor without external sensors. However, a delta configuration of the coils causes the impedance between phases to be lower than in star configuration, thus requiring smaller drive voltages. [3]

The missing null point in a delta connection can be replaced with a virtual zero, though. Forming the virtual null point requires three equal-size resistors, which are connected into star configuration between the poles of the motor. The null point of the resistor star is then the virtual null point. Now, the position of the rotor can be read from the virtual null point. As long as the resistance of resistors are magnitudes bigger than that of the coils, the structure will not cause excess load on the driver, either. [35]

The driver circuit consists of MOSFET (metal oxide semiconductor field-effect transistor) or BJT (bipolar junction transistor) bridge circuits. A half-bridge, as shown in Figure 21, is a unit consisting of two transistors: a high side driver and a low side driver. As there are three poles, also three half-bridges are needed. By setting either of the transistors on (high or low), a single pole of the motor can be driven to supply voltage or ground. The other end will be connected to the opposite terminal through a coil (delta connection) or multiple coils (star connection) of the motor.

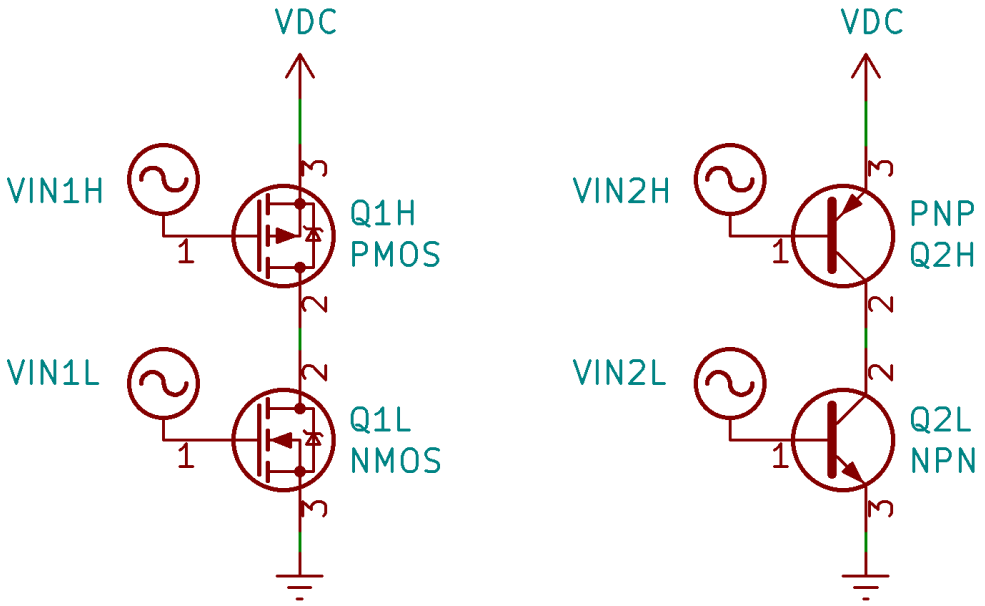

Figure 21. *Half bridge structures with MOSFETs and BJTs. VIN1H and VIN2H describe input signals of the high voltage transistors and VIN1L and VIN2L represent the control voltages of the low voltage transistors. The source VDC indicates the DC voltage of the supply.*

Usually the low side driver MOSFET is of enhancement mode N-channel type and the high side driver is an enhancement mode P-channel type MOSFET. In the BJT version, the high side driver is a PNP-type and low side is an NPN-type BJT. The half-bridge can also be made with two MOSFETs of the enhancement N-channel type, but ensuring a proper gate-to-source voltage, more complex driving circuits have to be made. An enhancement mode N-channel type MOSFET can be utilized as a high side driver, too but requires a separate driver circuit, since the source voltage is not fixed. Therefore, it has to be driven above the motor-driving voltage to ensure that V_{GS} is kept above the required voltage for on-state.

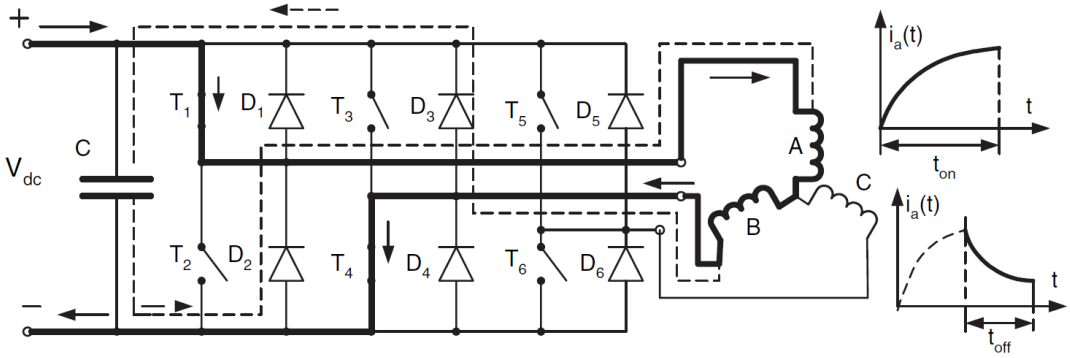

Figure 22. *Current flow through a star-connected BLDC and its control circuitry. [34]*

How the motor controller of a BLDC motor works is presented in Figure 22. BLDCs are very close to the structure of a permanent magnet synchronous motors, hereafter PMSM. Another name that PMSMs are known with is BLAC, which in turn comes from brushless alternating current. However, they're not the same and they shouldn't be confused with each other. The differences are listed in Table 1, where can be seen distinguished that the PMSM is more complex and expensive as a system, compared with the BLDC, yet with the benefit of nearly constant torque against the torque ripple of the BLDC. [3]

Table 1. *Differences of BLDC motors and PMSMs. [3]*

	BLDC Motor	**PMSM**
Back-EMF	Trapezoidal waveform	Sinusoidal waveform
Stator winding	Concentrated winding	Distributed winding
Stator current	Quasi-square waveform	Sinusoidal waveform
Driving circuit	Inverter (120° conduction)	Three-phase inverter (180° conduction)
Drive method	Simple, using low-cost Hall effect sensors	Complex (using high-resolution position sensor such as an encoder or a resolver)
Torque ripple	Significant torque ripple	Nearly constant torque
System cost	Low cost	High cost

Table 1 shows the main differences in BLDC and PMSM technologies. Structurally they assimilate each other but when it comes to characteristics, like winding structures, control waveforms and torque characteristics, they are rather different. [3]

2.2 Position controllable rotary electromagnetic motors

Position controllable rotary electric motors divide into two subcategories: stepper motors and servomotors. Stepper motors – as opposed to other motor types – have the ability of rotating by discrete steps. The very commonly used way of using a stepper motor is

to use a controller that receives direction signal and a pulse detector, like in Figure 23. The drive circuit (the controller) takes care of powering the stepper motor according to the drive signals. [13]

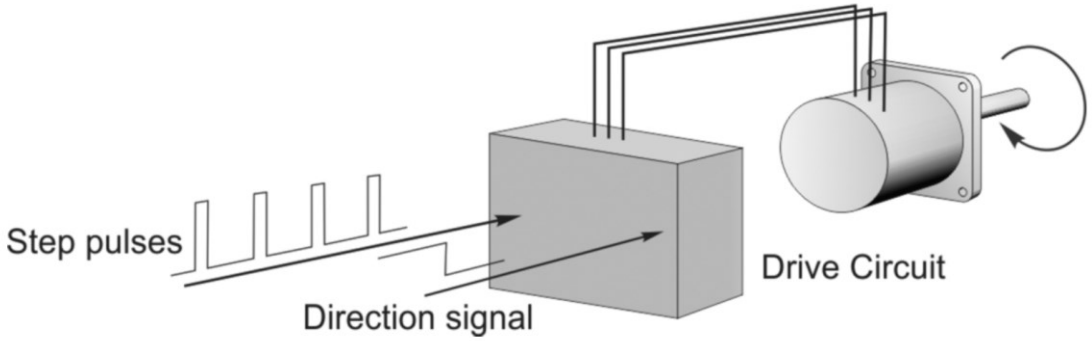

Figure 23. *Representation of a generic stepper motor and its controller. [13]*

Compared to other kinds of motors, stepper motors provide high torque in low speeds. The torque of a DC commutator motor of equivalent size may have only a fifth of the torque produced by an equally sized stepper. In many cases, a stepper motor is powerful enough to power element-to-be-moved directly, making use of gearbox unnecessary. [36]

A stepper motor and a servomotor differ from each other in the way, that a servo motor has internal position feedback and a servo motor isn't necessarily a stepper motor. A stepper motor in turn, by itself, is just an open loop actuator. An open loop system is a system, where no feedback about the system's output is used to control the input. Comparatively, closed loop system somehow gets information about the system's output, using it to modify the input and to correct possible error in the output. [37]

Yet, in case rotor position is important information, the position can be calculated by counting the steps fed to the controller after setting the position to a known position. In that case, it's provided yet that no stalling happens or stalling has to be detected. If for example insufficient power is fed into the stepper, it will not overcome the load torque, keeping the motor stuck in the position where it was before the load exceeded the produced torque. In addition to stalling in the beginning of the rotational movement, similar failure may occur in braking the motor. If the command pulses are stopped without a proper ramp, it may be so that the rotor continues movement over the commanded step count. Thus, if stalling happens, the position can no longer be determined, unless there is a position sensor for the shaft or the controller has integrated stall detection. There are stepper motor controllers with stall detection, too. Despite for some motor types overheating is a problem, for a stepper motor that should not be the default case,

as for many purposes not only precise movement but also precise position keeping is desired. [13]

A servo motor has a position sensing unit and a closed-loop control built in, it will attempt to reach the commanded position, until it reaches it or another setting value is fed for it. [2] For the stepper motor's lack of closed-loop control, there is a number of types of sensors that can be used for external feedback: rotary encoders, hall effect sensors, switches and fotointerrupters, to name a few. This way, one can create a closed-loop system with the motor and guarantee proper function of the device. [13]

2.2.1 Variable reluctance stepper motors

Variable reluctance stepper motors are rather similar compared to reluctance motors. Just as reluctance motors, they rely on ferromagnetic rotors and reluctance path minimization of salient pole rotor. The exception is that the saliency of the poles is designed for stepwise action. [13]

The rotor of the variable reluctance stepper motor is often of soft iron and it's surrounded by coils with ferromagnetic cores. When a pole is activated, the rotor aligns itself so that the reluctance path in the magnetic circuit is minimized. By the coil-induced temporary magnetization of the rotor, when the direction of the current in pole A, in Figure 24 below, is flipped, and the pole B is activated, the rotor will turn into its next position. A benefit of this type of motors compared to its counterpart – the permanent magnet stepper motor – is that the rotor doesn't have to be of expensive materials. [19] [36]

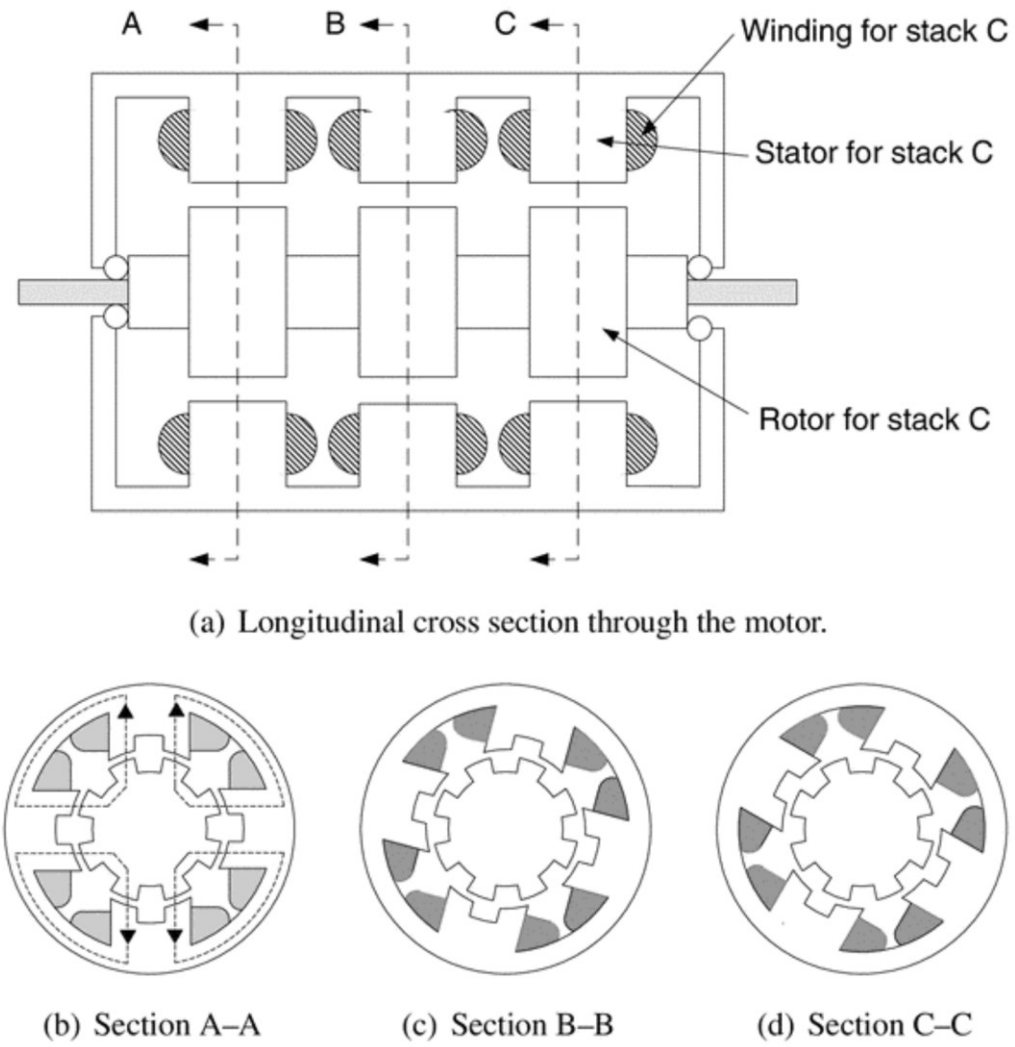

Figure 24. *Section views of a multi-stack variable reluctance stepper motor. Section A-A shows also the magnetic flux propagation through the motor. [19]*

Torque, as well as resolution of the stepper motor can be enhanced by stacking rotor and stator structures. As each stack can be offset from each other, the length of a single step can be divided for $\frac{1}{s}$ steps, where s is the stack count. By utilizing only 2 different alignments, like depicted in Figure 25 below, the additional stacks can be utilized to produce higher torque. [13]

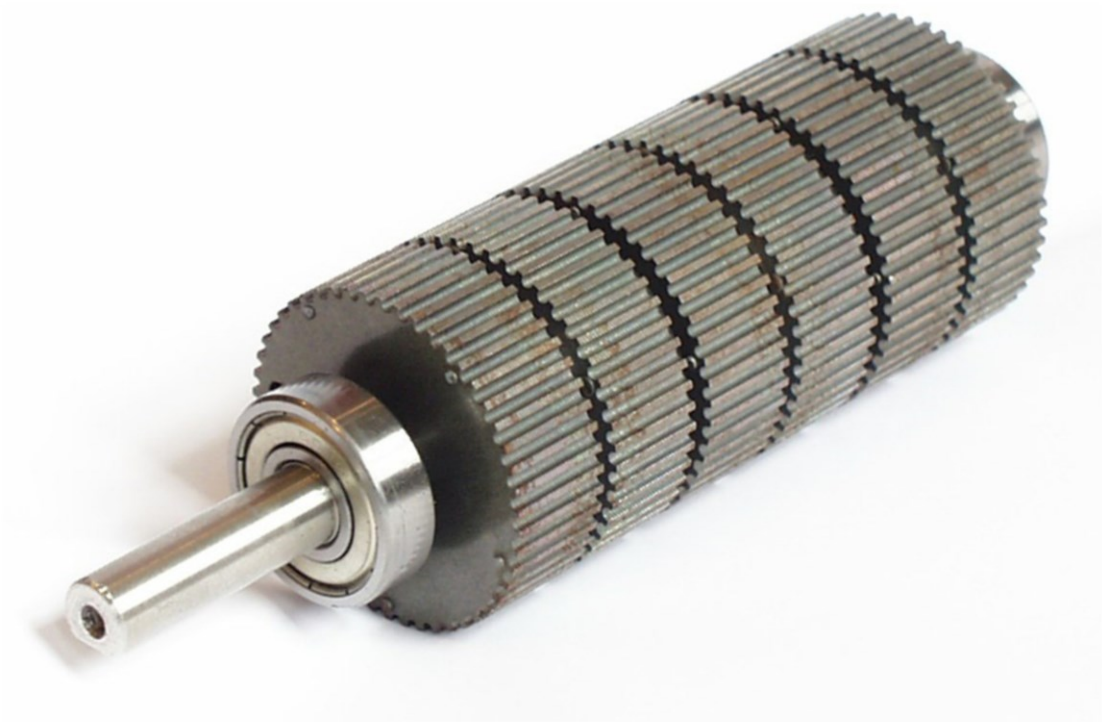

Figure 25. *Stacked rotor structure of a stepper motor. This exact rotor is from a multi-stack hybrid stepper motor but the (toothed) reluctance part of the rotor is based on the same principle as variable reluctance stepper motor. [13]*

There is a considerable characteristic for variable reluctance stepper motor, namely holding torque, while no stator coils are activated, i.e. detent torque. Unlike with other stepper motor types, there is no detent torque, which follows from the fact that no permanet magnets aren't utilized in the motor. [2] [13] [38]

2.2.2 Permanent magnet stepper motors

As the name tells you, permanent magnet stepper motors utilize permanent magnets to produce torque in cooperation with electromagnets. As with other motors, the working principle is based on the attraction of codirectional magnetic fields. In the case of permanent magnet stepper motors, the attraction forces are between permanent magnets in the rotor and (steered) magnetic fields of the stator coils. In the following structure, the magnetic fields are collinear with the rotational axis but the ferromagnetic stator material is chosen to lead the magnetic field towards the radial magnetic fields of the magnets. [19] [36]

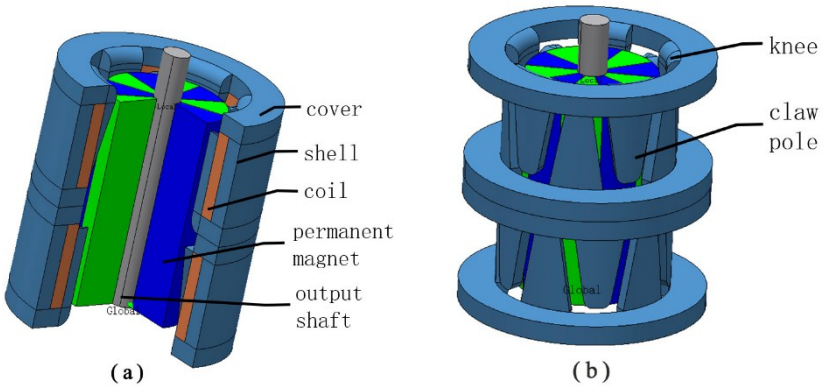

Figure 26. *The structure of a permanent magnet stepper motor. [38]*

The rotation of the stepper motor is controlled by two differently aligned stators as can be noticed from the claw-pole permanent magnet stepper motor in Figure 26. This structure is known also as can stack structure. In order to produce motion, the magnetic poles' polarity is changed on the stator by reversing the direction of the coil's current. The stator poles match the ones on the rotor, so as to lock the rotational slipping between the rotor and the stator. Due to the rotor being ferromagnetic, the permanent magnet stepper exhibits detent torque. An alternative structure of a permanent magnet stepper is introduced later in this thesis. [36] [38] [39]

2.2.3 Hybrid stepper motors

Hybrid stepper motors combine the two aforementioned working principles: permanent magnet stepper motors and variable reluctance stepper motors. The rotor of the hybrid stepper motor is split into three parts: two ferromagnetic parts with equal tooth pattern and a magnetic layer separating them from each other. As the magnet is axially magnetized, making the other part North pole, and the other, South. The ferromagnetic parts are rotated by a single tooth's angle and fixed to each other via the magnet. Rotor, in turn, has a tooth pattern with equal dimensions to the rotor. [36]

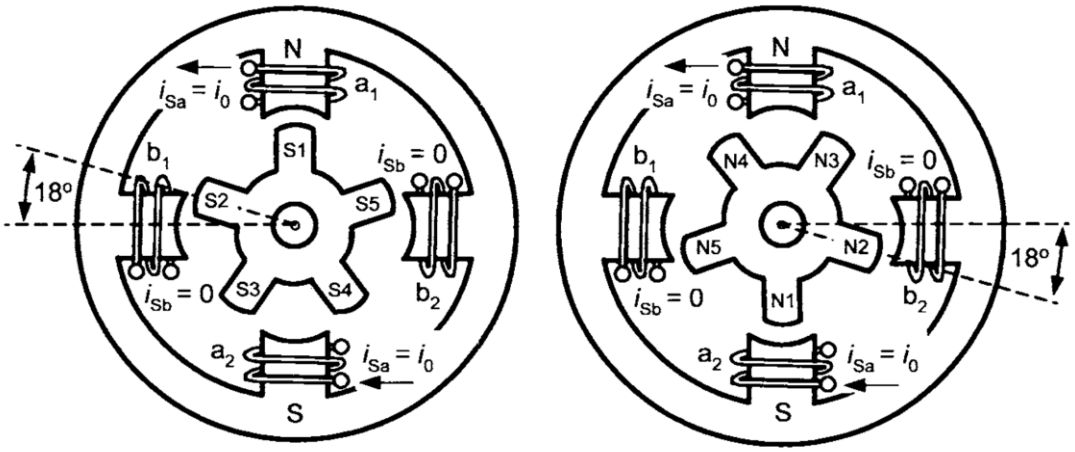

Figure 27. *Section view of the two poles of a hybrid stepper motor. [40]*

Figure 27 presents a simple hybrid stepper motor structure. On the left, there is the south pole stack. On the right, there is the similar section cut of the northern rotor pole. The working principle of hybrid stepper motor is based on these two or more misaligned layers on the rotor, as shown in Figure 25. As depicted in Figure 27 above, when phase a is activated with current i_0 the coil a_1 attracts south pole 1 (S1), the north pole 1 is attracted to the coil a_2. In these positions S5 are is misaligned by 18 degrees from pole b_2 and N5 from b_1 with the same 18 degrees. The same holds true for pairs N2- b_2 and S2- b_1. By powering the phase b ($i_{Sb}=i_0$ or $i_{Sb}=-i_0$), and powering off the phase a ($i_{Sa}=0$), S5 and N5 or S2 and N2 will align with the activated phase, making the rotor rotate. The displacement will be 18 degrees clockwise or counterclockwise in the direction, where opposite polarities on stator and rotor match. [40]

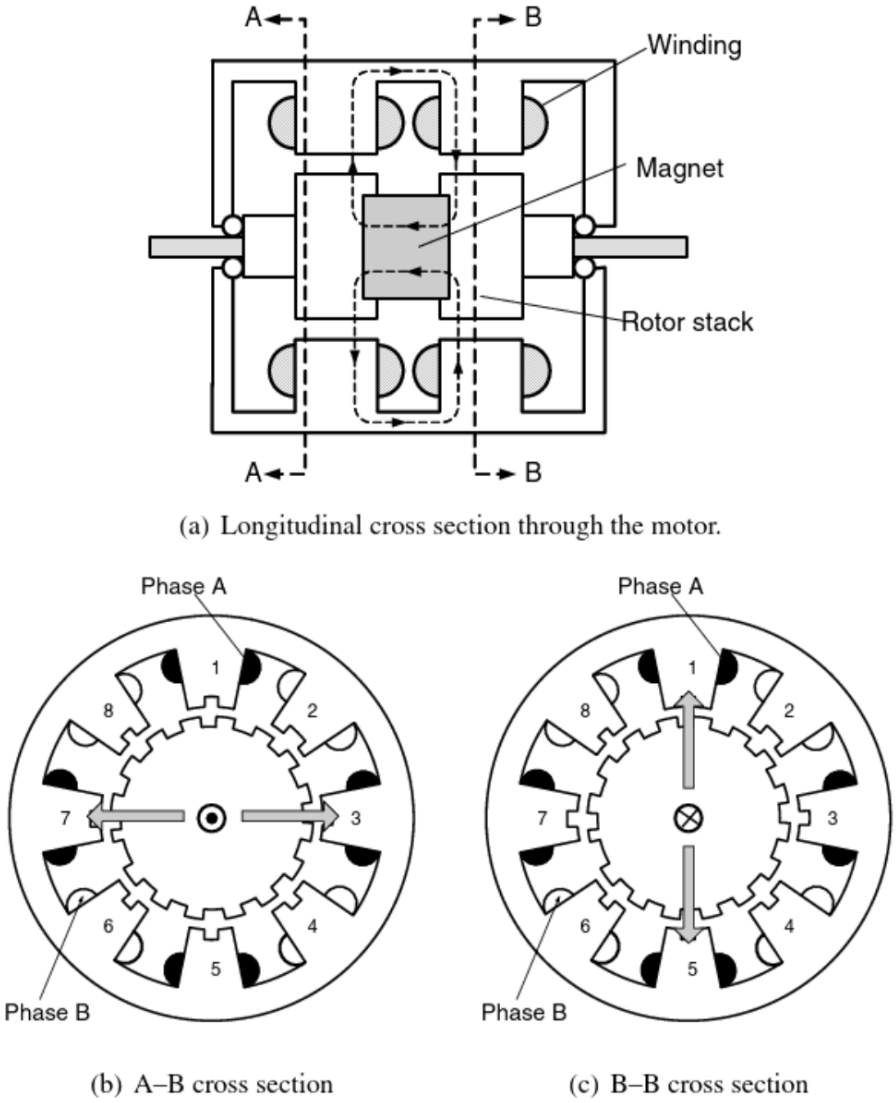

Figure 28. *8-pole 2-phase hybrid stepper motor structure with additional saliency of the rotor and stator poles. Section A shows the propagation of the magnetic field in the direction of the rotational axis, and the sections (b) and (c) show the section view of the different poles of the rotor. [19]*

A widely used structure with 8 stator poles shown in Figure 28, since it's one of the simplest possible patterns to achieve bidirectional rotation. The tooth pattern differs in different phases by the offsets. The most common structure involves two electrical phases, which are indicated black or white in the Figure above. The first two of the coils (1 and 2) are toothed with equal offset and another pair has inverted pattern. (I.e. tooth pattern offset by a single tooth.) These two poles form a single phase, and the other phase is formed of the remaining four coils: The teeth of the third coil pair is offset from the first pair by half a tooth, and the last pair, again, inverts the pattern of the third pair. [36]

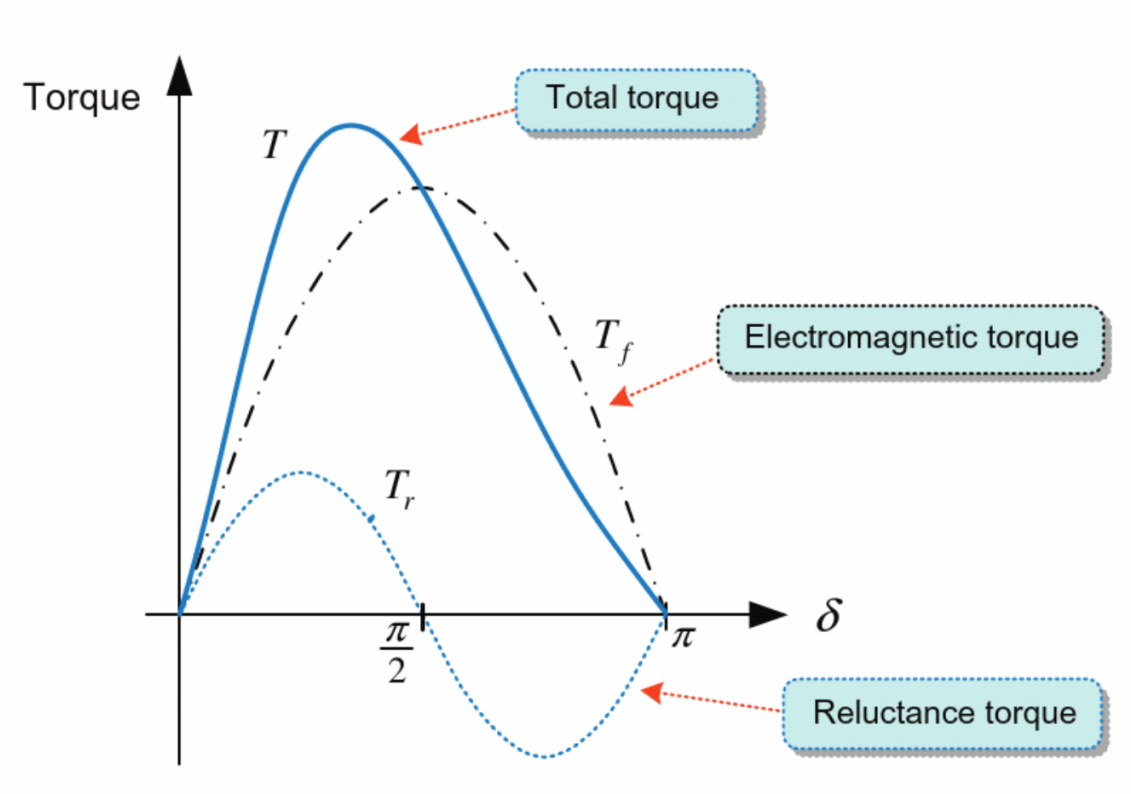

Figure 29. *Total torque formation of a salient pole synchronous motors over rotational angle δ. Hybrid stepper motors are structurally a relative to hybrid stepper motors. [3]*

The torque production of a hybrid stepper motor with both its base components is shown in Figure 29. The permanent magnet in the middle of the rotor produces a magnetic flux, and the magnetic circuit attempts to close via the surrounding stator. If there's no current flow in the coils, the motor will still attempt to stick in a position with the least reluctance path. This is what causes an inherent holding torque, as was the case for permanent magnet steppers in Chapter 2.2.2. [13]

2.2.4 Controlling of a stepper motor

As earlier mentioned, there is a tooth count for the motor, which determines the resolution of a stepper motor positioning. However, if some sacrifices in performance can be made, there is a way of bypassing the limitation of the base resolution, i.e. native steps, namely microstepping. Microstepping splits each step to a portion of the native one: ½, 1/4th, 1/8th , 1/16th of a step and so on, down to 1/256th with modern controllers and can be configured by the user. [41] [42]

The increase in precision, doesn't come without drawbacks, though. The torque production with microstepping is less than with native steps. The amount of torque

achieved in microstepping mode ($T_{\mu s}$) can be evaluated mathematically as follows [37] [43]:

$$T_{\mu s} = T_{fs}\left(sin\left(\frac{90}{\mu s}\right)\right) \quad (17)$$

Where T_{fs} is the torque achieved in full step mode and μs is the amount of full steps per full step. So, if the controller is chosen to use 1/16th of a full step, μs is 16. Unlike gear reduction, microstepping enables the use of the motor's full speed. Using microstepping modes also includes benefits like reduced mechanical wear on the load, and resonance-related problems. [37] [43]

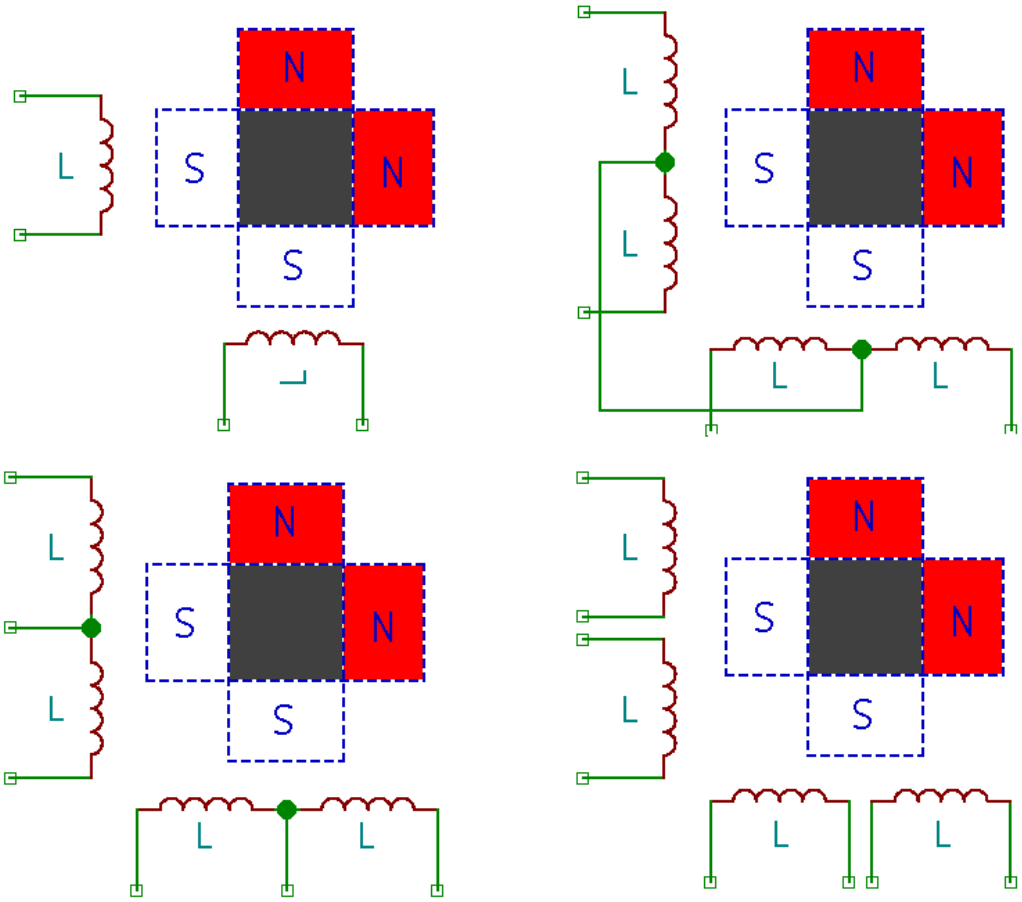

Figure 30. *Different types of electrical interfaces of a stepper motor. The bipolar connection is in the upper left quarter, 5-wire unipolar connection is on the upper right quarter. The lower left quarter shows the 6-wire and the 8-wire interface is on the right.*

The most common electrical configuration for stepper motors is two coils with 4 leads – the bipolar winding, shown in Figure 30 above (upper left quarter). This, however requires more semiconductor switches than the alternatives with 5, 6 or 8 wires, shown

in Figure 30's lower half and upper right quarter, which are called the unipolar configuration. The crucial difference between the configurations comes with the controlling of the stepper motor. The unipolar stepper motor doesn't require as many semiconductor switches as its bipolar correspondent. Configurations like 5-wire and 6-wire ones can be utilized with 4 semiconductor switches, as the center wires are coupled to the common voltage and the other can be switched on and off with a single switch per wire. Configuration with 8 wires also enables more applications since the coils can be connected in parallel. [36]

2.3 Linear electromagnetic motors

In addtition to rotating actuators, there are multiple types of linear actuators as well. They produce linear motion by design, each different type doing it by its own way. Perhaps most commonly known (and used) type of a linear actuator is a solenoid that has been utilized since the early days of mechatronics. As will be found later in this Chapter, some other kinds of linear actuators have been introduced in the recent years, such as permanent magnet linear motors and perhaps the most recent one, shape memory alloy actuators. The last mentioned have been under research for the recent years and are finding their place in the different kinds of actuators. When it comes to small motion, piezoelectic drives have provided an opportunity of producing extremely precise rotary and linear movement.

2.3.1 Solenoids

Perhaps the oldest and simplest type of electromagnetic actuators is a solenoid (plunger) which can be seen in Figure 31. A solenoid consists of soft iron core and a coil that surrounds it, hence, it is a subtype of reluctance machines. A (linear) push-pull solenoid works so that when the coil is activated, the core attempts to position itself into a position that minimizes the reluctance path [16]. When the coil is deactivated, the withdrawal must be induced by another force than that of the reluctance minimization and is often solved by a separate spring. A solenoid usually has two mechanically limited positions, between which it switches, responding the current applied on the coil. [2] [24] [44]

Figure 31. *Photo of a cylindrical solenoid actuator. [24]*

The motion of the armature between the extreme positions is limited by the saturation of the coil, since the maximum force will be achieved in the point where the coil saturates. In many use cases, solenoids are used in the extreme positions like magnetic circuit breakers, car starters and door locks. However, they can also be used in variable positions by adjusting the current, for example in adjustable hydraulic valves. There are also other types of solenoids like rotary solenoids and lever solenoids, the latter of which are utilized in reed switches and relays. [2] [44] [45]

2.3.2 Permanent magnet linear motor

Permanent magnet linear motors (hereafter PMLM) act by the same magnet-activated coil attraction as the brushless DC motor with the difference that they produce linear motion. However, they differ from voice coil motors in a definite way. As opposed to voice coil motors, the linear motion in permanent magnet linear motors is perpendicular to the active magnetic fields. The rotor of the PMLM consists of magnets with alternating directions of magnetic field – such as in the rotor of a brushless DC motor.

There are several benefits of the PMLM: the speed, the accuracy and the force. Compared to piezoelectric, friction-based actuators, the only surfaces that may wear out over time are the ones of the stator and the rotor that are in contact with each other, leaving the functional parts intact. In other words, it may impact the performance of the motor, but it doesn’t necessarily make it unusable. [46]

In many ways, the permanent magnet linear motors assimilate their rotary counterparts. Their torque ripple can be reduced by skewing the magnet structure (like in AC induction motors) and like rotary motors, they can utilize salient armature, having no permanent magnets in the armature itself. Linear hybrid stepper motors are developed as well, and they utilize similar toothed structure and operational principle to rotary hybrid stepper motors. Both cases of hybrid stepper motors aim at the same goal – minimizing the permanent magnet volume needed. [47]

2.4 Piezoelectric actuators

Despite their recent uprising in the market of actuators, ultrasonic motors and piezoelectric actuators are based on an older invention that one might think. The first hints of direct piezoelectricity, surface charges under mechanical stress in some crystals, such as quarz, were found already in 1880. The piezoelectric material, $BaTiO_3$ was found already in the 1940s and during the same decade, the first patent of piezoelectric motor was applied for as well. More common utilization was hindered though, until the further development of materials and manufacturing processes. [48] [49]

Ultrasonic motors (USMs) are based ultimately on the piezoelectric effect. Piezoelectric effect is not inherently in the material but is made in a suitable material by heating the material up to high temperatures and then applying elecrical field on it. Then, after this poling process, applying voltage in the direction of the poling axis, the material either expands or retracts in lower temperature. This phenomenon is called converse piezoelectric phenomenon. Piezoelectric elements also present converse phenomenon, that is the direct piezoelectric phenomenon. Direct piezoelectric phenomenon shows up as a mechanically stressed piezoelectric element produces a charge. [50]

Piezoelectric elements are used in both, linear and rotational motors. They’re also most often driven with AC voltages with frequency over hearable frequencies, hence they’re often called ultrasonic motors. Rotational piezoelectric drives are widely used in camera lenses as autofocus actuators. Many of them are based on a wave-propagation method of rotating piezoelectric ring, and the first time, that technology was presented, was already in 1987 in a camera manufactured by Canon. Piezoelectric actuators are used in form factors, like piezoelectric stacks, stick and slip actuators, inchworms, to name a few linear-motion-producing ones. In addition to the linear motion production, a common type of piezoelectric actuator is the rotary traveling wave motor. [48]

Precision-wise piezoelectric actuators appear to be a favorable choice: In theory, the resolution of an actuator that is made of piezoelectric elements, would be infinite. In

practice, however, there is strong hysteresis and drift in piezoelectric actuators. In addition to that, they are sensitive to disturbances, as they are highly sensitive to voltage applied on them. This means that errors in supplying voltages – such as noise – induce errors in mechanical positioning of the actuator. Thus, the controller of a piezoelectric actuator has to be noise-insensitive and voltage-wise highly precise. [49]

2.4.1 Rotary ultrasonic (piezoelectric) drives

One possible structure of an ultrasonic drive is a wave propagation ultrasonic motor, or in other words, traveling wave motor. Figure 32 shows the structure and operating principle of this motor type. In traveling wave motor, single piezoelectric crystals are connected in series to form a ring. When a voltage is applied, those piezoelectric crystals will form a waved circle, coupling two round, parallel surfaces mechanically. When applying an AC voltage that is of the resonant frequency, the wave on the ring propagates, causing the contact surfaces rotate from each other. [48]

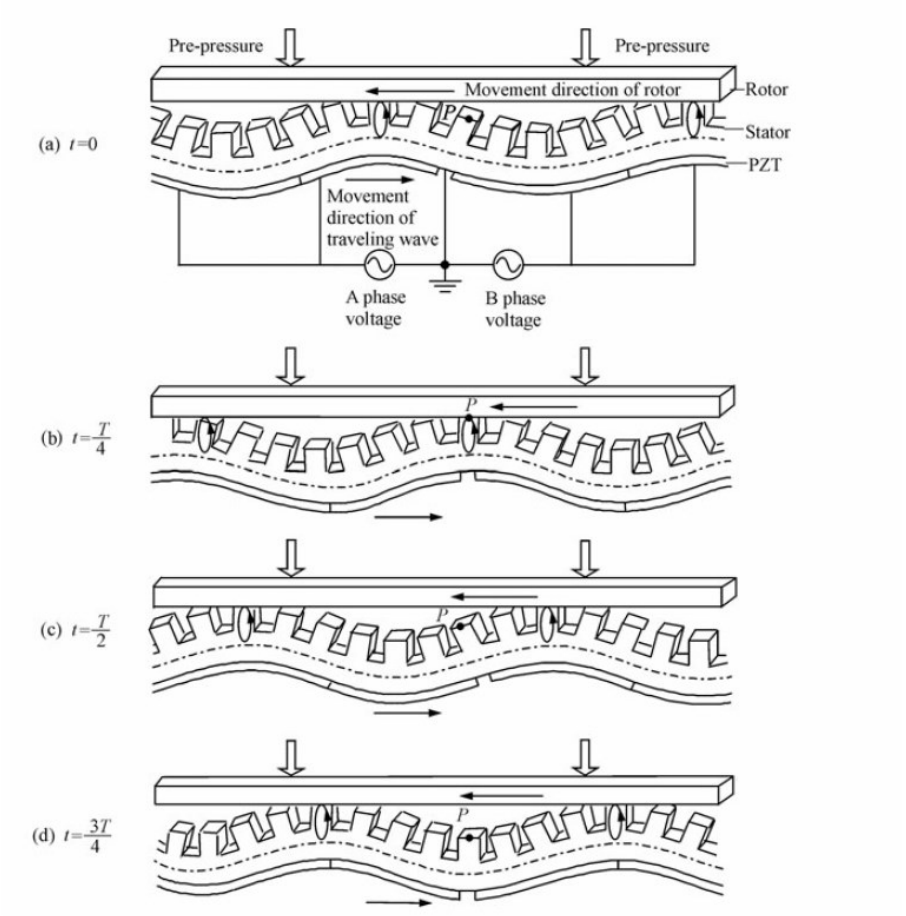

Figure 32. *The structure and operating principle of a traveling wave ultrasonic motor. In section (a) the wave is in its initial position and as the AC voltage is conducted to the different phases, the wave propagates along with the voltage. Phases (b), (c) and (d) show the wave's form over time. [48]*

Why ultrasonic drives are especially lucrative to camera actuators is due to multiple of their caracteristics. They are capable of precise actuation with high torque, even with low speeds. Due to their high torque capability, a common difficulty for elecrical drives is eliminated: gears. As they can produce high torque even with low speeds, they don't need gears to raise the initial torque. In addition to that, they are driven with AC current with frequency most often over the (approximate) hearing range of 20-20 000 Hz. [48]

Unfortunately, in piezoelectric motors there are downsides compared to motors that base their operation on electromagnetics. The movement, especially in the case of a traveling wave motor, is based on friction between the wear surfaces, thus limiting the lifetime. The wear track is worn abrasively along the direction of the rotor's rotation, and wear is affected by the contact materials. The life expectancy as well as the efficiency, reliability and stability of the motor can be affected by the choice of tribomaterials. [48]

Tribology is a science regarding the contact of two surfaces and the phenomena occurring in them, hence the science is also inevitable when discussing the properties of the ultrasonic motors. A part of tribology, which is near to the piezoelectric motors is wear mechanism classification. There are four mechanisms of wear: adhesive wear, abrasive wear, fatigue wear and corrosive wear. Adhesive and abrasive wear mechanisms are quite similar to each other but what differs them from each other is the surface pairs. In adhesive wear, the question is about two smooth surfaces which slide against each other whereas abrasive wear is about a hard and rough surface sliding on a softer one, deforming it. Fatigue wear regards wear during repetitive stress cycles, caused by either sliding or rolling contact between the surfaces. The corrosive wear occurs in a combination of sliding contact surface and environment that is corrosive. [48]

Tribological properties of the ultrasonic motor's tribopair are essential when it comes to the performance of the ultrasonic motor. For example, the elastic modulus of the tribomaterials affects the speed, torque and efficiency of the ultrasonic motor. Hardness, in turn affects the torque of the motor, as well as the friction coefficient. Increasing the frictional coefficient increases torque but it ceases to increase over a certain point. Going beyond the maximum torque only increases the wear of the tribolayer as well as causes increase in noise levels produced by the motor. Some materials' properties are depicted in Figure 33. [48]

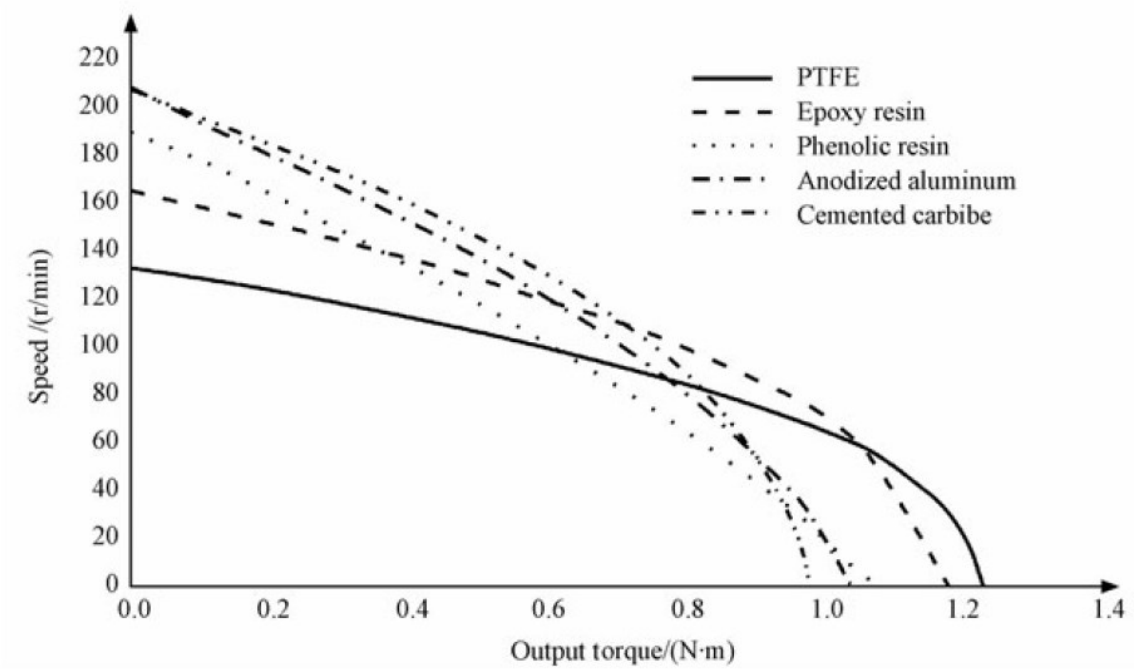

Figure 33. *Five tribomaterials and their effect on speed-torque characteristics of a traveling wave ultrasonic motor. [48]*

Electrically, piezoelectric elements can be seen as predominantly capacitive elements. Control-wise the elements are driven with AC frequency that is above audible frequencies – hence the name ultrasonic motor – which are most commonly in the range of 20 kHz to 100 kHz. Ultrasonic motors' 2 or 4 phases require 90° phase-shifted signals with a voltage of tens to hundreds of volts. With a voltage from the higher end of the range, higher output power is attainable but with a downside of heat output increase. [48]

2.4.2 Piezoelectric stacks

The size of the piezoelectric element is usually of miniature size. To achieve extensions and retractions of usable scale, the piezoelectric elements are most often used as stacks of multiple piezoelectric elements. Even in the case of a piezoelectric stacks, only relatively small strains, meaning the scale of 0.1-0.2 %, can be achieved. The problem can be overcome by using different kinds of amplifiers, such as mechanical levers or hydraulic amplifiers. In addition to the longitudinal expansion of the piezoelectric element, there will always be some lateral expansion, too, so supports may have to be provided. [49]

2.4.3 Piezoelectric inchworms

Piezoelectric inchworms consist of multiple separate piezoelectric actuators. The operating principle of piezoelectric inchworms reminds of the motion of an inchworm. A

visual description of the operation can be seen in Figure 34. In off state, all the actuators are in idle position. The motion phase begins by clamping two actuators, opposing the motion arm, gripping it. After that, the parallel-to-motion-arm actuators are either extended or contracted, depending on which phase of operation is in question. The operation of the piezoelectric inchworm is pictured in Figure 34.

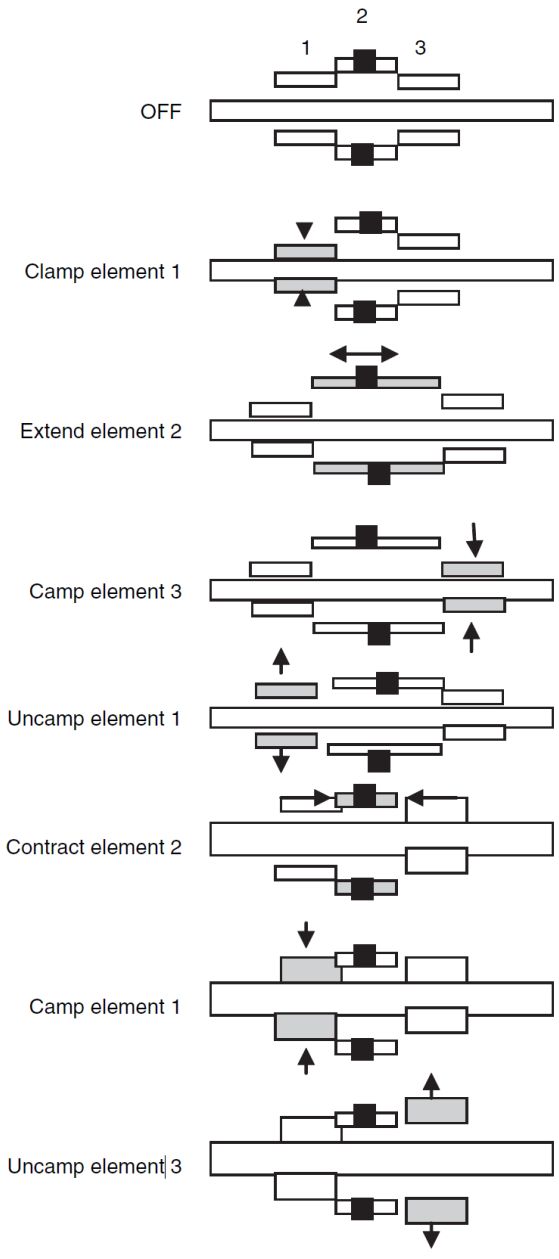

Figure 34. *The operating principle step-by-step of a piezoelectric inchworm actuator. [49]*

While at the altered position, the opposing elements, number 3 in Figure 34, are activated, gripping the motion arm. Then, the actuators labeled with number one can be deattached from motion arm, while the actuator pair #3 remains holding the motion arm

in place. The actuator pair #2 can then be contracted or extended, back to their original position and the element pair #1 can be reattached. Now again, the other gripping pair (#3) can be deattached from motion arm, and the cycle can be repeated in order to achieve a longer travel distance. By contrary steps, the motion can be reversed. [49]

Piezoelectric stick and slip actuators demonstrate a bit similar operating principle compared to the aforementioned piezoecectric inchworm. The difference is that skipping the grip-contraction/extension-grip phase, the stick and slip actuator sticks to the friction surface, and slowly proceeding moves the motion arm. After that it's quickly actuated back to its default position, so fast that the friction between the motion arm and the piezoactuator element is overcome, making the element slip. [49]

2.5 Shape memory alloy actuators

Shape memory alloy (SMA) actuators have their basis on the so-called shape memory effect (SME). Shape memory alloys are metal alloys, which operate between two different phases depending on their temperature. In the low temperature phase, i.e. the martensite phase, the structure of the material is highly crystalline. The higher temperature phase is the austenite phase, in which the material has a more organized, centered cubic structure. An illustration of both structures is introduced in Figure 35. [51]

The crucial part in SMA actuators' operation is that as the state is changed, through a thermal process, the form returns back to the form it was before in the same state. For example, if a (cool) spring of shape memory alloy is loaded, it will extend or retract elastically like an ordinary metal spring. However, if the SMA actuator is heated over the temperature of austenitic formation, while still keeping it under load, it will get back to its original form. When it cools down again, it will revert back to the loaded-spring form. [52]

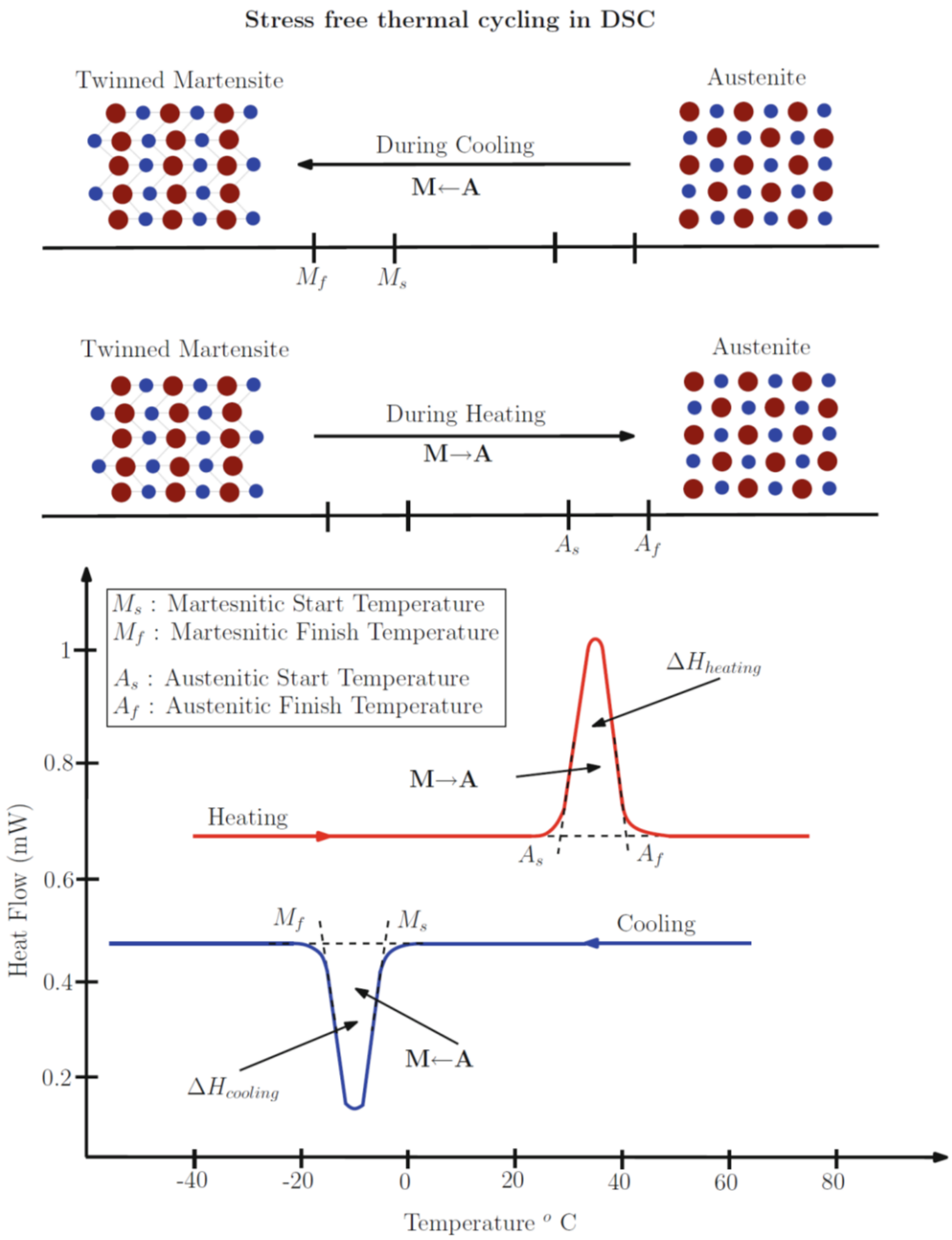

Figure 35. *SMA actuator transform processes. The upmost transition graph describes changes in the internal structure during cooling, the graph below it shows the structural changes in the inverse process and the lowest heat flow graph indicates their relation to each other by temperature. [52]*

Another distinguishing factor when it comes to SMA actuators is that it's been noticed, that they don't wear in the same manner as traditional phase-change materials. Whereas traditional phase-change materials have a definite matrix, where they return in each cycle, SMAs stuctures are refreshed each time as they cycle. Traditional phase-change materials aren't able to return back to the identical structure after each cycle but they receive it each time more imperfectly. SMAs don't present the same behavior, because

they don’t attempt to return to the same identical lattice each time they transform to the definite state. [51]

The inherent feature of thermal state change, however, might present a problem in the mobile device environment. Since the mobile devices have to be designed with the space requirement in mind, it’ s also difficult to provide exceptional heat dissipation at the same time. That in turn, may lead to that the device – as well as the camera module – may heat up to relatively high temperatures. In case that the austensitic temperature is low, it may cause problems with the performance of an antagonistic actuator. Antagonistic actuator configuration is a configuration, where the actuators operate on the same motion arm with but opposite directions. [51] [53]

There is a variety of metal alloys that can be used to manufacture SMA actuators, perhaps the most known of them being Ni-Ti alloy, also known as Nitinol. Some alloys were designed keeping biocompatibility in mind whereas for example copper-based alloys, such as Cu-Zn, were developed with the cheaper price in mind. [51]

2.6 System camera lens technology overview

There is a source that has disassembled some DSLR or mirrorless system camera lenses that are published in the past 10 years. Authored by Roger Cicala, the disassembly reports show more precisely than just the marketing materials, what the lenses and their focusing systems are made of.

A recent publication in the mirorless camera world is the Nikkor Z 24-70 mm f/2.8S lens, which was released in February 2019 [54]. The lens represents the high-end class of mirrorless zoom lenses, with the manufacturer’s suggested retail price, hereafter MSRP, for 2296,85 in US dollars.

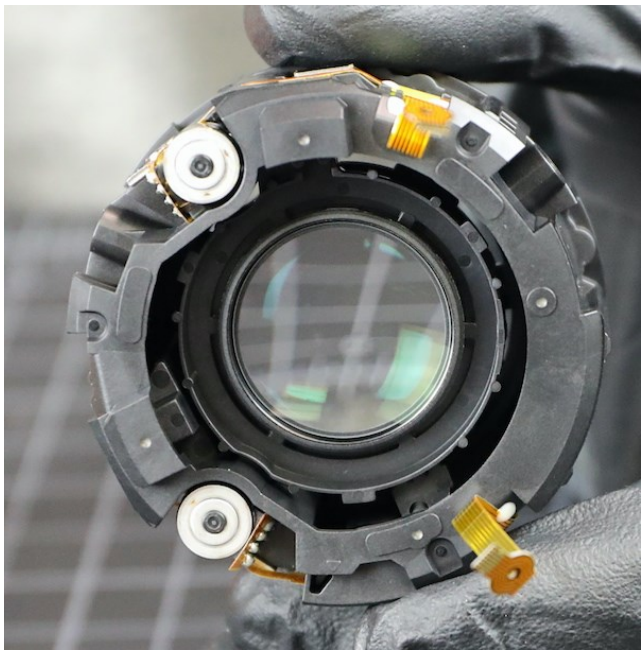

Figure 36. *The autofous lens group of a Nikkor Z 24-80 mm F/2.8 S lens. [55]*

The focusing system is using two rotational stepper motors, which, judging by Figure 36, seem to be from 5 to 10 mm in diameter. The assumption is supported by the 4-wire interface soldered to the ribbon cable that can also be distinguished from Figure 37 below. [55]

Figure 37. *Side view of the autofocus lens group of the Nikkor Z 24-70 mm 2.8 S lens. [55]*

From the side view of the lens in Figure 37, the stepper motor looks pretty much like a small-size rotational stepper motor. There is a metal cover on the output shaft side, so it can't be said, what actually is underneath, but a possible solution could be similar to the one presented in the aforementioned Samyang's solution of (supposed) linear screw.

Another rather recently published lens is a Canon RF 50 mm f/1.2. As the name tells, it's a fixed focal length lens, with the MSRP of 2299,00 $. As the price tag might hint you as well, it's one of the professional lenses for Canon's mirrorless cameras. [56] [57]

Figure 38. *Side view of the Canon RF 50 mm 1.2L. From the partially disassembled lens you can see the toothed ring of the ultrasonic autofocus motor. [57]*

From Figure 38 can be said that the autofocus motor is a travelling wave ultrasonic piezomotor of type. It's claimed that the same motor is used with the Canon EF 400 mm, presented in Figure 39, and the motor indeed looks very similar to the AF motor of that 50 mm lens in Figure 38. Also, another motor can be seen in Figure 39, which is the stepper motor above the white barrel, next to the distance indicator ring of the autofocus. [57] [58]

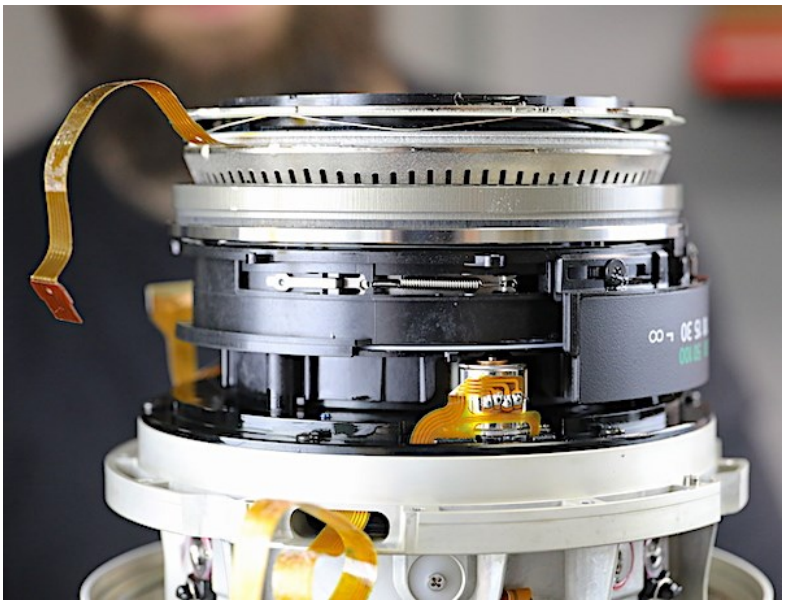

Figure 39. *Canon 400mm f/2.8L IS III disassembled. The ultrasonic autofocus motor with its loading spring is the topmost part of the parts shown. [58]*

An older lens, the Sony FE 70-200 mm f/2.8 GM, is Sony's first approach to the widely popular from 70 mm to 200 mm reaching zoom lens. What makes this lens interesting, that it has two focusing lens groups instead of just one, and uses both a linear and an ultrasonic motor. [59]

Figure 40. *Autofocus lens group actuated by linear motor in its extreme positions on a Sony 70-200 mm F/2.8 GM lens. [59]*

Figure 40 shows the lens group actuated by the linear actuator on a Sony 70-200 mm F/2.8 GM lens. The actuator itself is not distinguishable by this image and there is no explicit hint of its type, so it has to be declared unkown. Figure 41 below shows the ultrasonic motor of the same lens.

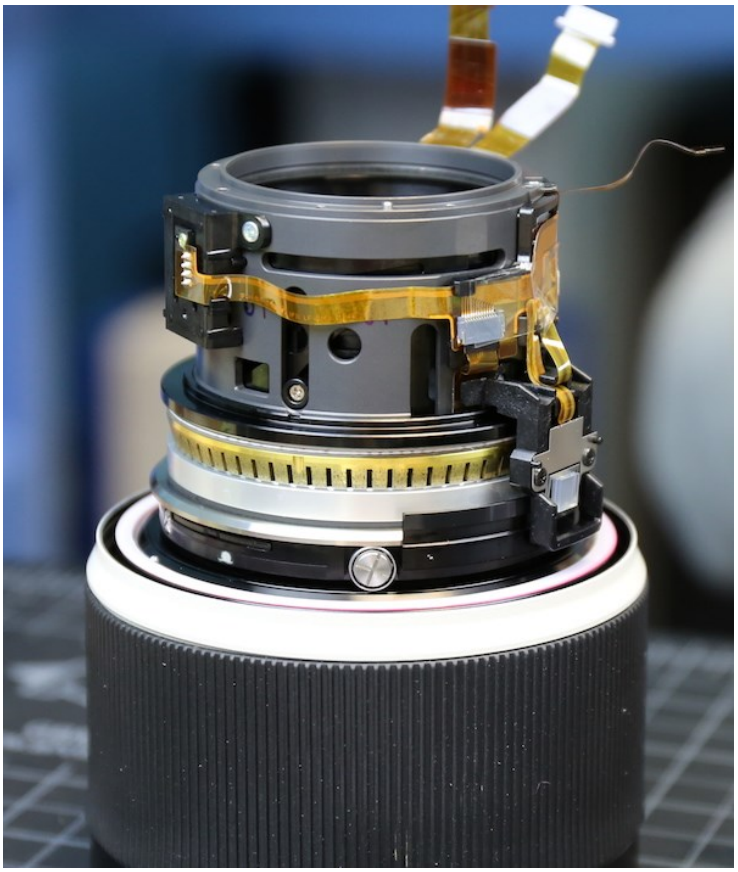

Figure 41. *The ultrasonic motor of the autofocus motors in Sony 70-200 mm GM lens. [60]*

So, what is the reason, why ring-type USMs are common? And why are the lenses' AF systems driven by small diameter stepper motors (with gears) and why is the stepper motor not a hollow-core one? If a hollow motor is designed based on the 20mm thick NEMA (National Electrical Manufacturers Association) compliant 17 hybrid stepper motor, is it realistic to expect torque close to the 100 mNm of a non-hollowed-rotor one? [33] [61]

Table 2. *Characteristics of different types of electromagnetic and ultrasonic motors. [48]*

Motor classification	Manufac-turers	Stall torque /(N•m)	Rotary speed without load /(r/min)	Weight /g	Torque density /(N•cm/g)	Maximum efficiency /%
EM, DC, Brush	Micro Mo	0.003 32	13 500	11	0.030 2	71
EM, DC, Brush	Maxon	0.012 7	5 200	38	0.033 4	70
EM, DC, Brush	Mabuchi	0.015 3	14 500	36	0.042 5	53
EM, DC, Brush	Aeroflex	0.009 88	4 000	256	0.003 86	20
EM, Alternating voltage /current, Three phases	Astro	0.075 5	11 500	340	0.022 2	20
USM, Standing wave, Longitudinal-torsional type	Kumada	1.334	120	150	0.889	80
USM, Traveling wave type, ∅60	Shinsei	1.0	150	260	0.385	35
USM, Traveling wave type, ∅60	PDLab	1.2	180	250	0.522	30

From the Table 2 above can be seen that the torque density is higher in ultrasonic motors when compared to its electromagnetic counterpart. Considering that for relatively small rotational movement between autofocus steps, the speed of the ultrasonic motor shouldn’t be too much a limiting factor for use in mechanical designs in optics modules. Depending on the mechanical design, the low speed may be even beneficial for the design, since the rotation doesn’t have to be slowed down by using gears, which in turn might induce acoustic issues.

3. DESIGN OF A HOLLOW STEPPER MOTOR

This Chapter and the following ones describe the development and prototype manufacturing parts of the Thesis in detail. The development process started by setting up the targets, was followed by choosing the technology for the task and then the work continued on by making a 3D-model of the design. With the assistance of the model, the design was simulated and prototype model was developed further with the obtained information, ending up in a real-scale prototype for camera applications.

3.1 Requirements

As for every design process, the design had set boundaries in which the motor should be able to perform. The features and specifications are listed in Table 3 below. In addition to the ones presented in the Table below, there were some other not that specifically determined. Perhaps the most important target of this work was to eliminate the noise coming from the gears that often were required to produce sufficient torque with the commercially available motors. Another very important factor was to keep the power consumption at bay, considering that mobile handsets are battery-powered and battery lifetime is a definite point of competition. A challenge that for example travelling wave piezomotors exhibit is the lifetime limitations because the operation is based on the frictional surfaces. Hence, this motor was to be designed minimizing the parts that would wear out.

Table 3. *Hollow stepper motor's specifications and their development over time.*

	Initial requirement	Re-evaluated	Final target
Minimum torque (mNm)	50	20	10
Diameter (mm)	25	26	26
Height (mm)	6	6	6
Middle hole diameter (mm)	18	18	18

Initially, the target torque was set to 50 mNm and the dimensions were determined by auxiliary equipment and size constraints (first revision, Chapter 4). As the motor's design proceeded and further knowledge was acquired about the mechanism to be driven, the targets were re-adjusted (from second to third revision, Chapters 5 and 6). As the prototype mechanism was developed concurrently, the torque target could eventually be set to 10 mNm (for the fourth revision, Chapter 7).

3.2 Concept analysis

The design goal was to create a hollow motor with as high torque capabilities as possible but with a mobile device compatible dimensions and precision. The steps-per-revolution target was that of a commonly used stepper motors, i.e. 200 steps per revolution. The exact demands weren't declared but the main goal for the design was to produce a motor that would not only be able to actuate a pop-up camera system but also drive the autofocus of the camera. To obtain sufficiently high speed for the pop-up mechanism, the motor would need high torque, but there's also need for precise actuation in order to minimize the complexity of the autofocus mechanics. For this project, 50 mNm was considered as the torque target.

The initial idea was to design a combined type of an actuator so that they could be used separately for separate purposes. The fast – and precision-wise undemanding – task for the motor was the popup phase. Here, however, fast rotation would be needed for satisfactory performance of the pop up. There is one type of an actuator that matched the charasteristics of the meaning particularly well: a BLDC. It's still difficult to achieve the needed precision for the autofocus movement, though. Since the mechanics use the rotation for both purposes, the precise motion has to be produced by some other way, or mechanics have to be more complex.

The decision was to combine the BLDC with some other actuator that would produce superior precision compared to the BLDC. Since there already was an electromagnetic system, it led towards the direction of another electromagnetic actuator. Because there was an intention to reduce mechanics-induced noise as well as minimize the mechanical losses, a non-mechanical-contact-driven actuator was preferred, closing piezoelectric actuator out. Adding the mobile devices' general demand for high efficiency and low power consumption, plus the permanent magnets, a combination of brushless DC and a hybrid stepper motor was considered worth further investigation.

Looking upon the other options available, there were other motor technologies that would be capable of filling the requirements of the motor sufficiently. However, they remained by some way inferior to the choice taken. A brushed DC motor would've been especially interesting of an option from the efficiency point of view according to what was studied by T. Verstraten et al. As was noticed in the study, a DC motor can be driven with high efficiencies even at low speeds using a gearbox. [27] Another point making the DC motor a feasible option, was the convertability to stepper motor by means of a gearbox as experimented by D. Venkantarao et al [26]. However, taking the wear of the carbon brushes and especially the electrical noise produced by the commutation (addressed in

Chapter 2.1.4), this would be no option. Adding the requirement of gears to the mechanism would also have been too heavy a compromise.

For the destined purposes, the variable reluctance stepper motor would've been mass-production-wise a really compelling option, since there's no need for magnetizing parts like with the other counterparts: hybrid and permanent magnet ones. However, bearing in mind that the device we're drafting the design for, is battery powered, and there is a requirement for consuming as little power as possible. Here, as earlier noticed, hybrid stepper motor and permanent magnet motors having the inherent holding torque, stand out as an optimal direction of development.

The next phase was to consider, how it would be possible to combine the chosen two different types of motors, minimizing excess parts, due to the fact that in mobile phones it's vital to minimize the size of the mechanical structures. First solution draft combined two motor types: a BLDC and a hybrid stepper motor. However, the solution was deemed unnecessarily complex when it comes to manufacturing and creating a prototype with satisfactory performance on both types of motors. A BLDC alone would not suffice precision-wise, leaving the stepper motor as the only option. It was found out that a widely available 20 mm thick NEMA 17 hybrid stepper motor was relatively close to the dimensions demanded of this design, so its performance was further researched. According to specifications, the torque produced by the motor is 100 mNm, which would be sufficient for the design. It was assumed that the new design's torque would be less than the reference but even in the case of reaching only 50 per cent of that, the torque would be sufficient. Because the maximum torque would be used only for short bursts (the pop-up phase), the 1 A current required by the 20mm thick NEMA 17 stepper would be allowable. [61]

As the rotor may rotate freely without a load, the detent torque moves the rotor to a position minimizing the reluctance of the magnetic circuit, i.e. so that the closest rotor teeth – stator teeth pair will match, as was concluded in Chapters 2.1.3, 2.2.1 and in the context of hybrid stepper motors' Chapter 2.2.3. Whether the phenomenon helps optimizing the power consumption with these mechanics, it is yet mere speculation and varies also by microstepping mode, power supply etc. The reason for that is that there are multiple mechanical contacts in the pop-up system, which in turn prevent the motor from rotating freely. Whether the cogging torque would overcome those forces, depends on the strength of the rotor's magnet and the misalignment tooth size as well as the position of the teeth.

3.3 Magnetic materials

Designing magnetic devices requires knowledge of magnetic materials. There are some few elements that are useful in handling magnetic fields, which are ferromagnetic materials. Iron (Fe), cobalt (Co), nickel (Ni) and gadolinium (Gd) are the elements, which are utilized in magnetic materials. Most of them are of *3d* or *4f* materials, with regard to electron structures. There are also so-called soft magnetic materials, such as steels (Fe) used with silicon (Si), iron as an alloy with Ni or Co, Zn combined with Mn or Ni and some metallic glasses, whose magnetic properties are linear as opposed to the hysteretic B-H relation of the hard magnetic materials. Linear magnetic materials' properties can be described by relative permeability (μ_r) in a certain range of internal magnetic field: [14] [28]

$$\boldsymbol{B} = \mu_0 \mu_r \boldsymbol{H} \tag{18}$$

Where $\boldsymbol{B}$ is the flux density of the internal magnetic field and $\boldsymbol{H}$ is the auxiliary magnetic field strength. Nonlinear magnetic materials' magnetic properties are described by a $B - H$ curve presented in Figure 42 below. [14]

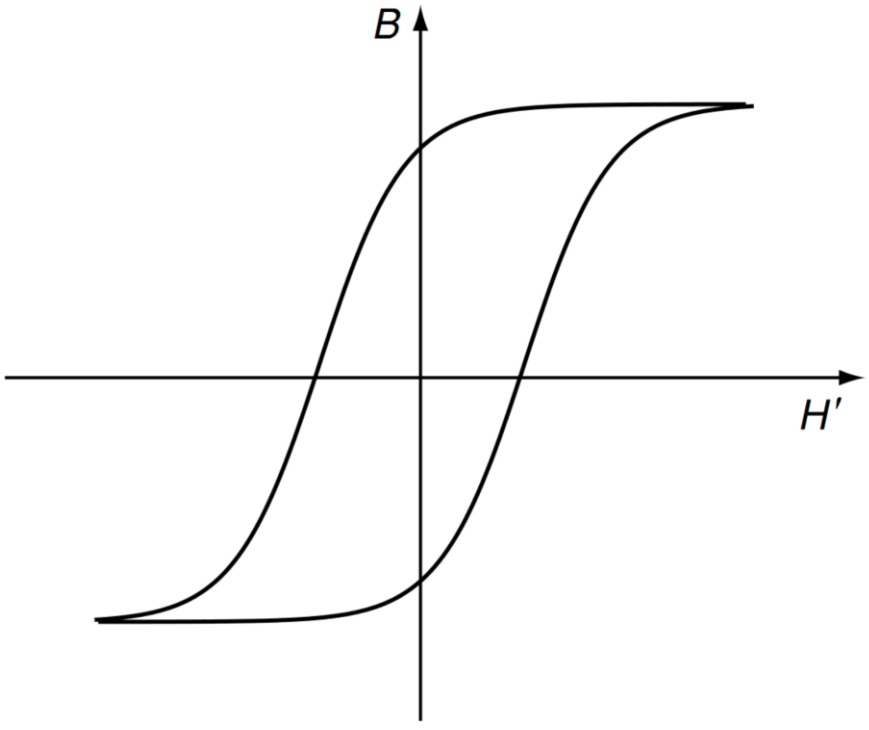

Figure 42. *The B-H curve of a magnetic material. [14]*

The strength of the magnetic field of a magnet array can be enhanced by arranging the magnets into a Halbach array. In a linear Halbach array with the width of a single magnet, each magnet turns 90 degrees compared to the previous one. The magnets, whose field

is collinear with the rail, strengthen the magnetic poles on either of the perpendicular sides as shown in Figure 43. On this side of the array, the magnetic field strengthens but on the other side it weakens. The array can be utilized in permanent magnet stepper motors, but often the other side of the non-Halbach array can often be used for another set of coils. [47]

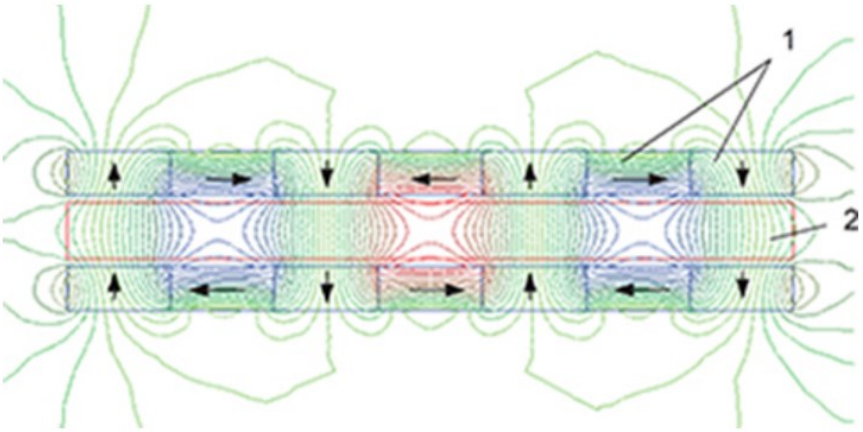

Figure 43. *Two Halbach-arrays. Magnetization direction of the magnets is presented with arrows and magnetic field curves are indicated. Denser lines indicate denser field. [47]*

As can be seen from Figure 43, rather than propagating through a magnet uniformly and returning back to the magnet from the reverse side, the magnetic field bends to form a dense circuit between the opposing layers. As the magnetic flux is more focused into the gap between arrays, the magnetic flux density is significantly reduced on the outside. [47]

3.4 CAD modelling of the hybrid stepper

As the form of a 20 mm thick NEMA 17 stepper motor was already quite similar to the intended design it was mimicked with some differences. First, in a mobile-device sized device, it would be a waste of space to keep the body as thick as it is in the aforementioned hybrid stepper. The aluminum shells could be opted out, since the movement of the rotor can be limited down to rotational movement with the mechanics where the motor is attached to. The caps, where bearing is attached to, is made of aluminum, and the relative permittivity of aluminum is 1.0002 whereas for iron $\mu_r \approx 10^3 - 10^4$. [14] [28] Hence, replacing the cap material with some other non-ferromagnetic material, is possible. [61]

First, the 20 mm NEMA 17 hybrid stepper was attempted to be hollowed and shrunk down to match the design target as well as possible. However, turned out that it wasn't worth the effort to modify the available hybrid stepper into a motor with hollow rotor at

that size with the available tools. This is why the design process eventually lead into designing a completely new motor and ordering parts from a manufacturer capable of doing parts of that scale.

Simultaneously with simulations, some variations of CAD (computer assisted design) designs were developed. Due to schedules, the design of the real prototype was fast tracked and prepared while still doing simulations of the performance. 4 different designs were made, varying shell thickness, diameter of the whole motor, tooth thickness and width as well as the radial thickness of the coil. Since in the simulations done earlier with the single-piece rotor, it was noticed that the magnetic flux in the rotor was saturated. Each of them had different dimensions when it comes to rotor and stator design. Two of the motors were designed with tooth count of 50. The other two were with bigger tooth size, which in this case meant 33 tooths per revolution. One of both, 33-tooth and 50-tooth motor designs are shown in Figure 44.

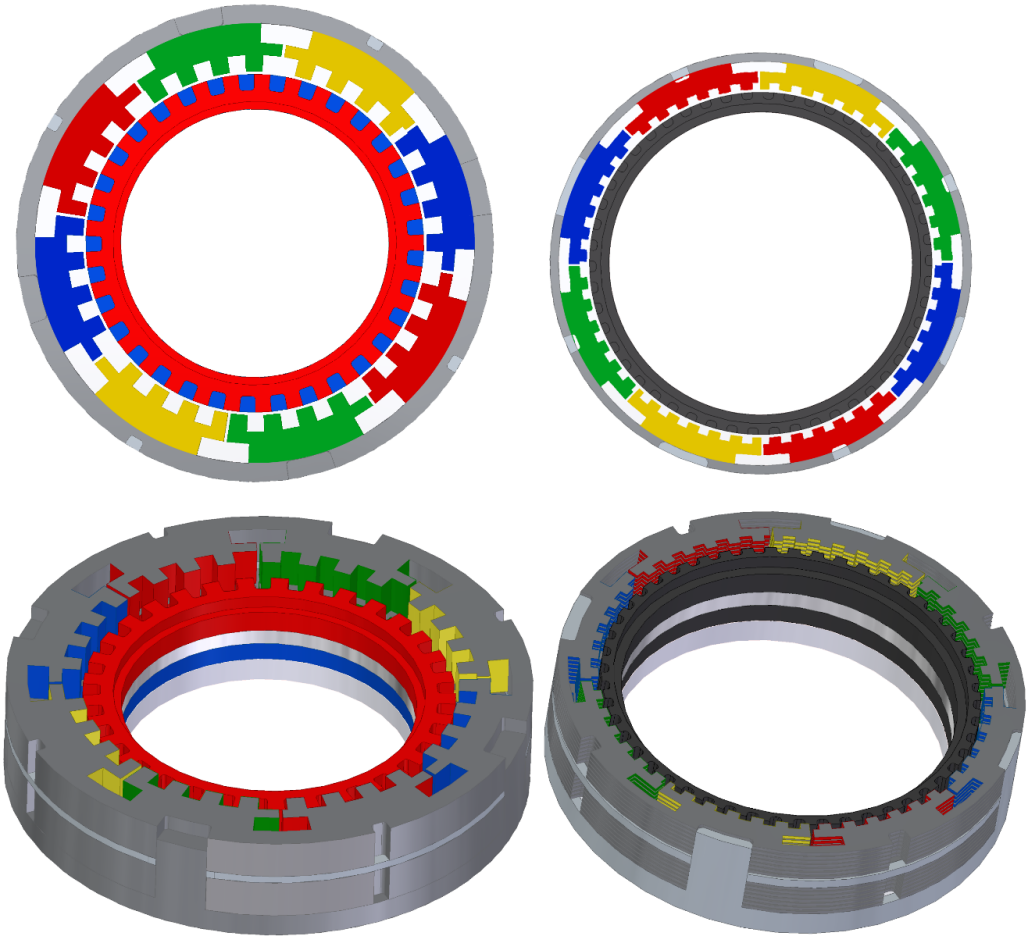

Figure 44. *The 33-tooth design of the hybrid stepper motor (on the upper left quarter) and the 50-tooth design (on the upper right quarter). 3D-versions of the structure are shown below respective images. The rotor of the 33-tooth design and the poles of both designs are coloured to emphasize the different alignment of teeth and the polarity of the rotor's magnetization. These colours do not describe the material properties in any way and the images are not in scale.*

The structure used is similar to the 20 mm thick NEMA 17 hybrid stepper, where red poles of Figure 44 has teeth matched to the **top** layer fo the rotor. Another pair of coils, namely blue, has teeth which are set off by one tooth compared to the aforementioned coil pair. In other words, they are aligned with the other half of the rotor. These two pairs (like red pair and blue pair) of coils form a single phase of the stepper motor. Two other coil pairs (yellow and green) duplicate this pattern, with the difference that each tooth is set off by a half tooth compared to the first 4 coils mentioned. When the rotor turns, the teeth of the coils (single color) are aligned one at a time. Thus, tooth count of 50 translates into 200 steps per revolution, which in turn means 0.9 degrees per native step of the stepper, and the 33-tooth version has 132 steps per revolution, meaning rotational angle of approximately 2.73° per step.

3.5 Simulations of the first revision

The performance of the rotor was evaluated along the design process in COMSOL Multiphysics 5.6.0.401 and 6.0.0.405. COMSOL is a multipurpose simulation software that's capable of FEM-based (finite element method) simulation [62] [63]. In this design task, magnetic fields and torques induced by magnetic fields were simulated.

First, the functioning of the basic principle was confirmed by simulating the torque produced by a two simultaneously activated coils. In this phase, no real-world coil windings or currents were used. Instead, somewhat sensible values (such as maximum allowable intermittent current) were used in order to evaluate the potential of the working principle. In order to perform the simulations in sensible time, only part of the motor was simulated in the early phases of the design process, meaning a motion through a single full step in the confirmed results. In order to make the process as fast as possible, some single point simulations in the maximum torque situation, i.e. half tooth misalignment, were used.

In first simulations, only a single coil was used but using another was significant getting valid results. This also represented a complete motor better: in a commercial hybrid stepper motor, the coils are connected magnetically by the soft iron rotor. The simulation of only two coils doesn't describe the exact performance of the motor but was sufficient measure for further development of the design and verification of the concept as it showed the function of a single magnetic circuit.

200 steps per revolution was the initial intended step count. However, because higher torques were a goal, the requirement for step count was reduced to 100 native steps in order to make the parts more manufacturable. In addition to better manufacturability, the

motor was intended to be used in half-stepping or some other microstepping mode in order to produce the demanded precision. Many of the commercial stepper drivers nowadays support microstepping in the aforementioned range. [42] [42] [64]

It was noticed that the hollowed 20 mm NEMA 17 stepper motor, has severely diminished torque compared to the unmodified version. For other kinds of motors as well, such as AC induction motors, the motor's rotor is not a single solid piece but a layered structure. This is a solution to minimize eddy current losses inside the rotor but didn't explain the low torque results. This was also concluded by splitting the stator structure and using air as a medium between the layers. The gap was simulated as air, because the relative permeability of air is relatively similar to most common plastic materials, as really few of them are ferromagnetic [65]. Commonly used materials for the rotor layers are 0.3 mm to 0.5 mm thick steel, silicon steel or soft iron, while some nickel alloys can be used as well. [3] [25] Eventually, it was concluded that making a hole to the rotor decreased the torque.

4. FIRST REVISION: HYBRID STEPPER

3D-models and simulations were done aiming at a design that would be custom made to the needs of the mobile phone camera module and maximum allowable dimensions. The structure was included into patent application PCT/EP2022/061667, available in public approximately July 2023. The plan was to manufacture the metallic parts of the motor and perform assembly and the necessary coating for stator lamination by oneself. However, there were changes in the plans, which affected the schedule so much that there was no chance to get the parts in time for this thesis work. The plan had to be adjusted to the schedule, and the idea was to prove that this design could be manufactured within reasonable performance gap from the requirement.

The alternative for the real prototype parts and assembly was to get back to the originally abandoned plan of modifying a 20 mm NEMA 17 motor. A reason for reattempting to modify the 20 mm NEMA 17 was that considering coil windings, it would've been possible to make the motor with smaller diameter of wire and thus make the magnetic field produced stronger than that of the original design. That would yield in higher torque as can be concluded from Equation 3 in Chapter 2.12.1.4 .

Simulations showed, that the solid rotor of the motor would provide more torque than the hollow one. If sufficient torque could be achieved with that motor with a modified hollow shaft, it would be enough to point out, that it is feasible to go on the development of the current motor, and take it to a motor manufacturer for further optimization. If a reasonable torque with the original stator could be received, it would also be possible to rewind the coils with a thinner diameter wire. In order to see, whether the motor can perform inside the small volume of a mobile without overheating itself or heating up surroundings too much, the motor was planned to be measured with a thermal camera.

Several rounds of simulations were done with different variations on the rotor. However, most of them resulted in torques less than 1 mNm, which was way less than the target, since an 8mm stepper motor with proper gears would be capable of producing over 50 mNm. Compared to the 100 mNm of the 20 mm NEMA 17 stepper, the result was also only under 1% from the torque with a motor approximately the same size. There was an attempt to enhance the torque with thicker shell of the rotor, since the thinner shell sizes presented saturation of the material, which for soft iron is around 2.1 T in the used soft iron model of Comsol, as can also be noticed from Appendices 5-8.

Thickening the shell and coils did not make the desired change in the performance of the motor, so the rotor was the next component to be looked upon. It was noticed that there is a distinguisthable drop in the torque produced, when there was a hole of *any* size in the rotor. That wasn't quite expected, considering that the radial field strength is greatest in the proximity of the motor's teeth. There was no difference noticed in varying the rotor (radial) thickness, so the explanation was searched in the hollowness of the rotor. The simulations were performed with the filled rotor, and with different hole sizes. The simulated diameter sizes were 10mm and 1mm, to see, whether there's a dependency on the area of the magnet.

5. SECOND REVISION: PM STEPPER

As the first attempts with the hybrid stepper motor were performed, deeming the torque production insufficient, alternative solutions were considered. Around the same times, more precise information about the torque needed, was acquired. By these results, it was estimated that 15 mNm would be sufficient to drive the mechanics the motor is designed for, so the requirement was lowered to that value.

Because there was a considerable dependency between the hybrid stepper magnet area, and the torque of the motor, permanent magnet motor was considered a solution for the problem. The performance of a permanent magnet stepper motor shouldn't be similarly affected by the hollowness of the rotor, as the magnetic flux density is dependent on the magnetization. Permanent magnet steppers tend to produce more torque than their hybrid counterparts [36]. Another supporting factor for using permanent magnet rotor was that other miniature steppers are using the same structure all the way from 28BYJ-48 geared stepper motor [66], (which is familiar for probably every electronics hobbyist) to a minuscule 6 mm diameter stepper motor manufactured by Minebea. [67]

Reflecting upon the Minebea's 6 mm stepper motors, increasing the torque from 0.23 mNm to 50 mNm in the size of an 25 mm diameter hollow stepper was considered a possibility at least. Hence, the structure was simulated in order to get a better grasp on the torque production capability of the motor. The magnet pole amount of the rotor was set to 36, since that would be somewhat close to the amount desired. 200 steps per revolution could be adjusted in the upcoming revisions or, again, reached with microstepping. The preliminary torque tests showed that the torque surpassed easily the prior hybrid stepper motor design, almost reaching the target of 50 mNm with only 0.5 A current. This case being simulated with only 25 turns per coil, it seems that permanent magnet stepper motor will be the more feasible option to continue developing on.

As can be seen in the Appendix 7, the peak torque for the motor with both phases activated seems to be in the range of 30 to 50 mNm. The possible causes for the fluctuation may be the slightly insufficient density of the simulation network in some minor surfaces on the motor shown in Figure 45 below. For further development, changes were made. There was a rather large cylindrical surface facing towards the magnets in each of the rotor pieces that would face both magnetic poles simultaneously – leaving a low reluctance path for the magnetic circuit to cut short. This shorctut wouldn't be beneficial

for torque production, so it was to be eliminated. In order to restrict the non-torque-inducing magnetic field propagation, the proximity of teeth in the rotor were cut out, leaving the teeth only, inmost part of the rotor. As the gaps also left empty space, the teeth were extended to fill it, enlarging the tooth area facing the rotor.

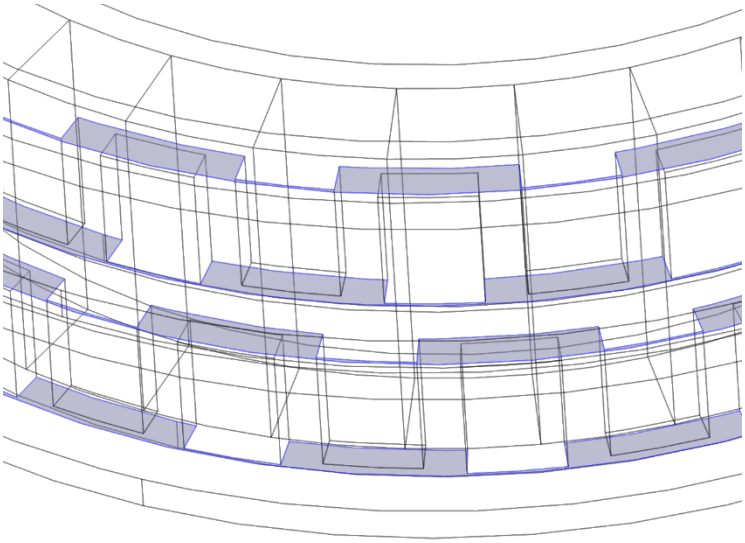

Figure 45. *Thin regions of the PM stepper motor.*

That, however, constraints the options of bearing. In this design, using a bearing in the middle of the rotor, locking the along-axis movement becomes difficult, since there's no more cylindrical surface against the rotor. This is why there has to be either two flanges with cylindrical bearing surface, one on each side of the motor, or a single flange on one side, and some other kind of mechanical restraint on the other. Since the rotor's magnetic field is facing the stator, it might also be possible to design a bearing structure on the stator itself, so that when assembled, the rotor is supported. Direct contacts of the size of a magnetic pole would also beneficial considering that the smaller the air gap, the less there is reluctance on the path of the magnetic circuit. Hence, the forces between the rotor and the stator should be bigger yielding in higher torques as can be concluded by Equation 1.

The first results weren't enough to prove the functioning, though. The simulations were performed without addressing the issue of slightly insufficiently dense simulation network, which induced errors to the simulation. The inherent holding torque was simulated, too, by disabling both of the coils. With the denser network, the simulations took considerably longer time, so the displacement steps were reduced to 1.25°/step in order to get to know the vital points of the torque curve. As the rotor had 36 poles, translating into 10° per pole, the size of a single step forward is half of that, i.e. 5°. The zero point was set to where magnets were aligned with either of the stators and

displacement sweep was performed towards both directions. This way, the peaks of the curve seen in Appendix 1 as well as full step zeros. Some things that were seen as improving the design, were also done at this point. The teeth were elongated to sink into the base plate of the opposing pole with an air gap of 0.2mm to maximize the pole area towards the rotor. The resulted geometry is shown below in Figure 46 and slightly further modified structure is presented in magnetic field simulation Figure 59 and Figure 60 in Appendix 3.

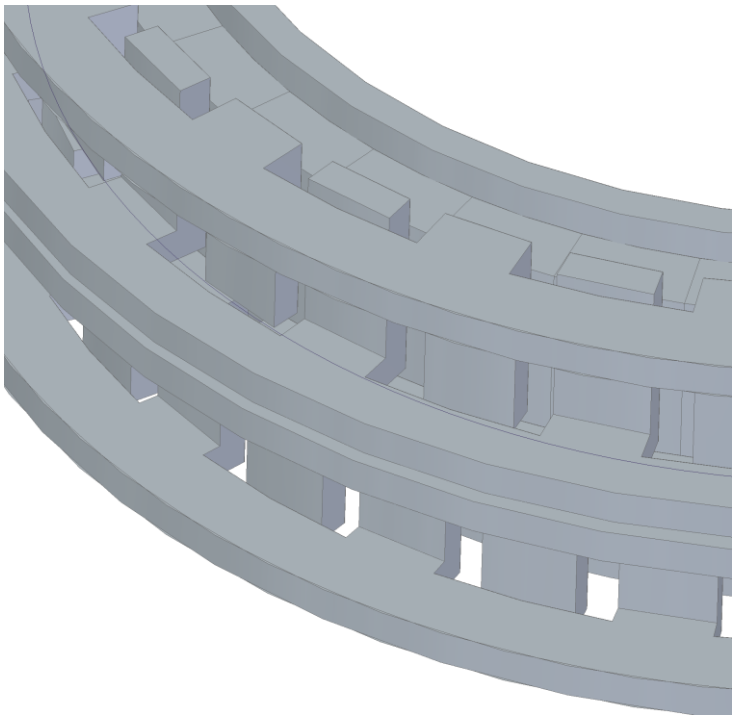

Figure 46. *The modified structure of the permanent magnet stepper motor.*

From Appendix 2 can be seen that the torque towards either of the assemblies are practically the same independent of the holding torque. Thus, the torque is actually caused by the magnet's attraction towards the stator structure, not the combined effect of the magnetic field of the permanent magnets and the magnetic field of the stator.

There were a couple of factors, which were seen as a solution for this. First one is decreasing stator tooth size. By narrowing down the teeth, the flux would be more focused on the side adjacent to the rotor. It would also provide a bigger air gap between the teeth of different poles, increasing the reluctance of the path between the poles. There would be less magnetic flux leakage between the stator poles, thus yielding higher torque production. Another factor to prevent the magnetic flux leakage between the stator irons is to make the air gap between the stator base plate and teeth bigger.

The last ways to improve torque production would've been increasing the current of the coil, wire turns per coil or both. This, however, was considered least lucrative an option,

since the aim was to consume as little space as possible and keep the power consumption at a reasonable measure considering battery-powered use. Yet, as the aim of the simulations of the motor was to prove the functioning of the design, increasing turns per coil by simply changing the parameter in the simulation was found the best step forward. The examination provided results as presented in Appendix 3.

Looking at the results of the aforementioned sweep in Appendix 3, it can be noticed that there are some inconsistencies. When comparing the upper blue torque curve, (towards the rotor magnet,) the corresponding torque with the coil inactivated (red curve) a difference of 10 mNm can be seen in the curve. With the black curve, the stator part with the other coil activated, the result is very similar compared to the one with two coils activated. In this position, the other phase of the stator is aligned with the teeth of the rotor, making no torque at all (magnetic fields' directions on the rotor and stator match).

From the other point of view, the torque to the stator assembly, (torque to coil assembly, green curve) the torque is around 6 mNm with a single coil activated. The corresponding result without coil activation is the cyan curve, showing marginal difference to the aforementioned. However, with the other coil activated (yellow curve), the torque goes some millinewtonmeters higher in torque. Yet, in both situations, the torque induced by activating the coil doesn't exceed the inherent holding torque (i0 = 0 A and i1 = 0 A).

6. THIRD REVISION: OUTRUNNER MOTOR

Considering the schedule of the project, and the required verification by simulations before the prototype could be manufactured by a third party, there was a demand for something that could provide for something measurable with a geometry that could be modelled and simulated. There was a couple of identical brushless DC motors available, and by rewinding their stators according to Figure 47, it could be used as a half of a stepper motor stator. As can be seen from Figure 47, the motors to be modified were outrunner BLDCs introduced in Chapter 2.1.5 in Figure 19. Misaligning them by half tooth, and combining them would yield in a stator structure that could be easily manufactured as well as made a simulation model of.

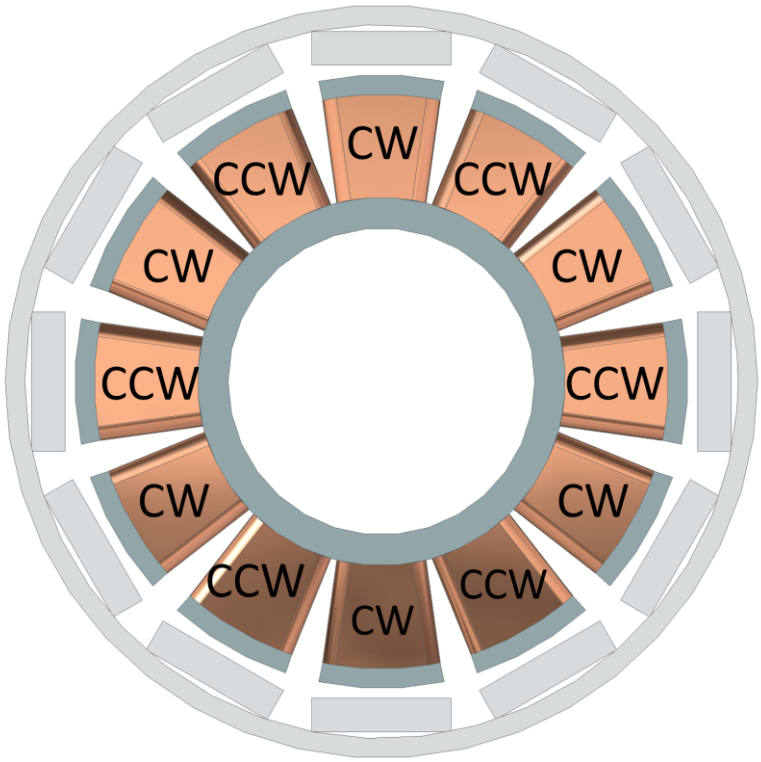

Figure 47. *BLDC stator structure with modified coil winding and magnets. CW indicates coil that has been wound in clockwise direction (from outer radius perspective). CCW, in turn, indicates coil that has been wound counterclockwise from the same perspective. As opposed to the original structure, the pole count is equal for permanent magnets and electromagnetic poles.*

The BLDC motors used for the modification had 12 electromagnetic poles (on the stator) but 14 magnetic poles (on the rotor), so the magnets were stripped off and 12 of them rearranged in the same polarity-alternating pattern as the stator. Dimension-wise, this motor wasn't that far away from the desired size, either. Its outmost dimension was 27 mm. However, the thickness (in the rotational axis' direction) for the functional parts

(without the bearing), was about 12 mm, which would be simply beyond compromise for an integration on a handset. The overall structure of the motor with its bearings and an external wheel for rotation speed measurement is shown in Figure 48.

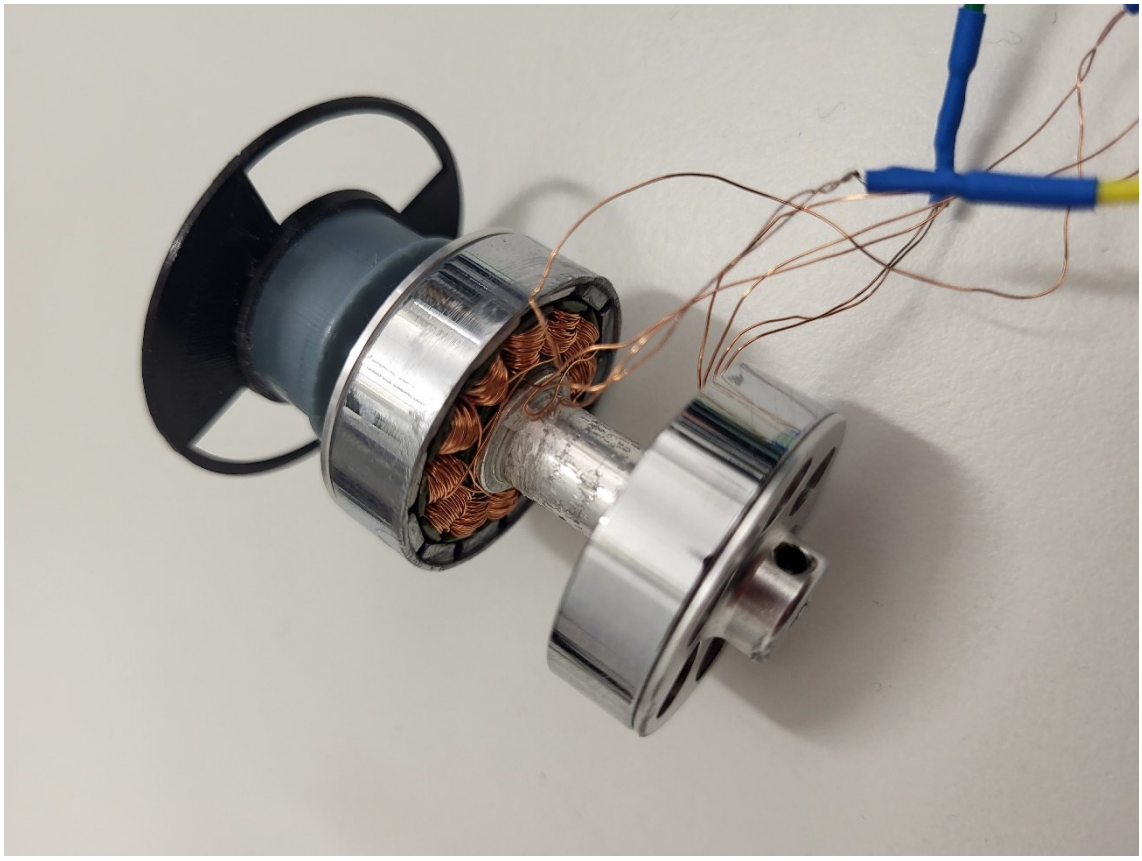

Figure 48. *The stepper motor modified out of two BLDC motors. The two stator parts were connected to each other with the aluminum pipe of the original BLDCs and the original power shaft was replaced. As the rotors were attached to the shaft, they were misaligned by one tooth. The black encoder wheel was attached to the motor to measure rotational speed during the torque measurement process.*

The bearing was left out from the simulation geometry, and the magnets were combined so that the rotor didn't have 24 separate poles but 12. This assembly, in total, was as thick as the rotor and stator halves altogether. The simulation model with the aforementioned changes to the structure is shown in the following Figure 49.

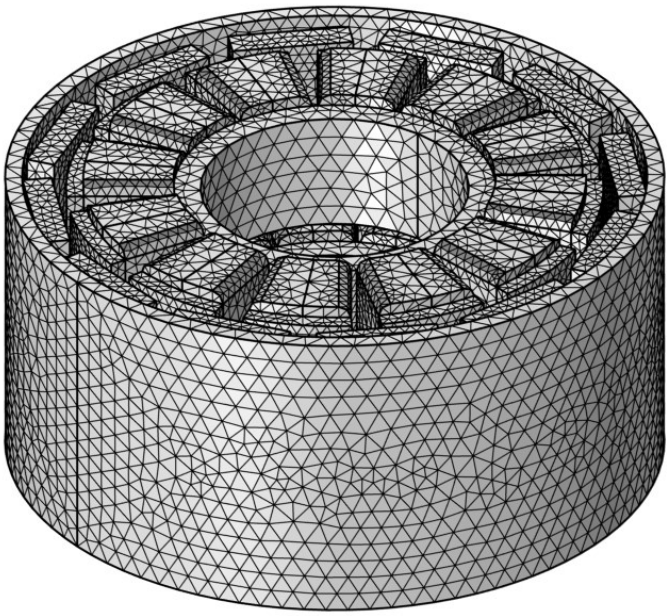

Figure 49. *Meshed simulation geometry of the stepper motor prototype modified out of two BLDCs.*

To simplify the simulations, the number of activated coils was decreased to a single coil, and the same displacement sweep was used for the rotor displacement. In this model, the starting point is, where the activated coil is between two magnets. As there are 12 poles, the displacement of a single tooth is 30 degrees in total, hence the sweep ranged from -15 degrees to 15 degrees of displacement.

Eventually, to match the simulation results with the physical prototype measurement, a simulation with all coils enabled was made. Despite taking longer time, the simulation presented a result that is explainable by examining the magnetic fields. The torque curve shows also a quite similar form compared to the curves in the measurements. The results are presented in the Appendix 7, in total 4 torque peaks can be noticed: Starting from -15 degrees' displacement, -35 mNm peak downwards at approximately 12 degrees, the next one up at around -4 degrees, then down again at 4 degrees, and finally upwards peak at around 12 degrees.

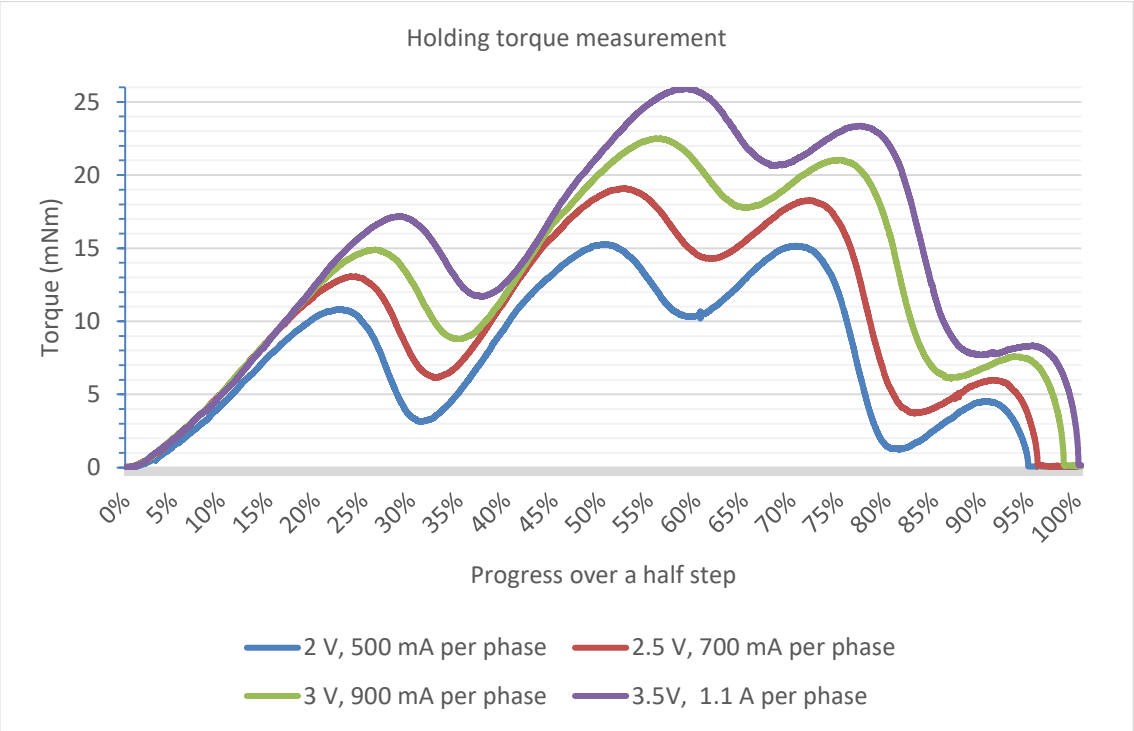

Figure 50. *Holding torque measurement of the BLDC-based modified stepper motor. Based on measurement data acquired by Nico Koski.*

From Figure 50 we can see a waveform that assimilates the torque curve in Appendix 7. The peak of the highest curve in the simulated torque curve in Appendix 7 is around 55 mNm, meaning that in reality only around 34 % of the simulated torque was reached, comparing the results for same phase current. Even with the higher current, the simulated result cannot be reached as the prototype produced only 47 % of the higher torque of 1,1 A with higher current. Possible causes for that are misalignments of the motor assembly shown in Figure 51 and friction of the bearing parts.

7. FOURTH REVISION: DOWNSCALING

As the torque curve forms approximately matched, a prototype in proper dimensions was made. The whole motor was manufactured with suitable materials, most importantly the shell and stator being structural steel. The other parts were made of non-ferromagnetic metals and magnets were commercially available rectangular block magnets made of NdFeB with a grade of N52. A patent of the structure has been applied with application number PCT/EP2022/079642 and will be public on approximately on February 2024.

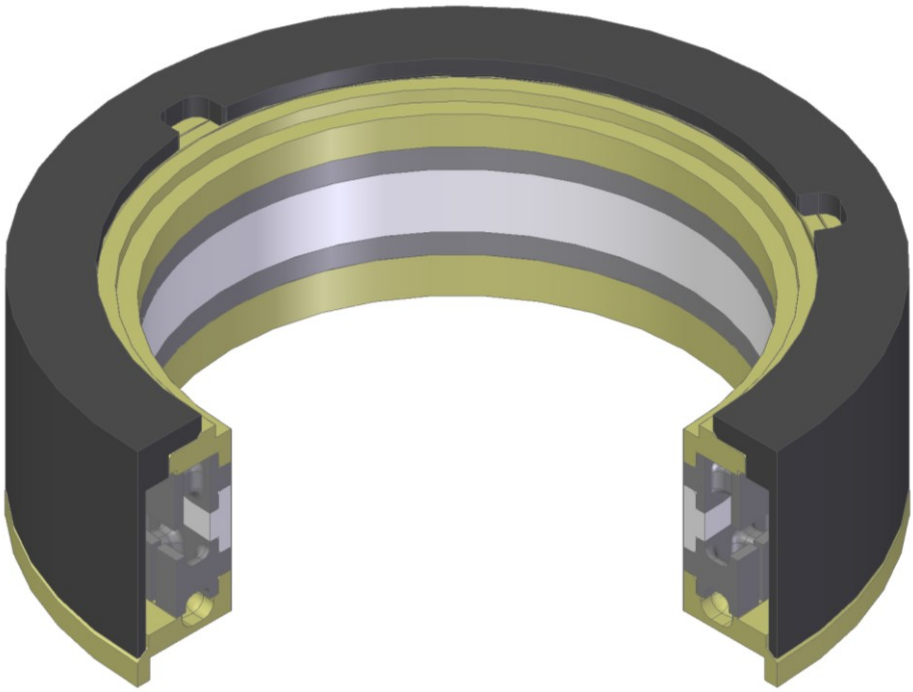

Figure 51. *Section view of the final motor structure without coils and magnets.*

As the motor was assembled for the first time, it was noticed that there is high rotational resistance in approximately a rotation of one tooth step. At first, it was deemed that it was due to magnetic torque induced by variable reluctance of the path between magnets and stators: the loop that circulates from the magnet to the ferrite part, propagating to adjacent poles and then back to the corresponding magnets and through the shell back to the magnet. The first attempt to run the motor failed, as the mechanical resistance was way too high. 0,1mm coil wire was used with 20 revolutions per pole. With further examination with a single magnet-coil pair, it was noticed that the coil wouldn't lift a magnet off a single pole with the desired current. Considering that, it was reasoned that it would be improbable that the motor would spin even if there wasn't that much mechanical resistance.

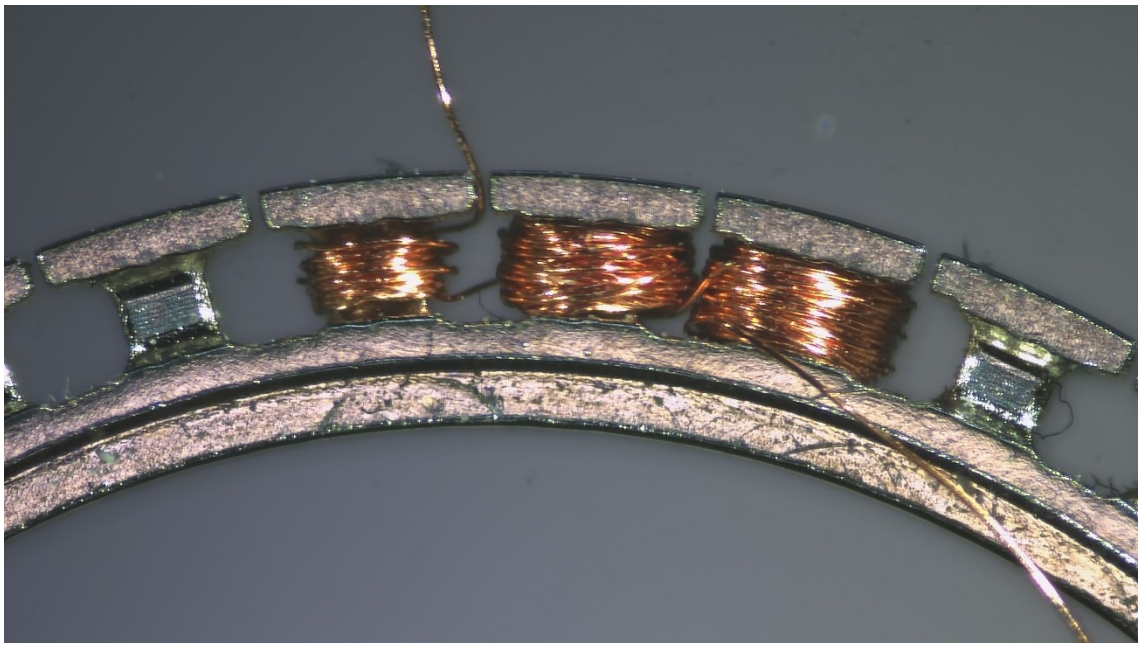

Figure 52. *An in-progress winding of a stator with the manufactured steel parts.*

Simultaneously, there was also a problem with the windings with the metallic parts: the gaps between the magnetic poles were so thin, the enamel coating stripped off really easily while winding. Figure 52 shows a winding in progress with 50 µm copper wire, and as can be seen, there isn't much extraneous space between the coils. The enamel stripping lead to shortcuts between coils, through the stator body, leaving multiple coils inactivated and making sufficient torque production simply impossible. As a first attempt to fix the problem, the gaps were widened by sanding them lightly. A rewinding of the part showed, that it had no significant effect. So as to prevent enamel coating from stripping off from the coil wire, a smaller diameter wire was used as a last resort in hand manufacturing. This either didn't make a difference, since for the wound stator, the measured impedances varied heavily, (in the extent of several ohms to tens of ohms,) reducing possible torque production. In this phase, though the more significant a factor was the mechanical jamming, so it remains a mystery, whether torque production would've been sufficient with smaller diameter wire.

In the same trial, pastic coil body was compared with the already manufactured iron one, shown in Figure 53. As it was possible to hold a single magnet's weight with a single activated plastic-cored coil, a plastic version of the stator body was made with a 3D printer for trial purposes. Since the 3D printing process required a couple of iterations and test fittings, it was also noticed, that the air gap between the magnets and stator's coil bodies varied quite much. There was a collision between magnets and stator, causing the step-like resistance when rotating the rotor by hand. To prevent further

delays on the project, an assembly with plastic stator parts was made, even if equal performance wouldn't be guaranteed.

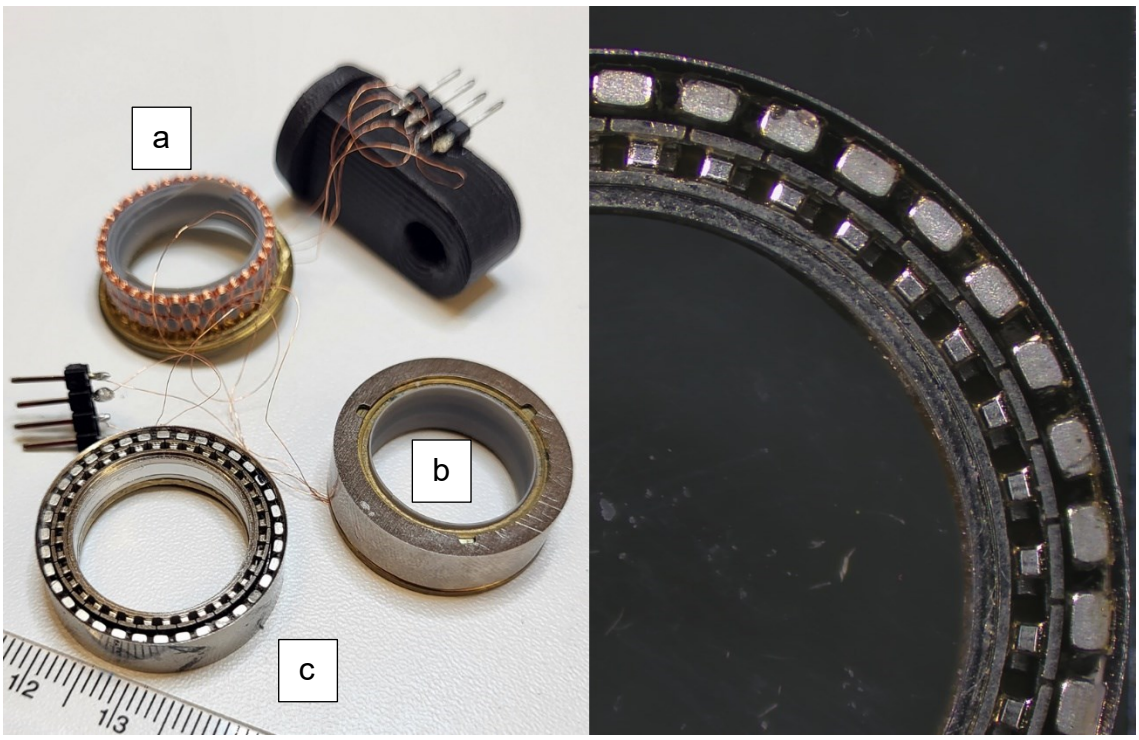

Figure 53. *Assembled motor with plastic stators (a and b on the left half).* A microscope image of the structure with steel stators (c) is shown on the right half.

With the single-coil–single-magnet test that was made for the iron stator part, too, it was noticed that greater force could be achieved with a wire of smaller diameter and increased revolution count while keeping the volume of the coil approximately equal. The limiting factor was heat dissipation: the less revolutions and the greater the diameter of the wire, the more current it would require to produce equal force with a magnet-coil pair, see Chapter 2.1, Equation 3. The plastic (Phrozen TR300) used wasn't a good thermal conductor, (despite specific thermal conductivity not provided by the manufacturer, nor measured in the scope of this thesis) meaning that the heat would build up faster inside the coils compared to the iron parts. [68]

As usual for prototyping, several iterations of the wound stator were made with the goal of maximum turns per coil and as good mechanical fit as possible. The structure was kept the same but some roundings and dimensional adjustments were made in order to get the parts fit and to reach greatest possible torque. A couple of attempts were successful. The main problems were with the shrinkage of parts printed with resin printer along with the mechanical properties of the parts printed with different resins. Some of the wound phases also showed significantly lower resistances than their counterparts, so in some cases, there probably were shortcuts via the other metallic parts. The exact

reason remains unclear because visual inspections didn't show any damage on the coils and the motor couldn't be inspected visually after assembly. There were also some difficulties with the stator colliding with the magnets.

Eventually, a build with no mechanical collisions and quite similar impedances between the phases was manufactured. Some changes were made to help proper assembly and avoid damage to the coils, including some extraneous support structures to be removed after assembly. The phases of the motor consisted of 122.4 Ohms resistance with 264 µH inductance and 155.46 Ohms with 322 µH inductance. These results were measured with B&K Precision LCR Meter 880 [69]. Each phase included 36 coils, each of which had 70 rounds of wire (probably deviating a few rounds for some coils due to human error). First test runs were performed with a stepper driver ST's STSPIN220 using full step mode and with 6.5 V voltage, which resulted in approx 80 mA current consumption from the supply. At this voltage, the current produced slightly more voltage than what was needed to make the motor spin: the motor could not spin with 5.5 V supply. Results of around 0.5 mNm were achieved until the motor was driven with a high enough voltage to melt the insulation of the coil wire, making the motor stall and break down.

Since the attempt to run higher currents through the 0.05 mm wire was unsuccesful, the next revision of the stator structure was printed with slightly modified dimensions to make assembly easier and enable winding with a larger diameter wire. The wire was chosen to be 0.1 mm, as it was available at the moment of assembly. With the larger diameter wire, the resistance was decreased, increasing the current carrying capability of the windings without overheating. With the larger diameter wire the motor was tested, providing the results shown in Table 4 below.

Table 4. *Results of the torque measurement. Based on data acquired by Nico Koski.*

Voltage	**4V**		**5V**		**6V**	
PPS	**Pull-out (mNm)**	**Pull-in (mNm)**	**Pull-out (mNm)**	**Pull-in (mNm)**	**Pull-out (mNm)**	**Pull-in (mNm)**
50	0.595	0.242	0.826	0.437	0.907	0.581
75	0.554	0.308	0.639	0.289	Not acquired	Not acquired
100	0.556	0	0.637	0.251	Not acquired	Not acquired

The motor wound with 0.1 mm wire had 20 revolutions a coil and it was succesfully tested to revolve with no load with the voltage of 4 volts. As it was tested, the voltage was raised to 5 V and 6 V, with results remaining around 0.6 mNm, peaking up to 0.8 mNm. Reflecting upon the target set to drive the mechanics, the increase was still far from sufficient. As the revolutions per coil were decreased, so decreased the torque

production, as can also be judged by Equation 3. Even though the current could be increased, and its effect on torque production is quadratic as could be seen in Equation 6 in Chapter 2.1.3, it could not increase the total torque production sufficiently to clearly surpass the prior version with 0.05 mm wire coils.

Another cause for deficient torque is the changes that had to be made in the test setup to make the measurement more precise. To enhance the precision of the torque measurement setup, the diameter had to be shrunk. The reason for this was that measurement setup the different motors were measured with was prony brake of type and the force sensoring system that was used. Naturally, the motor's outer dimensions could not be shrunk but an additional 3D printed part was attached to the rotor part in order to add a smaller axis cocentric with the rotor body. The added part is shown in Figure 54. This, however, increased the frictional torque as this torque measurement setup causes forces attempting to tilt the axis. [70]

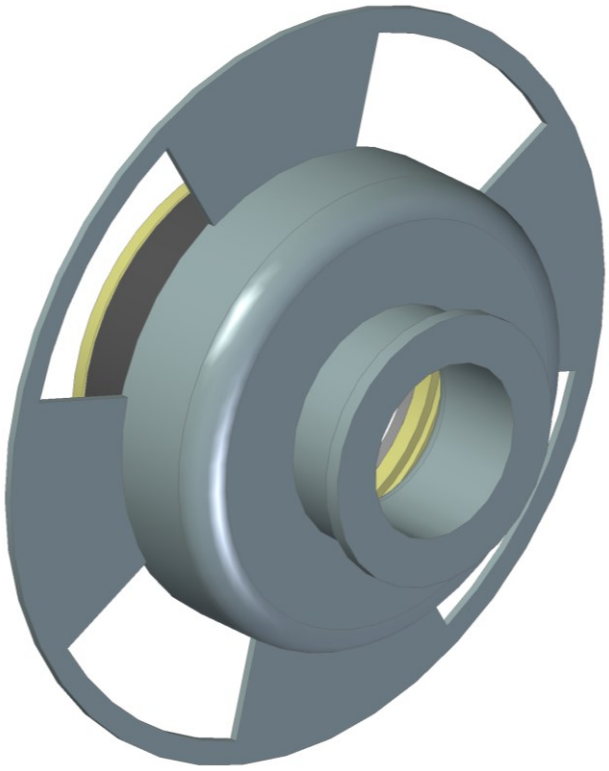

Figure 54. *The auxiliary part attached to the motor in order to shrink the measurement axis' diameter.*

Despite the attempt to build a working motor was not successful, it was found necessary to understand the torque-decreasing factors. The simulations performed, did not include friction, and thus, understandably would have inherent bias towards higher torque results. The friction was considered too small to explain the lower torque results alone. As the material had to be changed and reluctance for iron core was known to be a lot

smaller than that of air, (which was seen equivalent to plastic) it was seen as the major cause. The basis of the expectation was by both, examples and facts: As described in Chapters 2.1.3 and 2.2.1, reluctance motors' torque can be increased by decreasing reluctance of the active magnetic flux path. Various BLDC motors for hobbyist multicopters that were inspected, included only ferromagnetic stators.

This assumption was to be confirmed by means of simulation. Results are presented in Appendix 8: Simulated Stator material comparison. To optimize the time used for simulation, a section of 2 magnets on the rotor and 2 coils on the stator were used as the geometry and the final results were extrapolated to match the torque of the complete motor. This meant to multiply each torque point by number 18 as combining 18 of the equivalent setups would result in the geometry of the complete motor. Despite not necessarily an exact representation of the performance scaling, it was assumed to be sufficiently precise to describe the scale by which material selection affects the motor's performance. The simulated materials were soft iron and air, as the magnetic properties of the used steel quality weren't known and plastic was considered magnetically close to a material with relative permeability of 1 as concluded in Chapter 3.3. According to these results, selecting a ferromagnetic material enhances the torque production by multiple times, compared to a non-ferromagnetic one.

8. CONCLUSIONS

This thesis was started by technology scouting to find a suitable camera actuator for a pop-up camera development project. The currently available actuator types and already-in-use solutions were evaluated to find out, whether a proper solution already exists. It was to be found out, that there were suitable types of actuators but none matched the requirements as and of itself.

As none of the solutions available suited the use case, the project was to proceed to designing a new kind of an actuator, eventually resorting to two new types. Both of them were modified types of stepper motors, utilizing a hollow rotor, making space for camera electronics in the middle. Their performance was evaluated with simulations as well as prototypes.

Considering the initial question, whether the requirements of precision and speed could be reached, they weren't. Unfortunately, the final prototype that was made, could only spin without a load, and the torque was little, as could be seen in Table 4. Despite the specified requirements weren't accomplished, the prototype achieved proof-of-concept level. As said, though, fixing the mechanical collision between the rotor and iron stator would arguably result in higher torque.

The original plan was straightforward proceeding from concept drafting to simulation and to prototype building, measurements and conclusion. There were multiple changes in plans and schedule, which brought their own challenges in proceeding with the project. In addition to that, prior experience in FEM simulation would've made easier to judge the simulation results' validity. Skillful and experienced designer would've avoided some of the pitfalls of configuring the simulations but after all, this was a process of developing something new. Despite some work was unnecessary, current proceedings provide a good basis of understanding the motor's performance charasteristics and further development.

Considering available solutions, there are a few possible alternatives to develop the hollow motor further. One solution would be to optimize the dimensions of the current PM stepper design. Taken that it would be possible to make a non-slipping (noiseless and long life) piezoelectric motor of this size, it would probably be able to produce better volume-to-torque ratio without gears, shrinking the size even more than the optimization of the PM stepper. There is no explicitly clear solution that would be the best one, but these two alternatives are the most compelling ones considering the requirements of

silent drive, speed and precision. Electromagnetic actuators possess the risk of disturbance to the surrounding circuitry of the handset, yet minimizing the mechanical contact. Piezoelectric drivers require noiseless high voltage power supply that is not inherently available in a handset but are very capable of precise as well as sufficiently fast movement.

REFERENCES

[1] K. B. Kahn, G. Castellion, A. Griffin, The PDMA Handbook of New Product Development, 2nd edition, John Wiley & Sons, Inc., 2004.

[2] C. W. de Silva, Mechatronics : A Foundation Course, 1st edition, CRC Press, 2010.

[3] K. Sang-Hoon, Electric motor control : DC, AC, and BLDC motors, Joe Hayton, 2017, 427 p.

[4] HSM (Hyper Sonic Motor) | SIGMA Glossary | SIGMA Corporation, Sigma, 2022 Available (accessed on 10.6.2022): https://www.sigma-global.com/en/glossary/hyper-sonic-motor/

[5] 100-400mm F5-6.3 DG DN OS | Contemporary | Lenses | SIGMA Corporation, Sigma, 2022. Available (accessed on 10.6.2022): https://www.sigma-global.com/en/lenses/c020_100_400_5_63/

[6] 11-20mm F/2.8 Di III-A RXD, Tamron, Available (accessed on 10.6.2022): https://www.tamron.eu/lenses/11-20mm-f28-di-iii-a-rxd/

[7] Silent and swift: The stepping motor in NIKKOR lenses – Nikon Technology - Nikon Middle East FZE, Nikon, Available (accessed on 10.6.2022): http://www.nikon-me.com/en_ME/learn_and_explore/nikon_technology?lang=&ID=templatedata/en_Asia/taggable_content/data/learn_and_explore/The-stepping-motor-in-NIKKOR-lenses&Category=learn-and-explore-new&Section=

[8] Samyang Optics AF 135mm F1.8 FE product page, Samyang, Available (accessed on 10.6.2022): https://www.samyanglens.com/en/product/product-view.php?seq=576

[9] Tamron 70-180mm F/2.8 III VXD product page, Tamron, Available (accessed on 10.6.2022): https://www.tamron.eu/lenses/70-180mm-f28-di-iii-vxd/

[10] Sony FE 70-200mm F2.8 GM OSS II product page, Sony, Available (accessed on 10.6.2022): https://electronics.sony.com/imaging/lenses/all-e-mount/p/sel70200gm2

[11] A. Emadi, Advanced Electric Drive Vehicles, 1st edition, Taylor & Francis Group, LLC, 2020, 604 p.

[12] A. Salam, Electromagnetic Field Theories for Engineering, 1st edition, Springer Science, 2014, 315 p.

[13] A. Hughes, B. Drury, Electric Motors and Drives: Fundamentals, Types and Applications, 5th edition, Elsevier, 2019.

[14] J. M. D. Coey, Magnetism and magnetic materials, Cambridge University Press, 2010, 614 p.

[15] B. Bilgin, A. Emadi, M. Krishnamurthy, Design Considerations for Switched Reluctance, *IEEE transactions on industrial electronics,* vol. 59(10), 2012, 12p.

[16] T. J. E. Miller, Electronic control of switched reluctance machines, 1st toim., Boston: Newnes, 2001, 266 p.

[17] C. Bianchini, F. Immovilli, E. Lorenzani, A. Bellini, M. Davoli, Review of Design Solutions for Internal Permanent-Magnet Machines Cogging Torque Reduction, *IEEEE transactions on magnetics,* vol. 48(10), October 2012, pp. 2685-2693.

[18] J. W. Jiang, B. Bilgin, Y. Yang, A. Sathyan, H. Dadkhah, A. Emadi, Rotor skew pattern design and optimisation for cogging torque reduction, *IET Electrical Systems in Transportation,* vol. 6(2), September 2015 , 10 p.

[19] R. Crowder, Electric Drives and Electromechanical Systems, 1st edition, Elsevier, 2006, 287 p.

[20] Y.-U. Park, J.-H. Cho, D.-k. Kim, Cogging Torque Reduction of Single-Phase Brushless DC Motor With a Tapered Air-Gap Using Optimizing Notch Size and Position, *IEEE transactions on industry applications,* vol. 51(6), November/December 2015, pp. 4455-4463.

[21] S. Ghosh, Electrical Machines, 2nd ed, Pearson India, 2012.

[22] Y. Yang, B. Bilgin, M. Kasprzak, S. Nalakath, H. Sadek, M. Preindl, J. Cotton, N. Schofield, A. Emadi, Thermal management of electric machines, *IET Journals,* vol. 7(2), July 2016, 13 p.

[23] J. Pyrhönen, V. Hrabovcová, R. S. Semken, Electrical Machine Drives Control : An Introduction, 1st edition, John Wiley & Sons Inc., 2016, 527 p.

[24] J. R. Brauer, Magnetic Actuators and Sensors, 2nd edition, John Wiley & Sons Inc., 2014, 397 p.

[25] P. Moreton, Industrial Brushless Servomotors, 1st edition, Newnes, 2000, 205 p.

[26] V. Dadi, S. Peravali, R. Busi, Conversion of geared DC motor into stepper motor using switching delay time signals, *SN Applied Sciences,* vol. 3(4), 2021, 18 p.

[27] T. Verstraten, G. Mathijssen, R. Furnémont, B. Vanderborght, D. Lefeber, Modeling and design of geared DC motors for energy efficiency: Comparison between theory and experiments, *Mechatronics,* vol. 30(16), 2015.

[28] M. Kazimierczuk, High-Frequency Magnetic Components, 2nd edition, John Wiley & Sons, Ltd., 2014, 729 p.

[29] A. Butterfield, J. Szymanski, A Dictionary of Electronics and Electrical Engineering, 5th edition, Oxford University Press, 2018.

[30] Y. Zhang, J. Wang, Y. Zeng, J. Zhang, Calculating method of MTBF for integrated circuit, *Journal of physics: Conference Series,* vol. 1053(1), 2018, 8 p.

[31] T. Mak, Truncation erroranalysis of MTBF computation for multi-latch, *Microelectronics Journal,* vol. 43(2), 2011, pp. 160-163.

[32] M. P. Pantelić, S. M. Bošnjak, M. Z. Misita, N. B. Gnjatović, A. Z. Stefanović, Service FMECA of a bucket wheel excavator, *Engineering failure analysis*, 2019, 15 p.

[33] J. P. Johnson, Brushless DC Drives in *Handbook of Automotive Power Electronics and Motor Drives*, 1st edition, CRC Press, 2005, 736 p.

[34] J. F. Gieras, R.-J. Wang, M. J. Kamper, Axial Flux Permanent Magnet Brushless Machines, 2nd edition, Springer Science + Business Media B.V., 2008, 364 p.

[35] M. S. Sarma, Introduction to Electrical Engineering, Oxford University Press, Inc., 2001, 853 p.

[36] J. F. Gieras, Permanent Magnet Motor Technology : Design and Applications, 3rd toim., Boca Raton, Florida: CRC Press, 2010, 601 p.

[37] F. G. Moritz, Electromechanical Motion Systems : Design and Simulation, 1st edition, John Wiley & Sons, Ltd., 2014, 294 p.

[38] X. Xi, Y. Sun, X. Wang, Y. Xin, Y. Yang, A Study on the Detent Torque and Holding Torque of a Micro-Claw Pole Stepper Motor, *Micromachines,* vol. 13(6), 2022, 15 p.

[39] E. P. Furlani, Permanent Magnet and Electromechanical Devices: Materials, Analysis, and Applications, ScienceDirect, 2001, 518 p.

[40] J. N. Chiasson, Modeling and High Performance Control of Electric Machines, John Wiley & Sons, Inc., 2005, 709 p.

[41] Trinamic Motion Control GmbH & Co. KG, Trinamic TMC2209-LA datasheet, Available (accessed on 1.12.2022): https://www.trinamic.com/fileadmin/assets/Products/ICs_Documents/TMC2209_datasheet_rev1.08.pdf

[42] Texas Instruments, DRV8889A-Q1 Automotive Stepper Driver with Integrated Current Sense, 1/256 Micro-Stepping and Stall Detection, Available (accessed on 1.12.2022): https://www.ti.com/lit/gpn/drv8889-q1

[43] G. Beauchemin, Microstepping myths, *Machine Design,* vol. 75(19), 2003, 86 p.

[44] I. Sinclair, Passive Components for Circuit Design, 1st edition, Newnes, 2001, 296 p.

[45] J. M. Hughes, Practical Electronics: Components and Techniques, 1st edition, O'Reilly, 2015.

[46] X. Wang, F. Chen, R. Zhu, X. Huang, N. Sang, G. Yang, C. Zhang, A Review on Disturbance Analysis and Suppression for Permanent Magnet Linear Synchronous Motor, *Actuators,* vol. 10(4), 2021, 27 p.

[47] J. F. Gieras, Linear Synchronous Motors: Transportation and Automation Systems, 2nd edition, Taylor & Francis Group, 2018.

[48] C. Zhao, Ultrasonic motors, 1st edition, Springer, 2011, 522 p.

[49] P. Zhang, Sensors and Actuators for Industrial Control, in *Industrial Control Technology : a handbook for engineers and researchers*, 1st edition, William Andrew Inc., 2008, 186 p.

[50] S.-B. Choi ja Y.-M. Han, Piezoelectric Actuators : Control Applications of Smart Materials, Taylor and Francis Group, LLC, 2010, 263 p.

[51] S. Ameduri, V. Antonucci, E. Artioli, D. Asprone, F. Auricchio, S. Barbarino, E. Boatti, A. Concilio, M. Conti, I. Dimino, G. Faiella, L. Lecce, S. Marfia, A. Martone, C. Menna, R. Pecora, E. Sacco, F. Stortiero, A. Vigliotti, E. Villa, Shape Memory Alloy Engineering, Elsevier, 2015.

[52] A. Rao, J. N. Reddy, A. R. Srinivasa, Design of Shape Memory Alloy (SMA) Actuators, 1st edition, Springer, 2015.

[53] C. E. English, D. L. Russell, Mechanics and stiffness limitations of a variable siffness actuator for use in prosthetic limbs, *Mechanism and Machine Theory, vol*. 34(1), pp. 7-25, 1998.

[54] Photography Life, Nikon NIKKOR Z 24-70mm f/2.8 S, Photography Life, Available (accessed on 09.12.2022): https://photographylife.com/lenses/nikon-nikkor-z-24-70mm-f2-8-s

[55] R. Cicala, Finally, the Nikon Z 24-70mm f/2.8 S Lens Teardown, Lens Rentals, Available (accessed on 09.12.2022): https://www.lensrentals.com/blog/2020/01/finally-the-nikon-z-24-70mm-f2-8-s-lens-teardown/

[56] Photography Life, Canon RF 50mm f/1.2L USM, Photography Life, Available (accessed on 09.12.2022): https://photographylife.com/lenses/canon-rf-50mm-f1-2l-usm

[57] R. Cicala, Disassembly of the Canon RF 50mm f1.2L, Lens Rentals, Available (accessed on 09.12.2022): https://www.lensrentals.com/blog/2018/12/disassembly-of-the-canon-rf-50mm-f1-2l/

[58] R. Cicala, The Great 400mm f/2.8 Teardown Comparison. Part 1 – The Canon 400mm f/2.8 L IS III," Lensrentals, Available (accessed on 09.12.2022): https://www.lensrentals.com/blog/2018/12/the-great-400mm-f2-8-teardown-competition-part-1-the-canon-400mm-f2-8-l-is-iii/

[59] R. Cicala, Lens Teardown of the Complicated Sony FE 70-200mm f/2.8 GM OSS: Part I, Lensrentals, Available (accessed on 09.12.2022): https://www.lensrentals.com/blog/2017/02/lens-teardown-of-the-complicated-sony-fe-70-200mm-f2-8-gm-oss-part-1/

[60] R. Cicala, Completing the Teardown of the Sony FE 70-200 f/2.8 GM OSS: Part II, Lensrentals.com, Available (accessed on 09.12.2022): https://www.lensrentals.com/blog/2017/02/completing-the-teardown-of-the-sony-fe-70-200-f2-8-gm-oss-part-ii/

[61] Stepperonline, Nema 17 Bipolar 1.8deg 16Ncm (22.6oz.in) 1A 3.7V 42x42x20mm 4 Wires - 17HS08-1004S, Stepperonline, Available (accessed on 3.8.2022): https://www.omc-stepperonline.com/nema-17-bipolar-1-8deg-16ncm-22-6oz-in-1a-3-7v-42x42x20mm-4-wires.html

[62] H. S. G. Rao, Finite element method vs. classical methods, New Age International Ltd. Publishers, 2007, 434 p.

[63] COMSOL, The Modeling Workflow in COMSOL, COMSOL, Available (accessed on 3.2.2023): https://www.comsol.com/learning-center/setting-up-and-running-a-simulation-with-comsol-multiphysics?autoplay=true

[64] STMicroelectronics, STSPIN220 Datasheet, STMicroelectronics NV, 2020.

[65] J. K. Fink, Metallized and Magnetic Polymers: Chemistry and Applications, 1st edition, Scrivener Publishing, 2016.

[66] ProgrammerSought, Stepper motor 28BYJ-48 teardown diagram, principle and 51/stm32 test program, ProgrammerSought, Available (accessed on 3.8.3022): https://www.programmersought.com/article/43161241941/

[67] MinebeaMitsumi Inc., Small diameter type | PM stepping motors | MinebeaMitsumi Product DataBase, MinebeaMitsumi Inc., Available (accessed on 3.8.2022): https://product.minebeamitsumi.com/en/product/category/rotary/steppingmotor/pm/Smalldiametertype.html

[68] Phrozen Technology, Phrozen TR300 Ultra-High Temp Resin for durable 3D Printed Parts, Phrozen Technology, Available (accessed on 3.2.2023): https://phrozen3d.com/collections/3d-printer-resins-phrozen/products/phrozen-tr300-ultra-high-temp-resin#specs

[69] B&K Precision, LCR Meter Model 880 Product Page, B&K Precision, Available (accessed on 23.1.2023): https://www.bkprecision.com/products/component-testers/880

[70] A. S. Morri, R. Langari, Measurement and Instrumentation : Theory and Application, 2nd edition, Saint Louis, Missouri: Elsevier, 2012.

APPENDIX 1: PRELIMINARY PM STEPPER TORQUE PRODUCTION SIMULATION

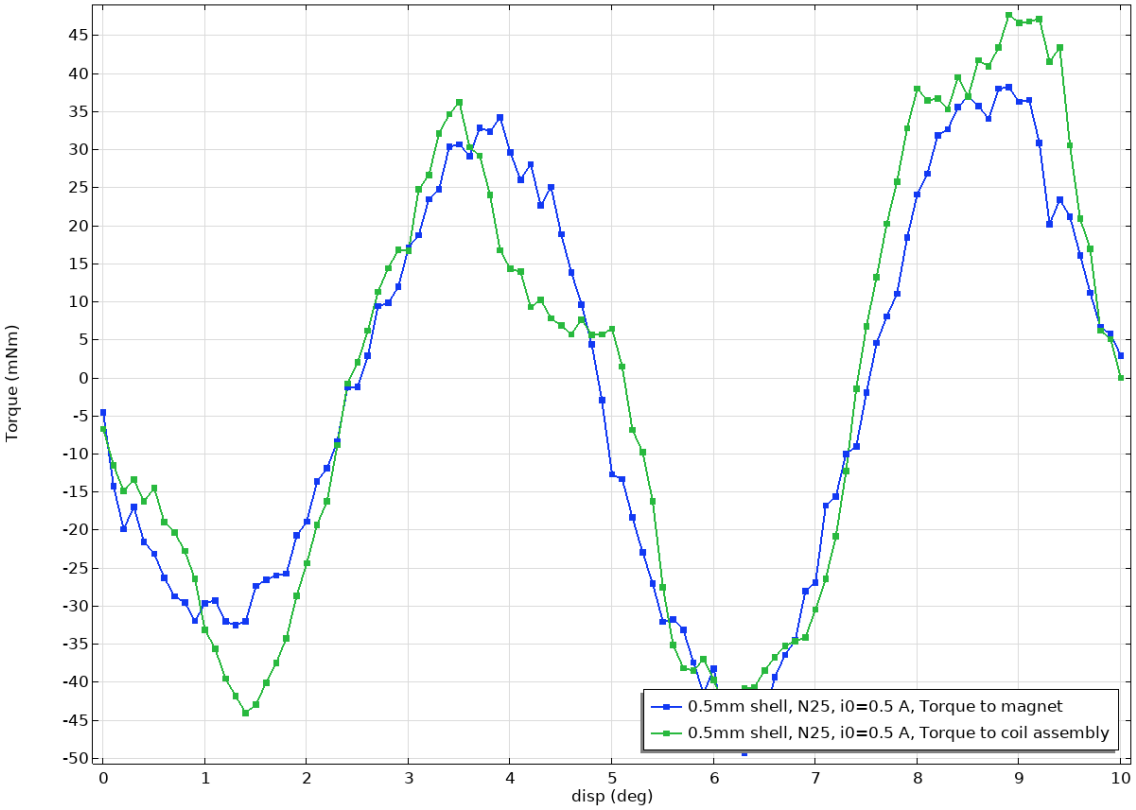

Figure 55. *Holding torque output simulation of the motor with 0.1 degrees rotational displacement step. As precise readers may notice, the waveforms towards rotor (magnet assembly) should be inverted compared to the ones towards the coil assembly. Here, however, the other waveform has been inverted to gain a better comparability between the results.*

Figure 55 shows the holding torque curve of the permanent magnet stepper motor introduced in Chapter 5. The different curves show the torques towards the different components of the motor. The torque towards magnets (blue curve) represents the torque against rotor and the torque towards the coil assembly (green curve) represents the torque towards stator structure. The other one has been inverted to see, whether the torques approximately match. That should hold true for a case, where the simulation's performed right and in this case it does.

APPENDIX 2: SECOND REVISION (PERMANENT MAGNET STEPPER) FIRST RESULTS

This Appendix includes the simulation results of the second motor design revision in Chapter 5. First, the torque curve is introduced in Figure 56, then the corresponding magnetic field results in Figure 57.

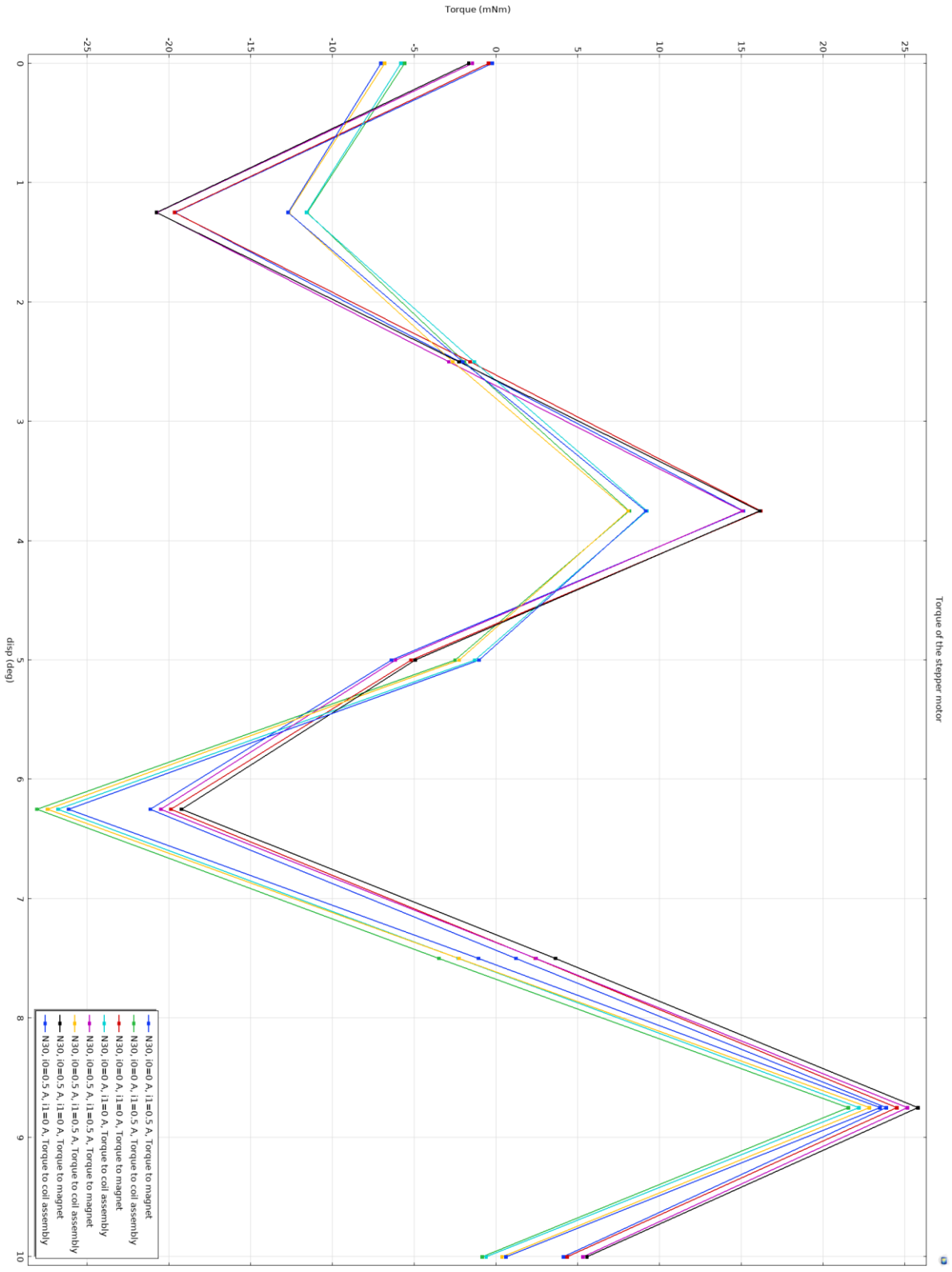

Figure 56. *The torque simulation of permanent magnet stepper motor with no coil currents (i0=0A and i1=0A), single coil enabled (i0=0.5A and i1=0A or i0=0A and i1=0.5A) or both coils enabled (i0=0.5A and i1=0.5A). For easier comparison between the torques towards different components, the other waveform has been inverted like in Figure 55.*

The Figure 56 shows the torque simulation of the second revision of the motor. Here, only the assumed vital points of the torque curve were simulated, to shorten the time of simulation and to determine the extent of modifications, that have to be made in order to reach the targets of the design.

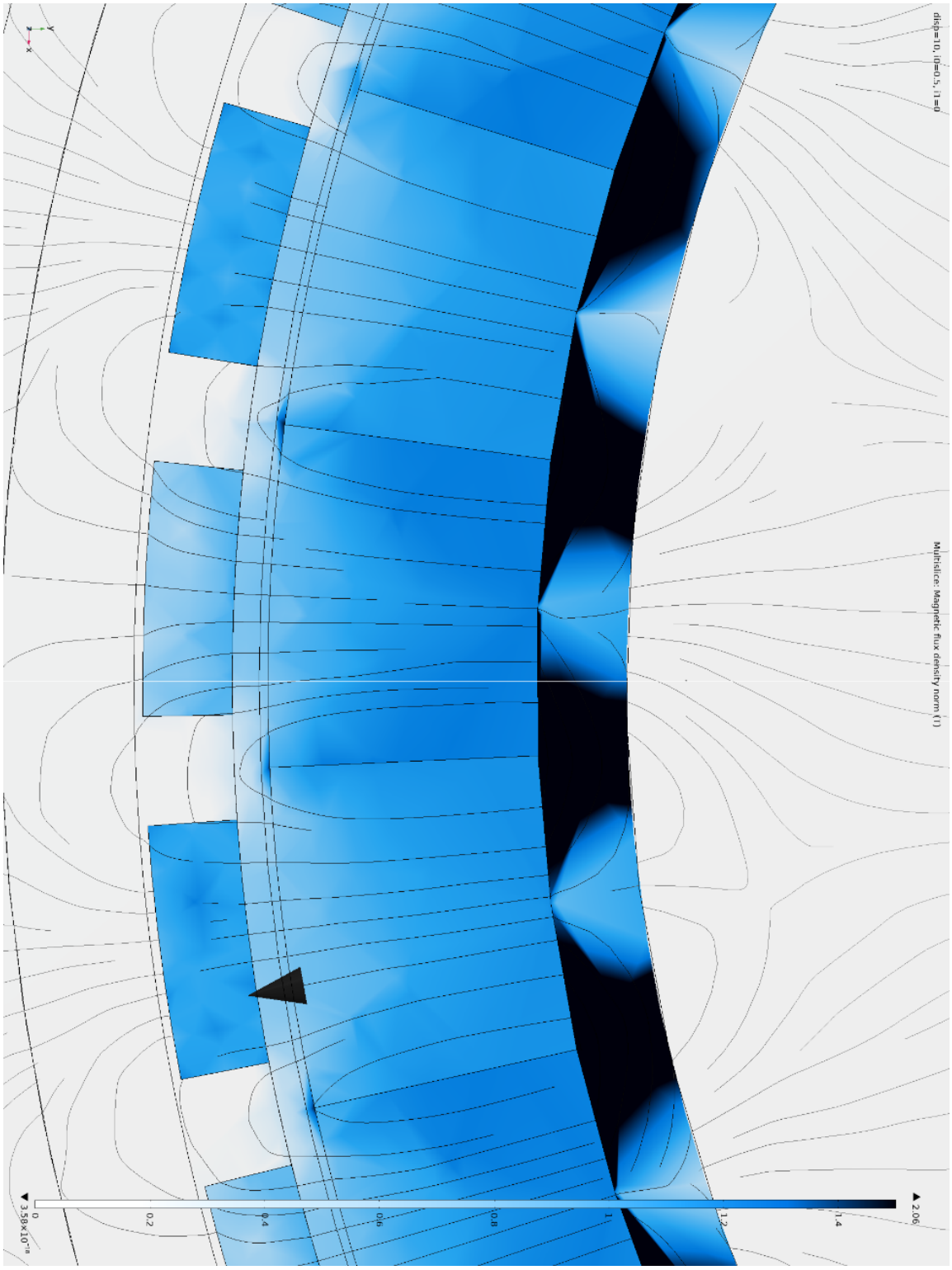

Figure 57. *Magnetic fields in the simulation of the second revision of the motor, introduced in Chapter 5.*

Figure 57 shows the magnetic fields corresponding the displacement of 10 degrees in the Figure 56. It can be observed, that the inner ferrite ring of the rotor is partially saturated, but no other parts are on this level. The magnetic field protrudes slightly outside the rotor, between the stator poles, which tells that there is a slight leakage of magnetic field between the poles.

APPENDIX 3: COIL TURN SWEEP

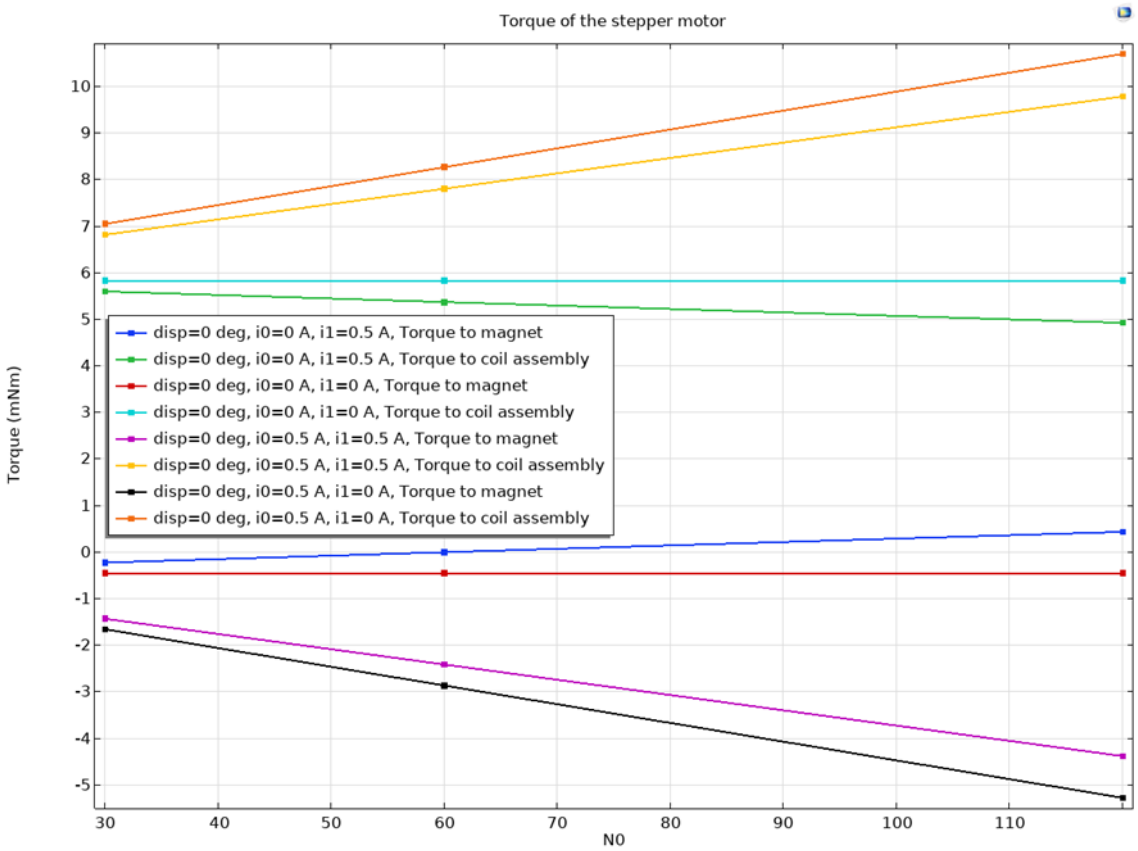

Figure 58. *Coil round sweep simulation results.*

The Figure 58 above shows the results of the coil turn sweep of the 36-pole permanent magnet motor model. From the results, it's apparent that the other phase, which is activated by current i1, is inducing very little torque but the other, energized by i0, makes a bigger difference. For some unrecognized reason, the torque curve towards the magnet assembly (rotor) isn't offset as its counterpart towards coil assembly (stator). However, activating the phase associated with i0 does create an offset compared to its deactivated counterpart, when comparing either torque curves towards the stator or the ones towards rotor. Comparing these offsets' magnitudes, they seem to be approximately the same, independent of whether comparing torques towards rotor or stator. In situations, where the phase connected to i1, its activation inflicts only a maximum of 1 mNm torque, which is due to the magnets being close to exactly aligned position with it.

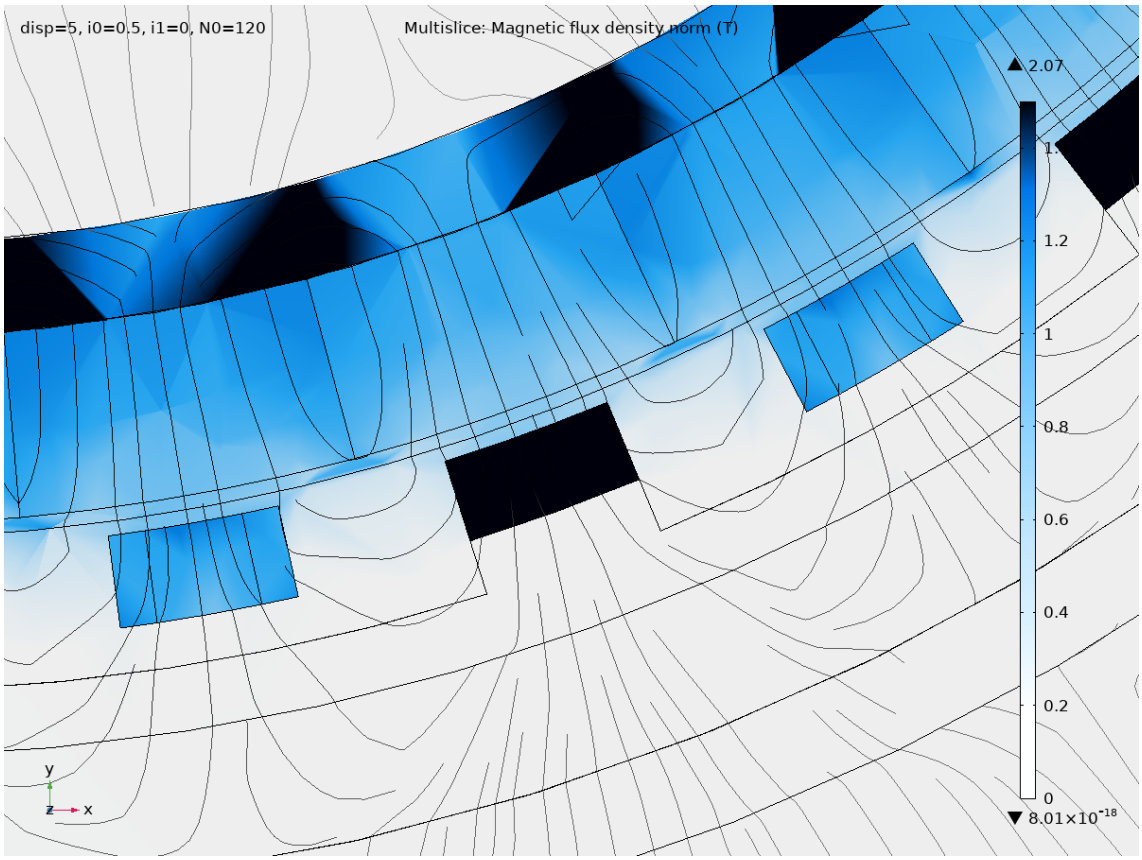

Figure 59. *Section view of the magnetic flux on the coil winding level. The highlighted parts the ones that are sliced whereas the strucures below can be seen as the wireframe in light gray color.*

The section view of the magnetic flux on the salient poles facing the magnets, in Figure 59 shows that the magnetic field inside the soft iron saturates, as the every other part is completely black. From Figures 60 and 59 can be observed that the magnetic field density increases moving from the extremes of the poles to the base plate level. The base plate level correspondent of the Figure above is shown in Figure 60 below.

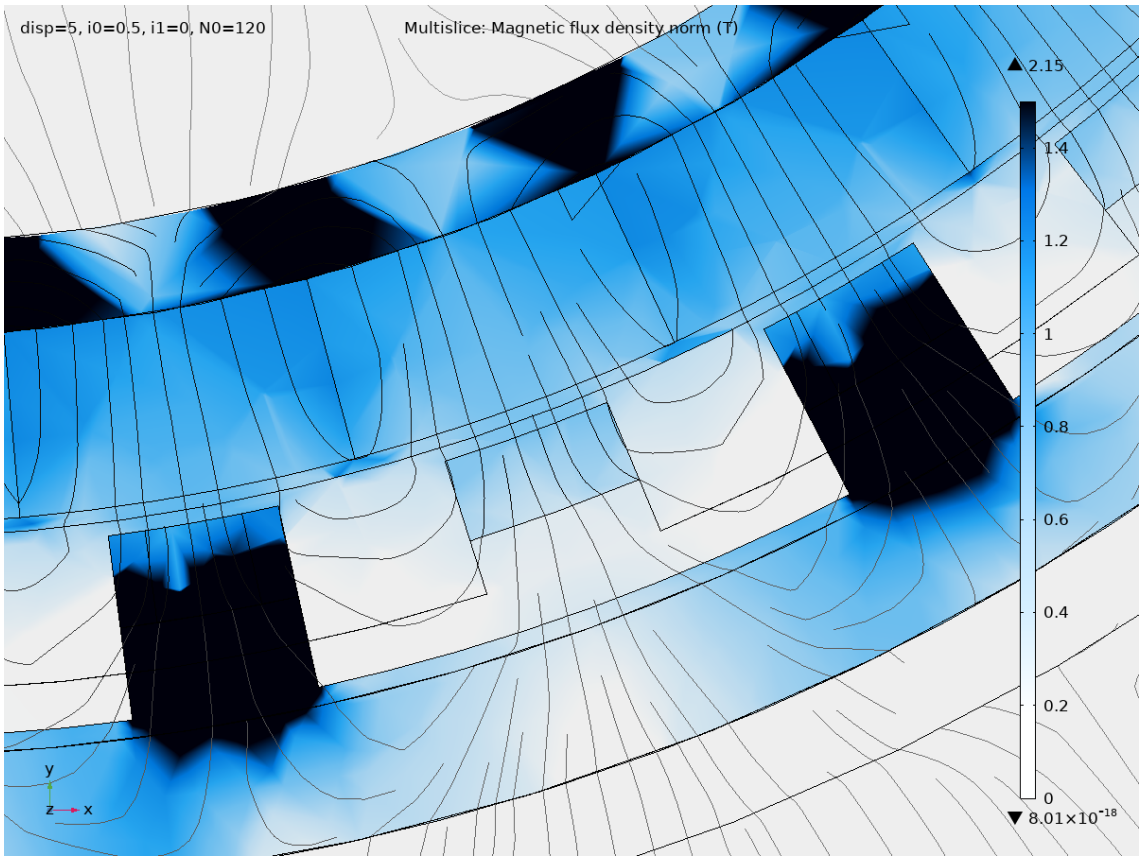

Figure 60. *Section view on the base plate level.*

The Figure 60 above presents magnetic fields at the base plate level of the stator structure. It shows that the magnetic field saturates in the narrowest part of the bending as it propagates to the salient that faces the magnet ring.

APPENDIX 4: TORQUE MEASUREMENT RESULTS

	4V		5V		6V	
PPS	**Pull-out (mNm)**	**Pull-in (mNm)**	**Pull-out (mNm)**	**Pull-in (mNm)**	**Pull-out (mNm)**	**Pull-in (mNm)**
50	0.595	0.242	0.826	0.437	0.907	0.581
75	0.554	0.308	0.639	0.289		
100	0.556	0	0.637	0.251		

Measurement data of the 36-pole permanent stepper motor described in Chapter 7. Measurement data collected by Nico Koski, Huawei Technologies Oy Finland.

APPENDIX 5: MF SIMULATIONS WITH SPARSE MESH

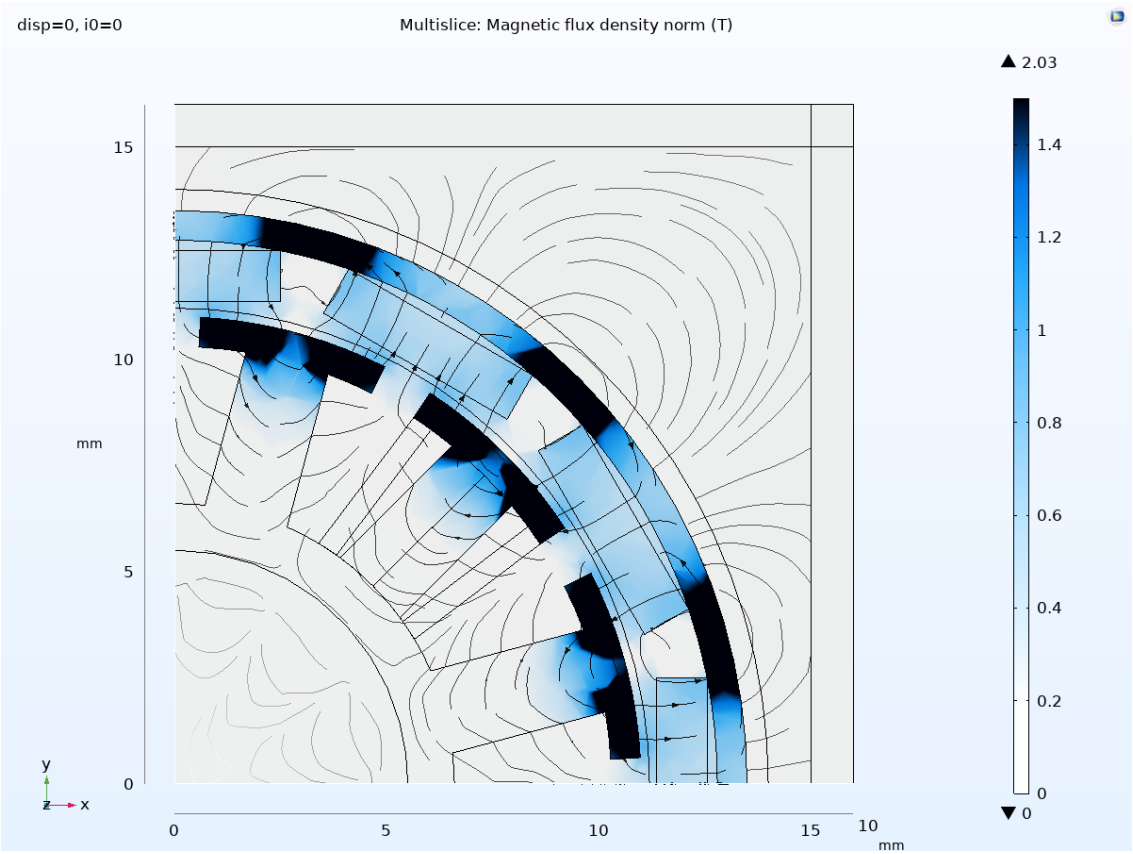

Figure 61. *The magnetic fields in permanent magnet stepper motor, when the motor is idling, i.e. the current i0 through the coil is 0 A.*

The magnetic fields presented in Figure 61 show that the magnetic flux paths are quite as expected. The magnetic field of a single magnet is strongest on the rotor side, as can be seen from the more saturated blue color between the rotor and the stator than between adjacent magnets.

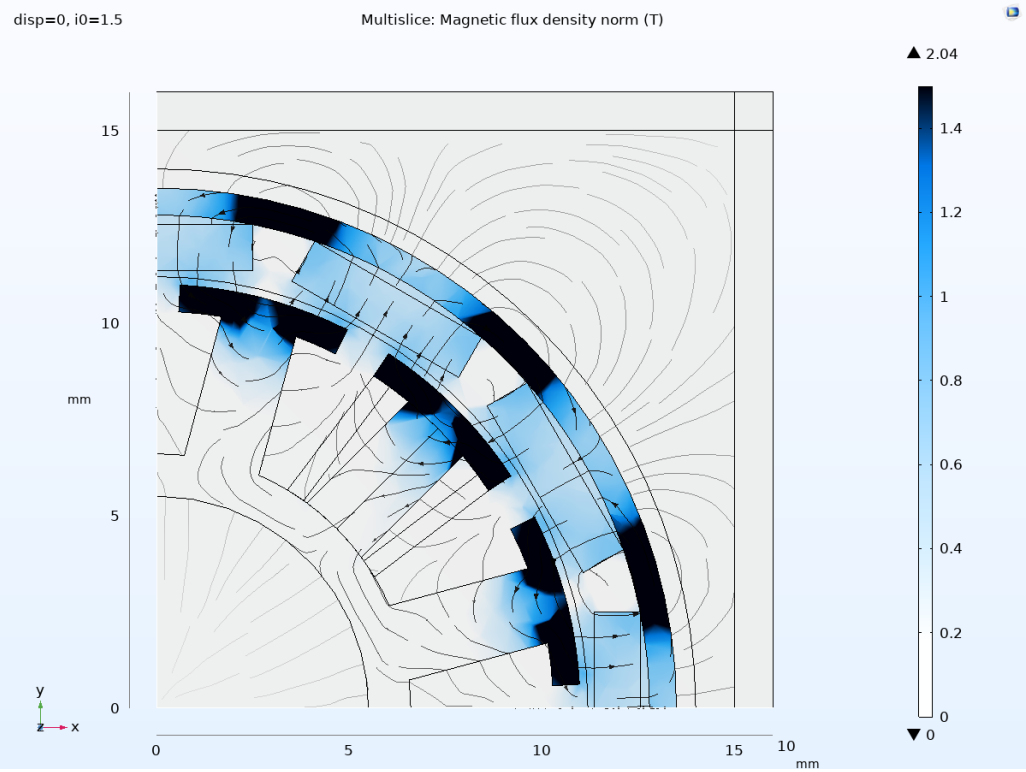

Figure 62. *The magnetic fields in motor revision 2, when the current i0 through the coil is 1.5 A.*

Figure 62 with an activated coil, presents slightly changed magnetic fields, with less flux between the adjacent magnets in the proximity of the activated coil. It can also be noticed, when comparing the two last Figures that the magnetic fields further away from the motor structure weakens, when the coil is activated.

APPENDIX 6: MF SIMULATIONS WITH DENSE MESH

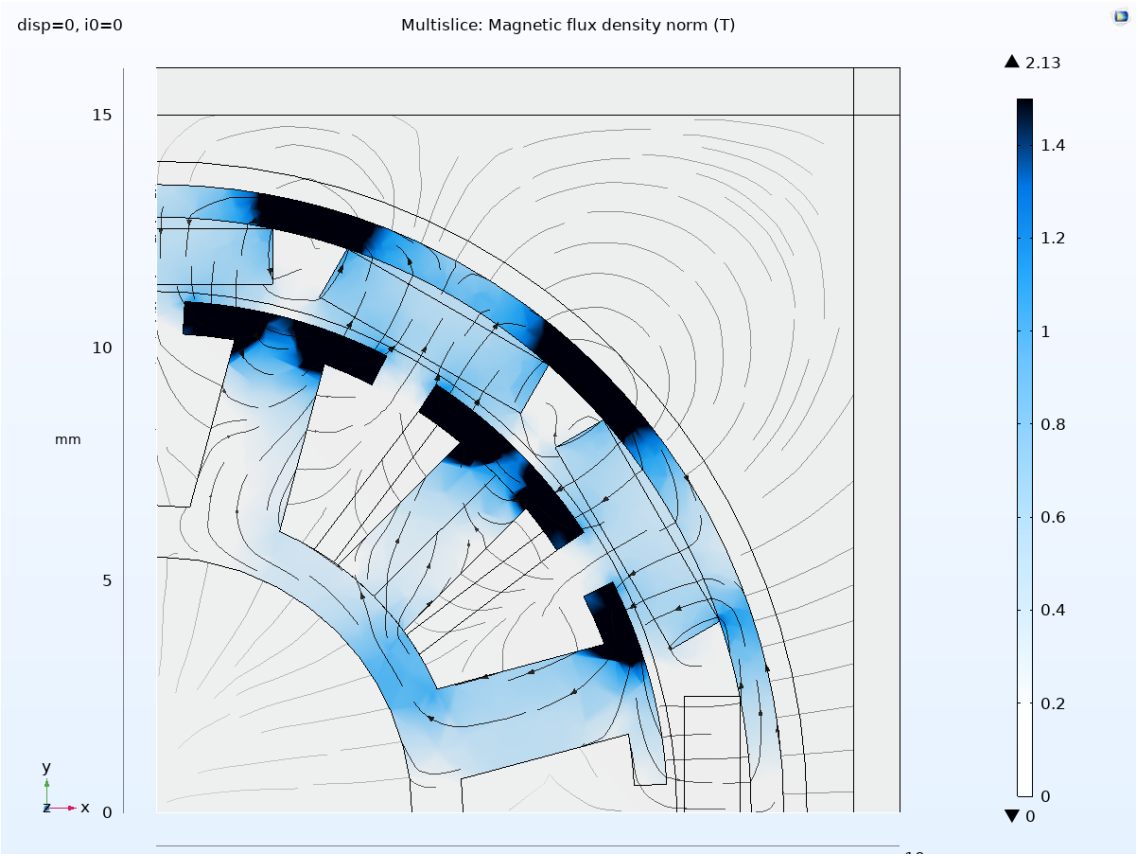

Figure 63. *Magnetic fields simulated in the brushless DC motor with deactivated coil and denser mesh than compared with the ones in Appendix 5.*

Comparing the results of Figure 61 and Figure 63, it seems that the denser simulation mesh makes a difference. There is a clear difference in the density of the magnetic flux in the inmost areas of the stator as well as in the coil core. Figure 64 shows the same view in situation, where the coil is activated.

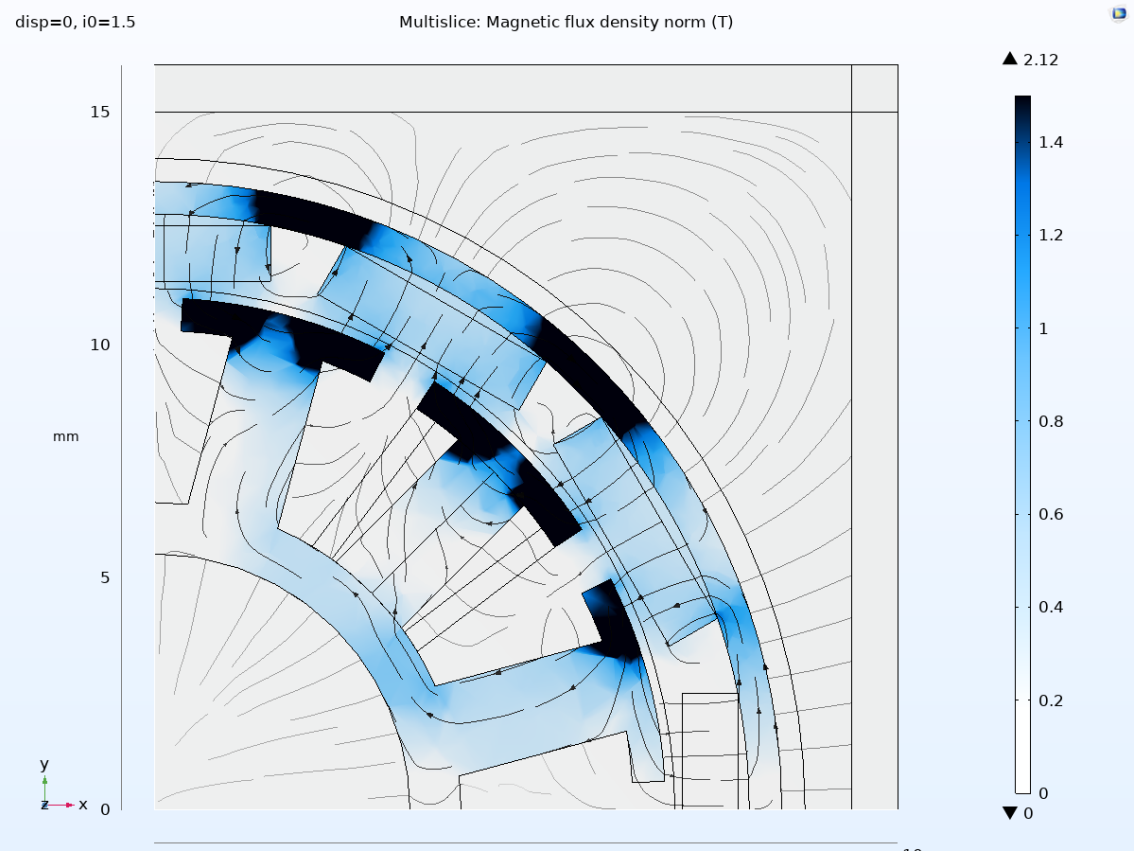

Figure 64. *Magnetic fields simulated in the brushless DC motor with activated coil and denser mesh than compared with the ones in Appendix 5.*

The cross-section of the motor with an activated coil with the denser mesh presents further spread magnetix flux on the adjacent poles of the one with activated coil. However, here can be seen that the magnet in the bottom part was disabled and the one cut in half along y-axis was not, so that's probably what caused distorted torque curve, shown in Figure 65.

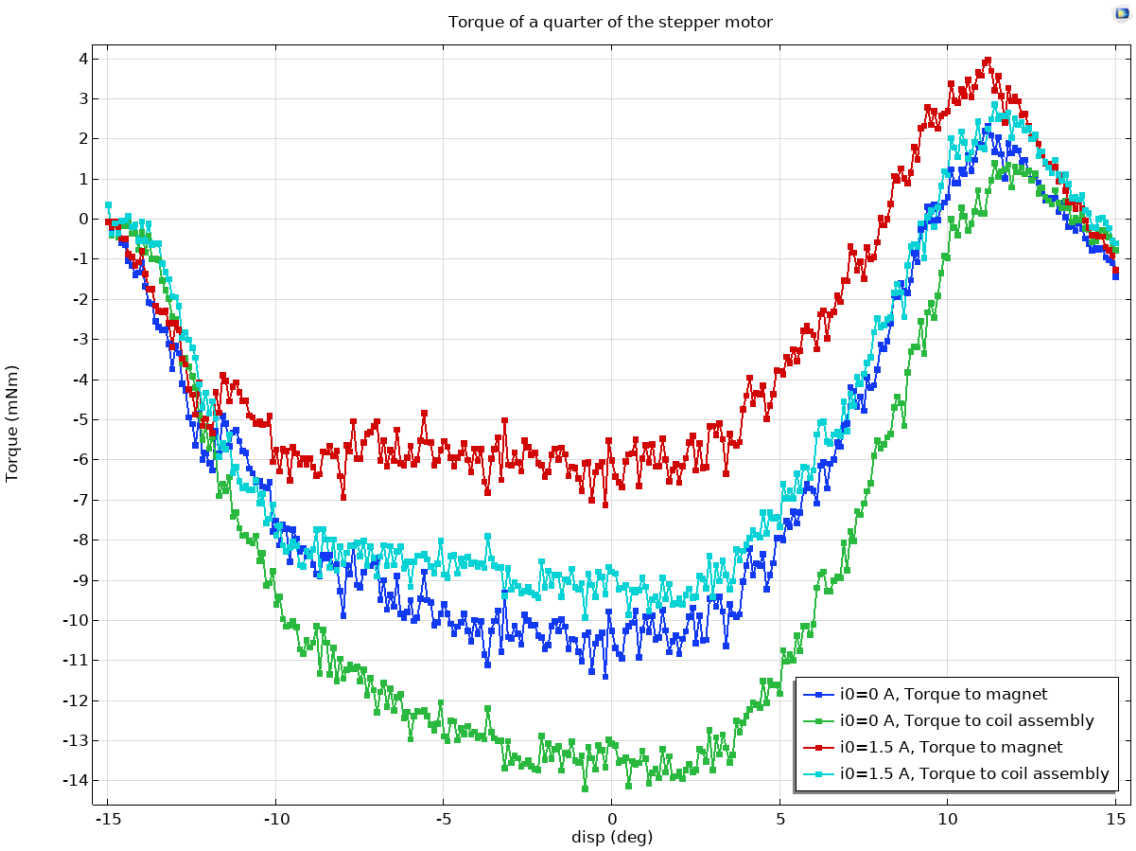

Figure 65. *The torque output curve of the denser simulation network results.*

APPENDIX 7: TORQUE SIMULATION OF THE MODIFIED PM STEPPER

This Appendix shows torque curve of the simulated structure that matches the motor made utilizing two BLDC motors, introduced in Chapter 6.

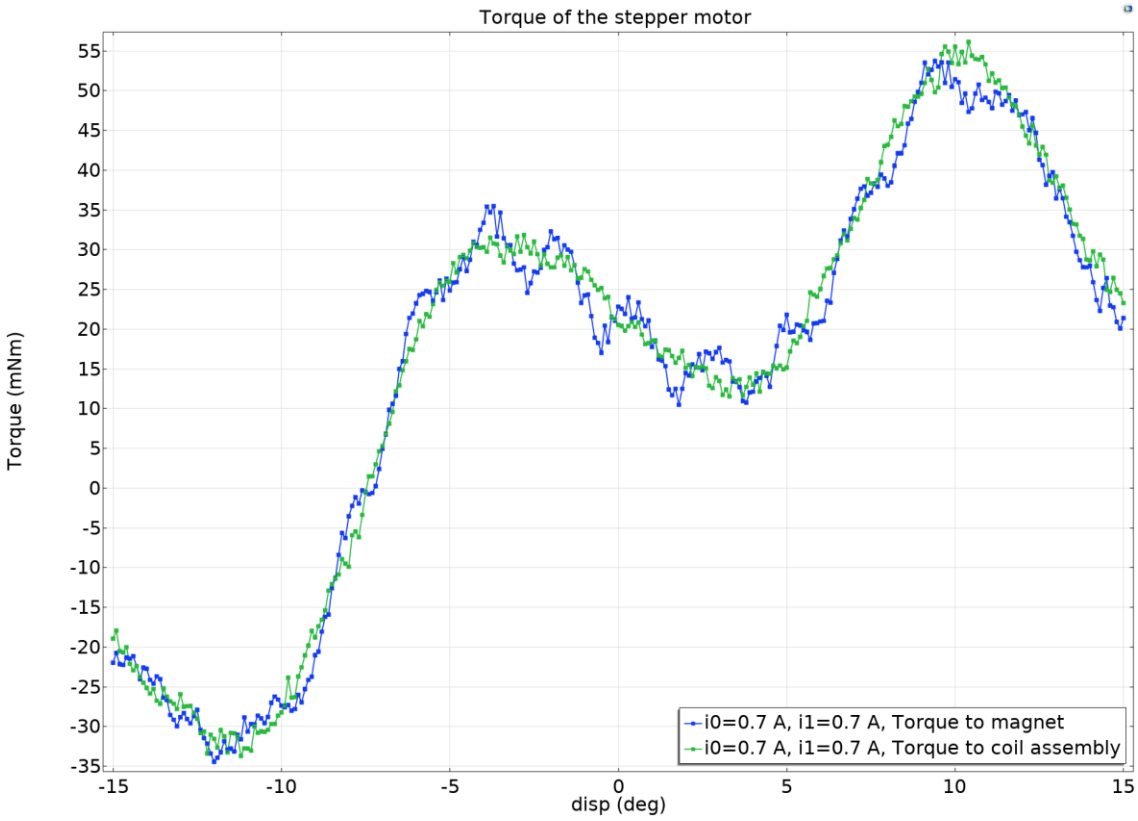

Figure 66. *Holding torque of the stepper motor manufactured in Chapter 6.*

The image above shows the displacement sweep results of the PM stepper motor equivalent to the PM stepper motor made of 2 BLDC motors' components, shown in Figure 47 and Figure 48. The magnetic field images below show and explain the significant points of the torque curve shown in Figure 66.

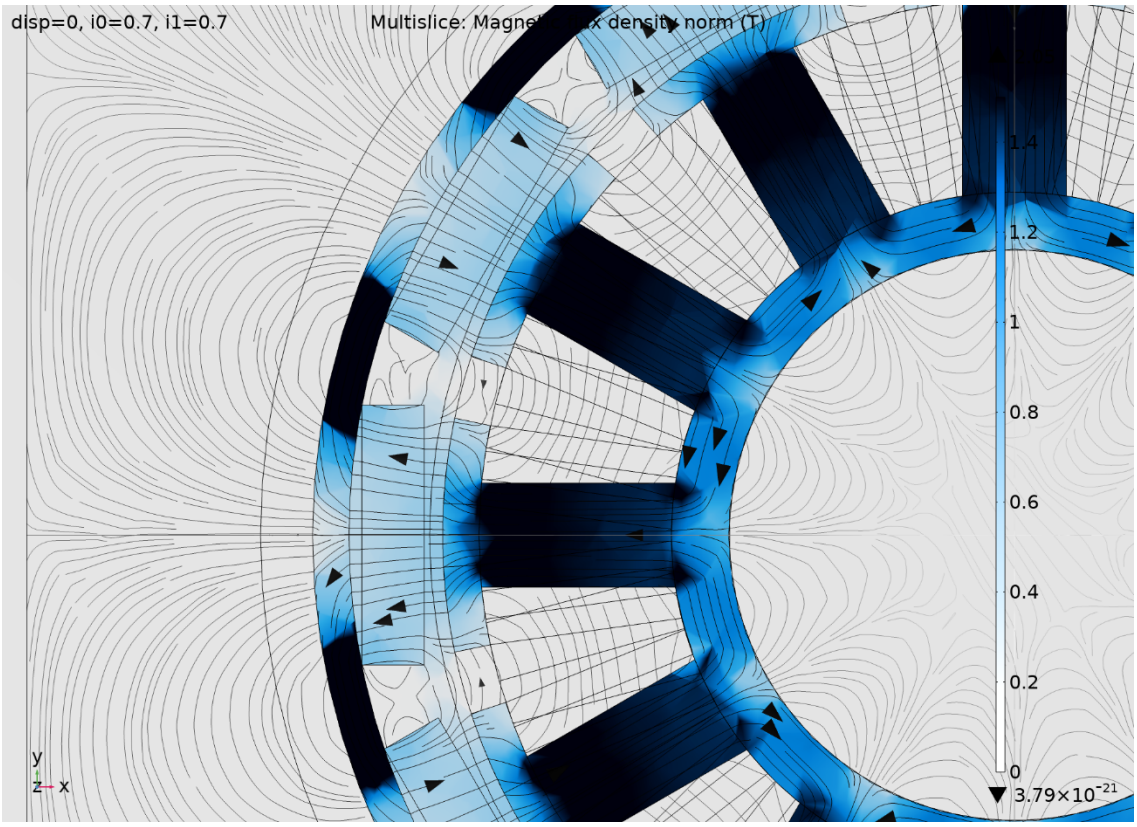

Figure 67. *View of the magnetic field results of the lower stator with the displacement of 0 degrees and both phases activated.*

At the displacement of 0 degrees, which is the intermediate position with the lower phase is aligned, (seen above in Figure 67) i.e. it causes barely any torque. The upper phase, in turn, is misaligned and induces torque, despite not the maximum. Following Figures 68 and 69 show the stators' flux in a position, where one of the peaks in Figure 66 is observed.

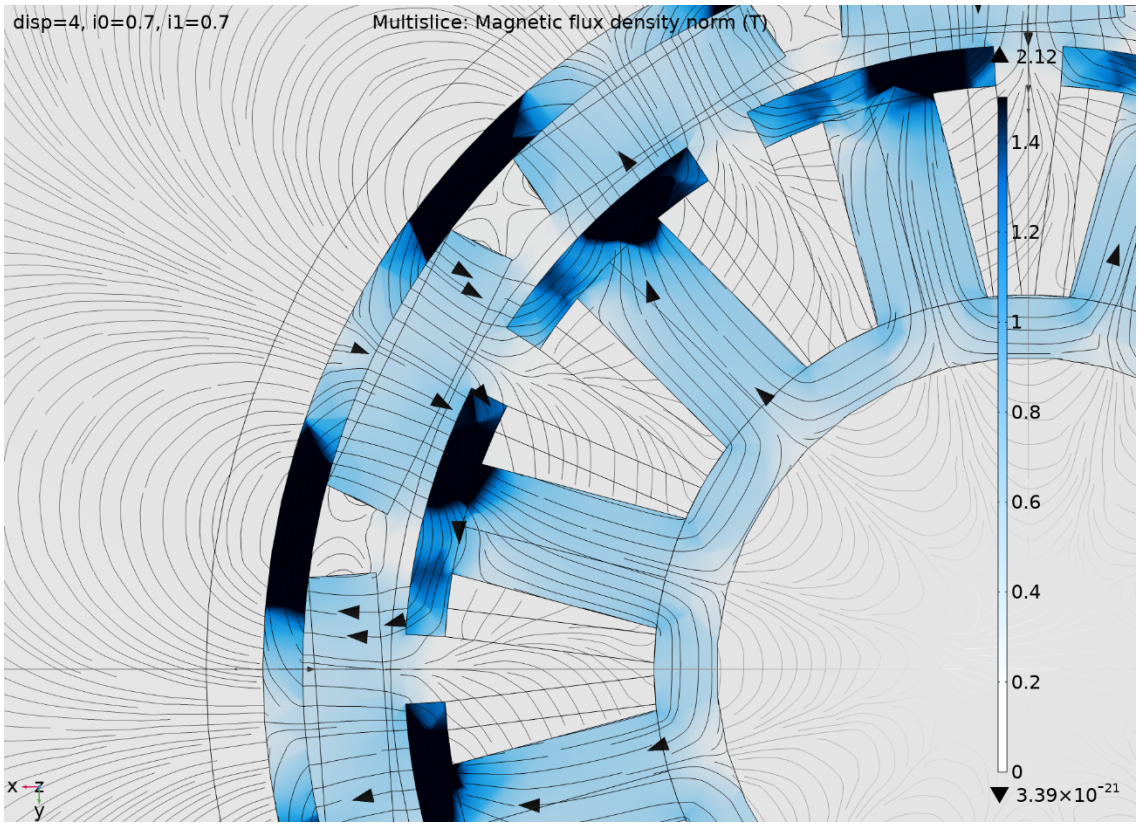

Figure 68. *View of the magnetic field results of the lower stator with the displacement of 4 degrees and both phases activated.*

In the intermediate position peak at 4 degrees in Figure 66 and in Figure 50 at approximately 40 % to 60 % can be noticed that the lower phase (Figure 68) induces torque towards the positive rotational direction of the rotor (note that the image of the upper phase, Figure 69 below, shows the motor from below).

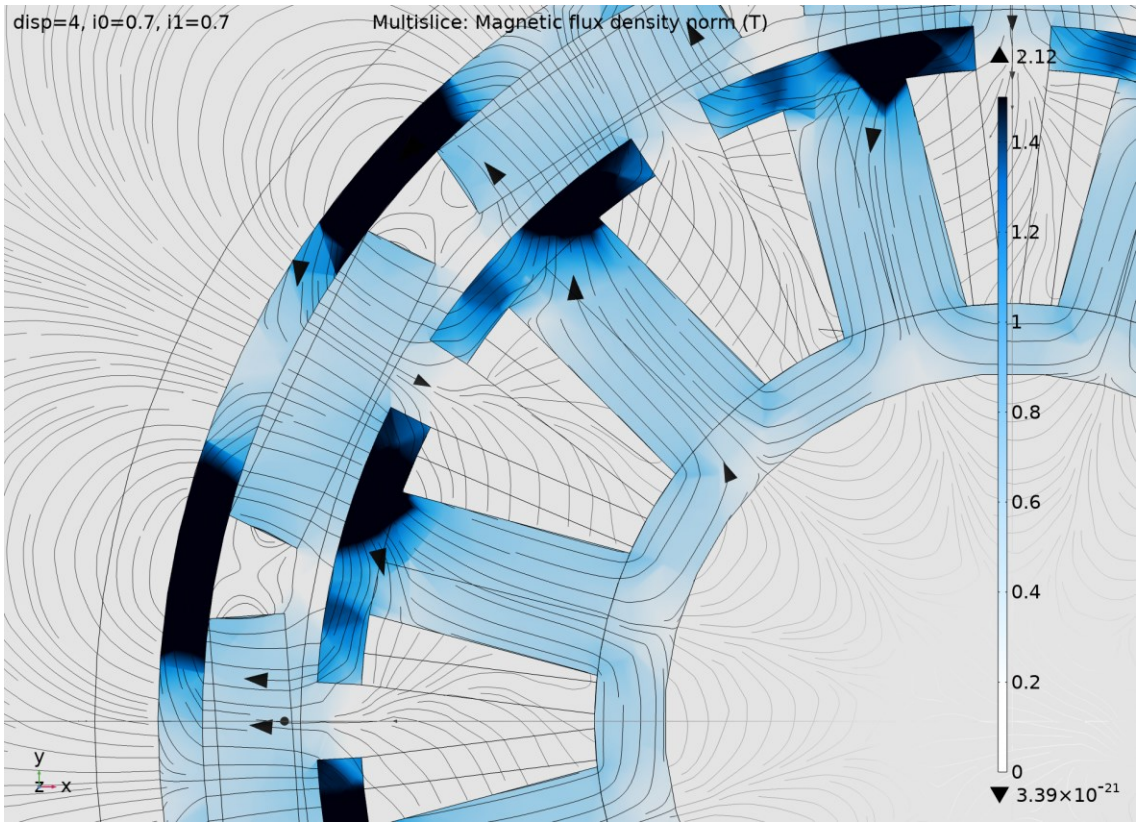

Figure 69. *View of the magnetic field results of the upper stator with the displacement of 12 degrees and both phases activated.*

The Figure 69 shows the situation at 4 degrees displacement from the upside of the model. As the magnetic fields would align, when the rotor would turn counterclockwise, the torque towards the stator is towards negative direction. However, the lower phase is closer to the position, where the reluctance path is minimized, so it remains dominant, yielding in positive total torque.

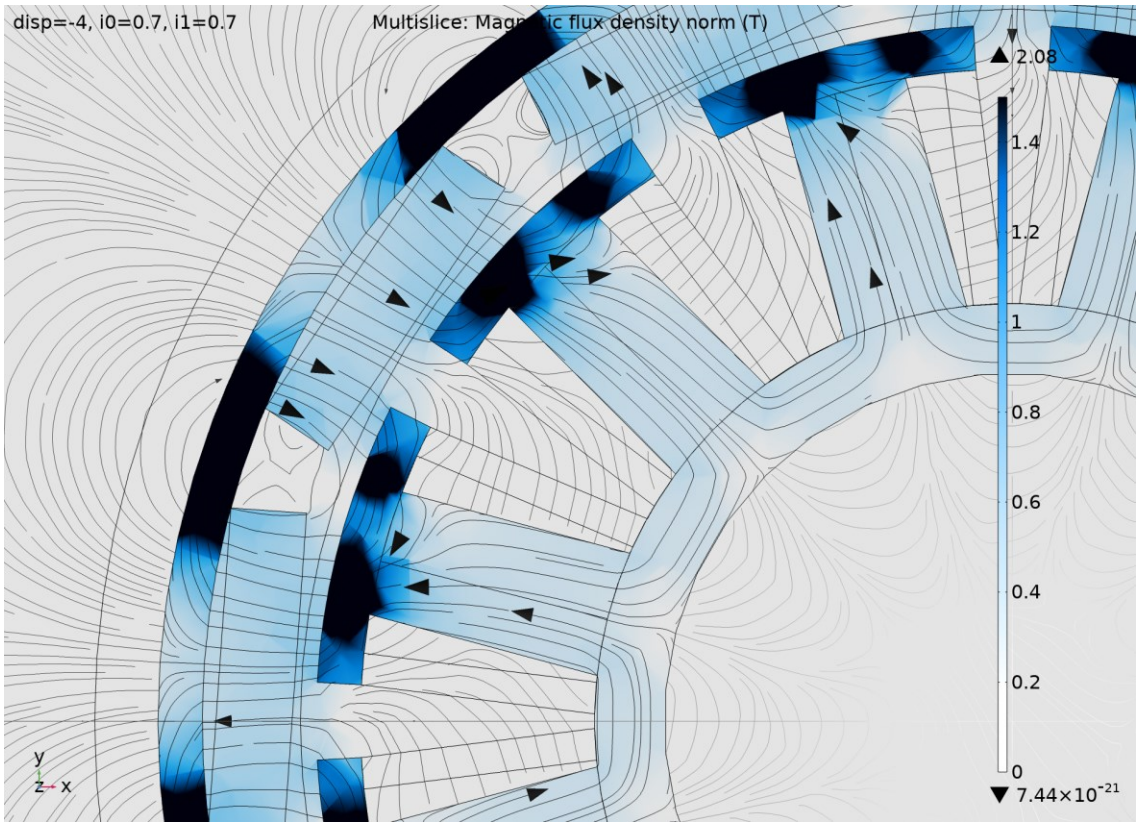

Figure 70. *View of the magnetic field results of the upper stator with the displacement of -4 degrees and both phases activated.*

At the displacement of -4 degrees from the perspective of top view, shown in Figure 70, the magnetic fields are nowhere near matching the magnetic poles. The rotor rotating into negative direction would result in matching magnetic fields, thus resulting in positive torque from the stator phase's point of view.

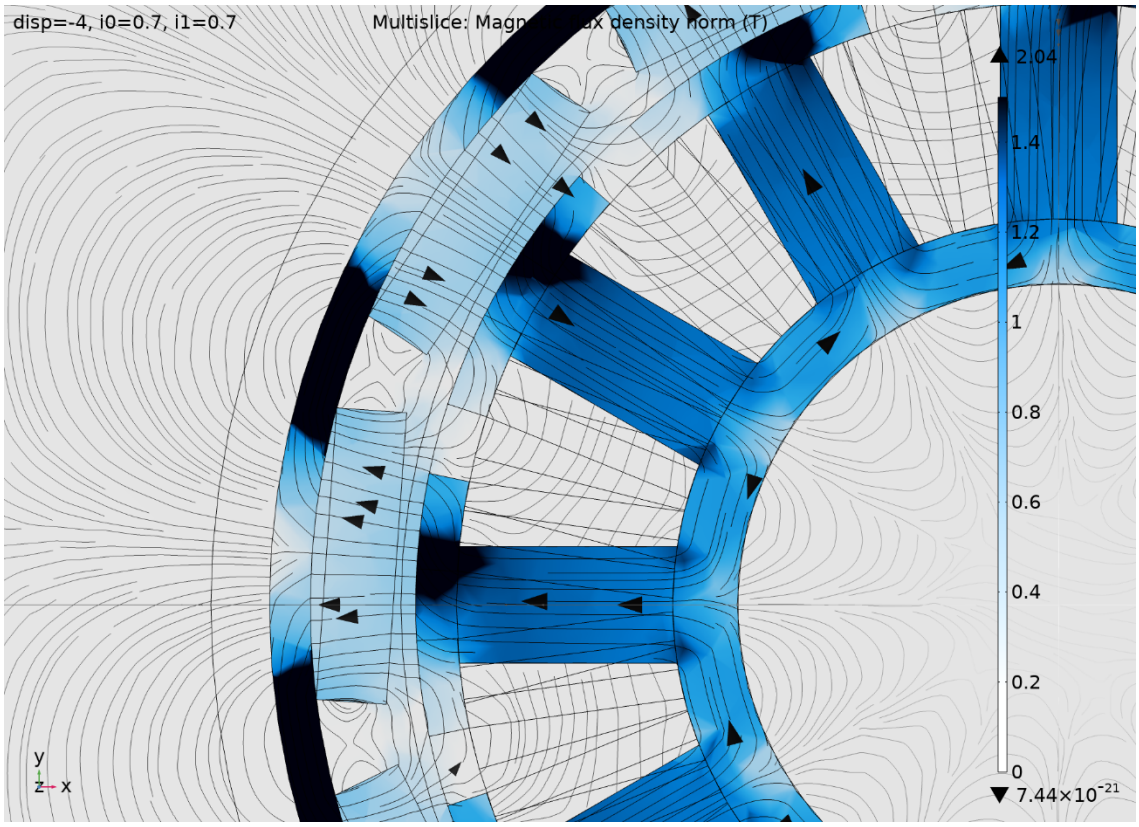

Figure 71. *View of the magnetic field results of the upper stator with the displacement of -4 degrees and both phases activated.*

In the same case, the lower stator is in a much more optimal position. This results in lower torque than the upper stator produces and since the optimal direction of the rotor's rotation is positive, the torque caused towards the stator by this phase is negative. In total, this translates into a positive torque peak in the torque curve in Appendix 7.

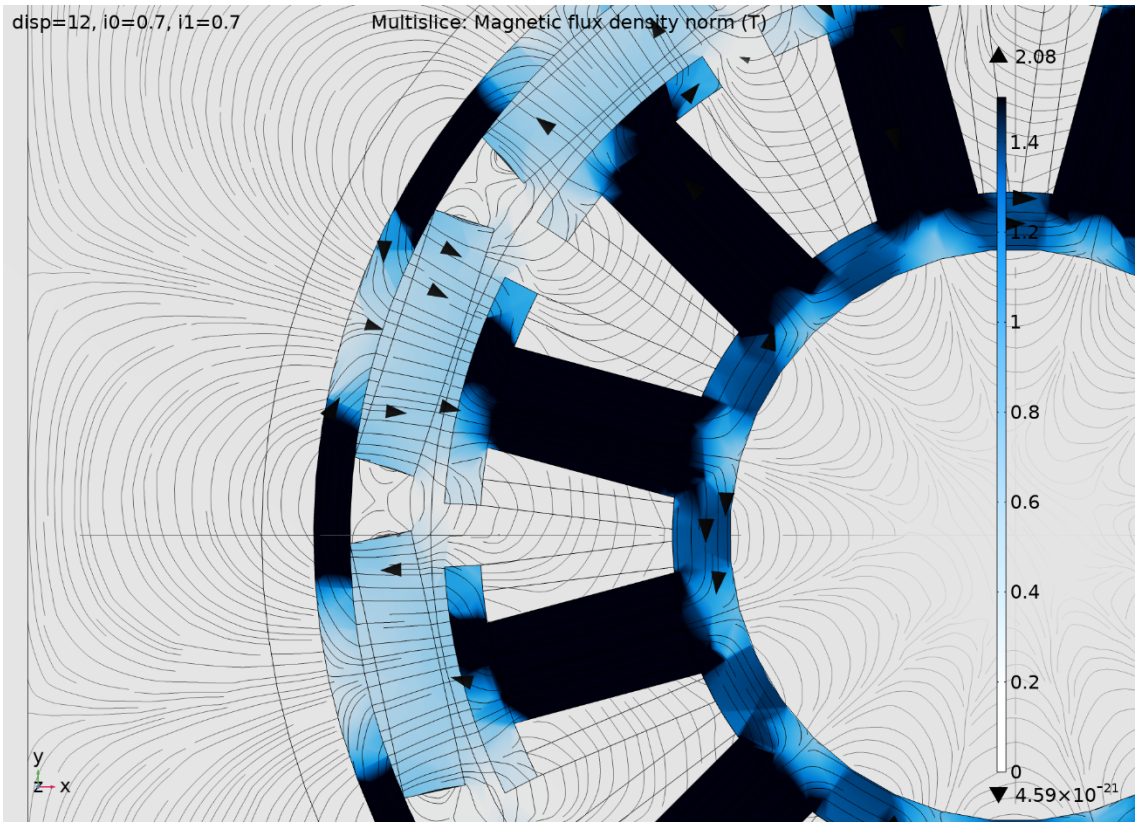

Figure 72. *View of the magnetic field results of the upper stator with the displacement of 12 degrees and both phases activated.*

When the rotor's been displaced for 12 degrees from the intial position, the magnetic fields of Figure 72 show heavy saturation in the upper phase. The coil cores are completely saturated for an understandable reason: The permanent magnets' magnetic field are nearly matching the electromagnetic poles of the stator, increasing the magnetic field strength.

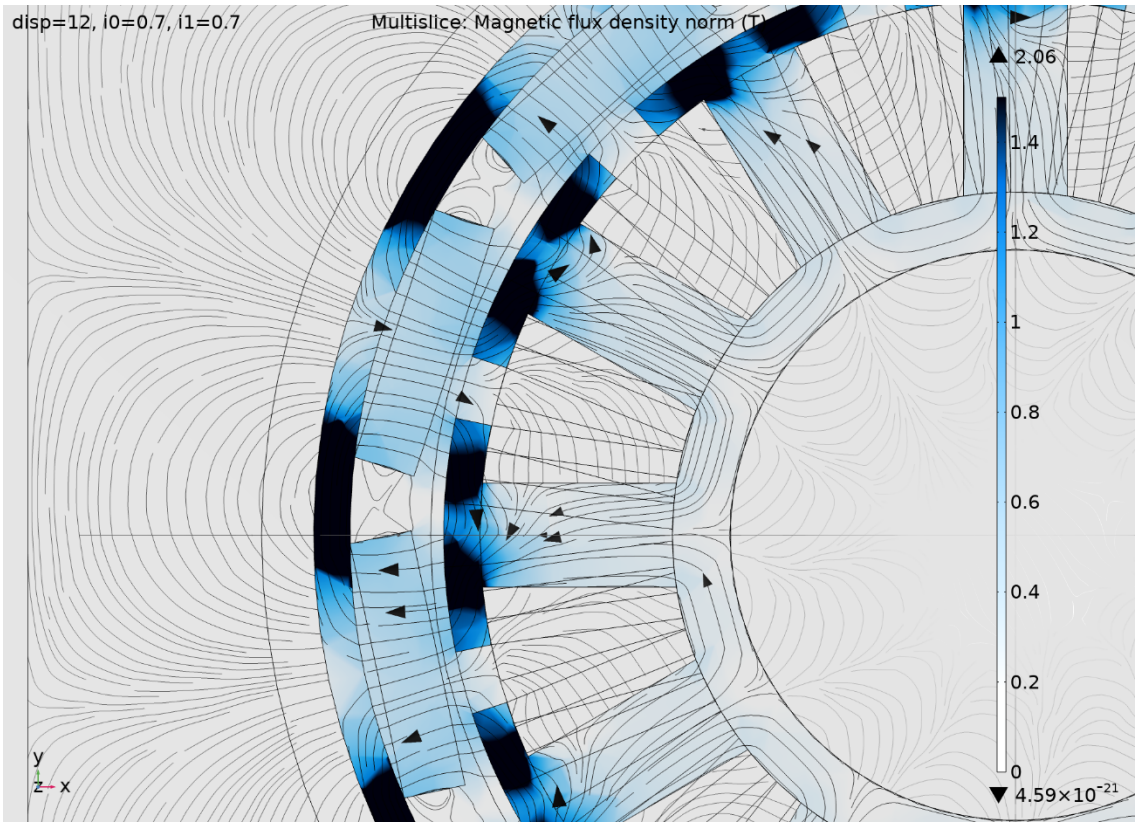

Figure 73. *View of the magnetic field results of the lower stator with the displacement of 12 degrees and both phases activated.*

In the same orientation as Figure 72, the lower stator looks very different when it comes to magnetic fields and saturation, as can be observed from Figure 73. The only place of saturation in the stator of this case is at the very end of the poles. The displacement of magnets is slightly past the middle of the pole gap of the lower phase, causing torque towards the positive direction of the stator rotation. (Of course, in a functioning motor of this structure, the stator doesn't rotate but the rotor rotates.)

APPENDIX 8: SIMULATED STATOR MATERIAL COMPARISON

The different materials and corresponding torque productions were studied by simulations. The materials to be compared were chosen to be plastic and soft iron, resulting in curves of Figure 74.

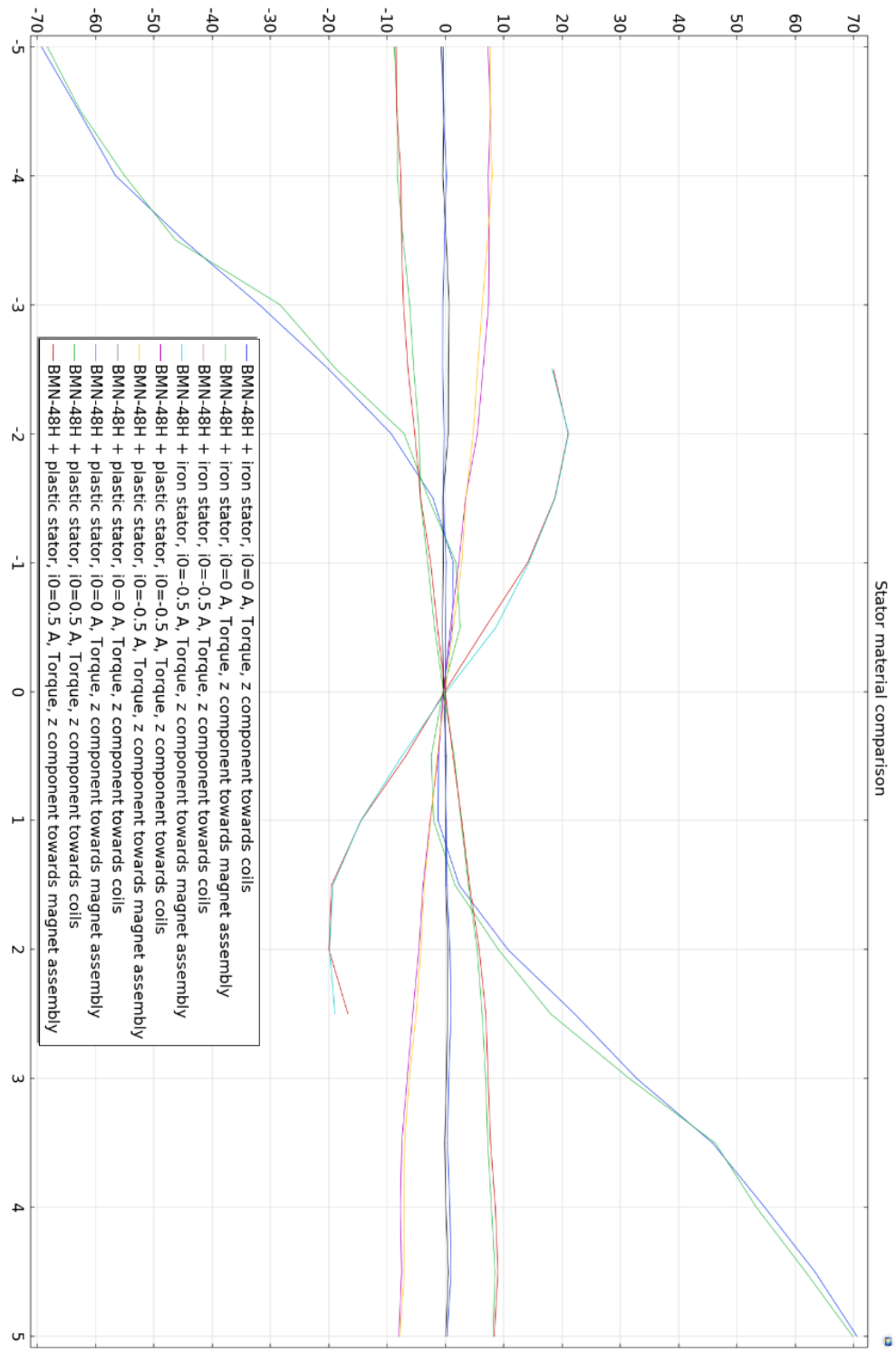

Figure 74. *Torque output comparison with the different stator materials.*

In this simulation, a partial model of the 36-pole permanent magnet stepper motor design was used. This section covered 18th of the complete motor, i.e. 1 pair of magnets and 1 pair of coils in the extreme position of -5° of the displacement sweep. The geometry is presented below. The Figure below shows only the active parts, as the others were left out, preventing distortion of the results.

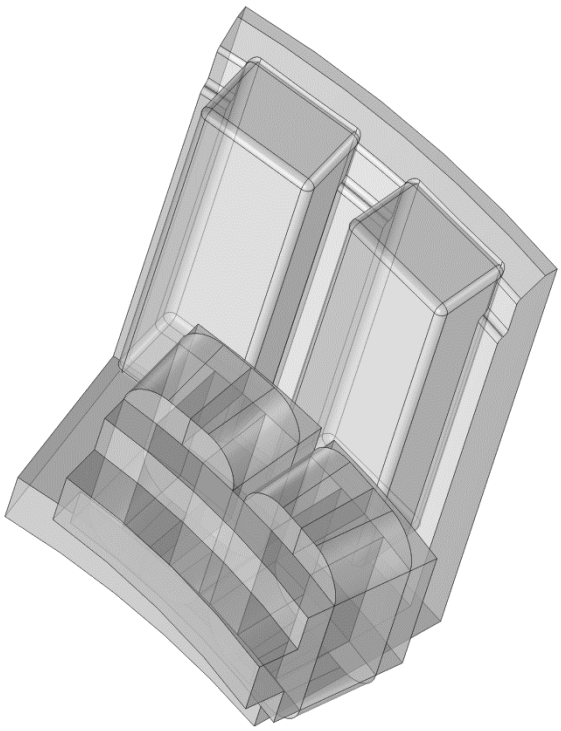

Figure 75. *The geometry used in simulations in Figure 74.*